Initial Characterization of Vaccinia Virus B6

by

Robyn-Lee Burton

A thesis submitted in partial fulfillment of the requirements for the degree of

Master of Science

in

Virology

Medical Microbiology and Immunology
University of Alberta

Abstract

Vaccinia virus, the prototypic poxvirus, is remarkably successful at circumventing the host immune response using an array of dedicated proteins. Studying these immune modulators and immunomodulatory strategies has lead to their use in therapeutics. The present work provides an initial characterization of the previously uncharacterized VACV-B6R, a potential addition to the immunomodulatory arsenal of poxviruses. Here we show that B6 is expressed early and localizes to the ER via a C-terminal transmembrane domain. Homologues of B6R are confined to a subset of orthopoxviruses, however some have become pseudogenes across evolution. Our data demonstrates that over-expression of B6 during infection induces novel ER morphological changes. Interestingly, while over-expression of B6 slightly decreases mitochondrial membrane potential, it also confers moderate protection against TNFα-induced loss of potential. These results were reminiscent of those obtained with expression of cellular Bcl-2. The underlying mechanisms for these phenomena have yet to be solved.

“Everybody is a genius. But if you judge a fish by its ability to climb a tree, it will live its whole life believing that it is stupid.”

- Albert Einstein

Acknowledgement

To begin, I would like to thank my supervisor, Dr. Michele Barry, for welcoming me into her lab first as a summer/499 student, and again as a graduate student. She always believed in me, especially in times when I doubted myself. Her support and encouragement throughout my stay allowed me to grow as a researcher and presenter, and ultimately gave me the courage to pursue my life-long dream. For this, I will be forever grateful.

Coming to work every day was a joy, thanks to my amazing work family. Kristin, we went through a lot together, and your constant words of encouragement taught me: “All you have to do is believe, my beautiful peach.” Bettina, all our therapeutic rant sessions and mutual love of wine and cats made the roughest days okay. Ninad, our token brown guy, your newfound love of inappropriate jokes and extensive knowledge of pretty much everything in life were priceless. Emeka, your kind heart and wisdom were a constant source of happiness and support, and the fact that you put up with our shenanigans speaks to what a great person you are. Ryan, within weeks of starting you were graciously proof-reading my thesis, and have become a wonderful addition to the Barry lab family. The tone of the lab was set by one incredible individual: John Thibault. His love of science and passion for research was infectious, inspiring everyone around him to seek knowledge in all forms. Though known for his love of comic books, superman, movie trailers, and chillatte’s, and his delightfully sarcastic wit, he will forever be remembered for the way he made people around him feel. John’s courage, strength, and positive attitude in the face of adversity were truly inspirational. Words can’t begin to describe how honoured and thankful I am to have known you, John. Though you are sorely missed, your legacy will live on in the form of love and laughter.

I am fortunate to say that within this lab, I genuinely learned from the best. When I began as a summer student I was assigned a graduate student mentor, Dr. Stephanie Campbell. One could not ask for a better teacher, or a more inspiring mentor. Others who have contributed to my success as a blossoming researcher are Logan Banadyga, Nick van Buuren, Kate Fagan-Garcia, Qian Wang, and Chad Irwin. To all of you: Thank you for your support and for all the memories.

I would not have survived this without the love and support of my amazing boyfriend, Mikey Thibert. I am so incredibly lucky to have you in my life and I am so excited for the next chapter of our lives together!

To my family: your endless encouragement and belief in me has allowed me to succeed in every way possible. For this, I dedicate this thesis to you.

Table of Contents

List of Tables

CHAPTER 1

CHAPTER 2

List of Figures

CHAPTER 1

CHAPTER 2

CHAPTER 3

Abbreviations Used in this Study

µCi	microcurie
µl	microliter
µM	micromolar
Aa	amino acid
ADP	adenosine diphosphate
APAF-1	apoptosis-activating factor-1
ATCC	American type culture collection
ATP	adenosine triphosphate
Bcl-2	B-cell lymphoma-2
BGMK	baby green monkey kidney cells
BH	Bcl-2 homology
BiP	binding immunoglobulin protein
bp	basepair
BrdU	5-bromo-2'-deoxyuridine
CARD	caspase recruitment domain
CD8+	cluster of differentiation 8
CEV	cell-associated enveloped virion
CHOP	C/EBP homologous protein
CHX	cycloheximide
cIAP	cellular inhibitor of apoptosis
CNX	calnexin
COE	chloroplast outer envelope
Cop	Copenhagen
CPMM	canine pancreatic microsomal membranes
CRT	calreticulin
CTL	cytotoxic T lymphocyte
CV-1	African green monkey kidney cells
DED	death effector domain
DEPC	diethylpyrocarbonate
DMEM	Dulbecco's modified Eagle's media
DMSO	dimethyl sulphoxide
DNA	deoxyribonucleic acid
dNTP	deoxyribonucleotide triphosphates
dsDNA	double-stranded deoxyribonucleic acid
ECL	enhanced chemiluminescence
ECTV	Ectromelia virus
EDEM	ER degradation enhancer, mannosidase alpha
EDTA	ethylenediaminetetraacetic acid
EEV	extracellular enveloped virion
EGFP	enhanced green fluorescent protein
eIF2α	eukaryotic initiation factor-2 alpha

ER	endoplasmic reticulum
ERAD	ER-associated degradation
EV	enveloped virion
FLICE	Fas-associated death domain-like interleukin-1β converting enzyme
GET	guided entry of tail-anchored proteins
HEK	human embryonic kidney
HI-FBS	heat inactivated foetal bovine serum
ICE	interleukin-1β converting enzyme
IFN	Interferon
IFNR	interferon receptor
IFNγ	interferon gamma
IKK	inhibitor of κB kinase
IP3	inisitol-triphosphate
IP3R	inisitol-triphosphate receptor
IPTG	isopropyl β-D-1-thiogalactopyranoside
ITR	inverted terminal repeat
IV	immature virion
IκB	inhibitor of κB
kbp	kilobase pairs
kDa	kilodaltons
LMP	low melting point
mA	milliamps
mg	milligram
MHC-I	major histocompatibility complex class I
mL	millilitre
mM	milimolar
MV	mature virion
NCS	newborn calf serum
NFκB	nuclear factor kappa B
NK	natural killer
nM	Nanomolar
nm	Nanometer
OAS	2',5'-oligoadenylate synthetase
OMM	outer mitochondrial membrane
ORF	open reading frame
PAGE	polyacrylamide gel electrophoresis
PARP	poly(ADP-ribose) polymerase
PBS	phosphate-buffered saline
PCR	polymerase chain reaction
PDI	protein disulfide isomerase
PFA	paraformaldehyde
pfu	plaque-forming units
PFU/mL	plaque-forming units per millilitre

PKR	protein kinase R
pmole	picomole
PVDF	polyvinylidene fluoride
RER	rough endoplasmic reticulum
RHD	rel homology domain
RIP	receptor interacting protein
RNA	ribonucleic acid
S.D.	standard deviation
SAR	sarcoplasmic reticulum
SDS	sodium dodecyl sulfate
SER	smooth endoplasmic reticulum
SLO	streptolysin O
SRP	signal recognition particle
SSC	standard saline citrate
ssDNA	single-stranded DNA
TA	tail-anchored
TAD	transcription activation domain
tBid	truncated Bid
TBST	tris-buffered saline plus Tween 20
TK	thymidine kinase
TMD	transmembrane domain
TMRE	tetramethylrhodamine ethyl ester
TNFR	tumour necrosis factor receptor
TNFα	tumour necrosis factor alpha
TNT	transcription-translation
TRADD	TNF receptor-associated death domain-containing protein
TRAF	TNF receptor-associated factor
TRC40	TMD recognition complex of 40 kDa
U	Unit
UPR	unfolded protein response
v/v	volume per volume
VACV	Vaccinia virus
VARV	Variola virus
vIAP	viral inhibitors of apoptosis
w/v	weight per volume
WHO	World Health Organization
WV	wrapped virion
X-gal	5-bromo-4-chloro-3-indolyl-β-D-galactopyranoside
$\Delta\Psi_m$	mitochondrial membrane potential

Chapter 1

Introduction

1.1 POXVIRUSES

The family *Poxviridae* comprises an extensive group of enveloped viruses tailored to infect a wide variety of hosts. Poxviruses encode large, double-stranded DNA (dsDNA) genomes and are distinguishable by their brick- or barrel-shaped virion (55). Most notably, these complex DNA viruses complete their entire life cycle exclusively within the cytoplasm of the infected host cell (55, 146). As such, poxviruses must encode all of the enzymes required for gene expression and DNA replication in addition to structural proteins (146). The remainder of the genome is dedicated to species-specific genes involved in host range dictation, host cell manipulation, and immune evasion (137, 146). Through studying these unique poxviral genes, scientists have gained considerable insight into the complexities of virus-host interactions, general virus biology, and host cellular pathways. Consequently, poxviruses are now being used as biological tools for gene delivery, recombinant vaccine vectors, and oncolytic therapies (81, 145, 219). Continued research into these highly successful viruses will enable us to better use them for medical applications in the future.

Poxvirus Classification. The *Poxviridae* family is sub-divided into those that infect insects (*Entomopoxvirinae*) and those that infect vertebrates (*Chordopoxvirinae*) (55, 146). The *Chordopoxvirinae* sub-family is further divided into nine genera based on genetic and host range similarity: *Avipoxvirus, Capripoxvirus, Cervidpoxvirus, Leporipoxvirus, Molluscipoxvirus, Parapoxvirus, Suipoxvirus, Orthopoxvirus,* and *Yatapoxvirus* (Table 1-1) (55). Members of the genera *Orthopoxvirus, Parapoxvirus, Molluscipoxvirus,* and *Yatapoxvirus* are capable of causing disease in humans, however most of these are zoonoses acquired by accidental infection from the natural host (55). These infections are typically benign and self-limiting, with little to no reports of human-to-human transmission (55). Interestingly, the only members which are sole human

Table 1-1 The *Poxviridae* family.

Sub-family	Genus	Species
Chordopoxvirinae	*Avipoxvirus*	Canarypox virus Fowlpox virus
	Capripoxvirus	Goatpox virus Lumpy skin disease virus Sheeppox virus
	Cervidpoxvirus	Deerpox virus
	Leporipoxvirus	Myxoma virus Shope fibroma virus
	Molluscipoxvirus	Molluscum contagiosum virus
	Parapoxvirus	Bovine papular stomatitis virus Orf virus Pseudocowpox virus
	Suipoxvirus	Swinepox virus
	Orthopoxvirus	Buffalopox virus Camelpox virus Cowpox virus Ectromelia virus Horsepox virus Monkeypox virus Rabbitpox virus Racoonpox virus Skunkpox virus Taterapox virus Vaccinia virus Variola virus Volepox virus Yokapox virus
	Yatapoxvirus	Tanapox virus Yaba monkey tumor virus Yaba-like disease virus
Entomopoxvirinae	*Entomopoxvirus α*	*Melontha melontha*
	Entomopoxvirus β	*Amsacta moorei* *Melanoplus sanguinipes*
	Entomopoxvirus γ	*Chrionimus luridus*

Adapted from (55, 65)

pathogens are variola virus (VARV, discussed more in section 1.1.2.1.), the causative agent of smallpox, and molluscum contagiosum virus (MoCV) (55). Other poxviruses, including myxoma virus (MYXV, *Leporipoxvirus* member) and ectromelia virus (ECTV, *Orthopoxvirus* member), provide excellent small animal models for studying poxviruses *in vivo* in rabbits and mice, respectively (66, 70, 106). Work done in these laboratory model systems has allowed for characterization of specific viral genes within the context of infection, and has provided a better understanding of smallpox-like diseases (70). The viruses that will be focused on in this study are described in the following section.

1.1.2. The Orthopoxviruses. The orthopoxviruses are the most extensively studied genus, as they consist of the most medically relevant species to humans (55, 72). There are now 14 species classified under this genus based primarily on morphology, serological cross-reactivity and cross-protection among members, and host range (55, 65). Despite evolutionary relatedness, member species exhibit diverse host ranges and disease spectra (55, 137). VARV and ECTV are restricted to single hosts (humans and mice, respectively), and elicit severe systemic infections with high rates of mortality (72). In contrast, vaccinia virus (VACV), cowpox virus (CPXV), and monkeypox virus (MPXV) can infect a variety of hosts, including humans, monkeys, cows, sheep, and rodents (55, 137). Interestingly, VACV and CPXV cause only a mild, localized infection that is cleared by the host immune response, while MPXV causes a disease that mirrors that of smallpox in humans (55, 160). The incidence of MPXV zoonoses has risen in endemic regions of western and central Africa since 1981, and is now regarded as an emerging zoonotic disease (160).

1.1.2.1. Variola virus. The most notorious member of the poxvirus family, and one of the most infamous viruses known to mankind, is VARV. This highly infectious virus causes smallpox: a systemic, febrile rash with its namesake pustular lesions, or ‘pockmarks’, leaving afflicted individuals with disfiguring

scars or dead (55). VARV has greatly influenced world history, as it has ravaged human civilizations worldwide for over 4000 years, killing more people than all other infectious diseases combined (71). Two variants of VARV exist: variola major, which caused mortality in up to 40% of infected individuals, and variola minor, which caused <1% mortality (55). Importantly, VARV represents one of the greatest achievements in the history of medicine, as it is the first human pathogen to be globally eradicated (71). Thanks to the early work of Edward Jenner and the dedicated efforts of the world health organization (WHO), the last reported case of smallpox was in 1977 (201). Though the world has been smallpox-free for more than 30 years, the use of the remaining stocks of VARV in acts of bioterrorism is still viewed as a potential threat (201).

1.1.2.2. Vaccinia virus. It was widely known that survivors of smallpox were immune to future infections; during the 18th century, English physician Edward Jenner, the father of immunology, made the keen observation that milkmaids who developed cowpox lesions on their hands were also immune to smallpox (11). We now know that CPXV is antigenically similar to VARV and thus confers serological cross-protection against smallpox (55). As a consequence of Jenner's observations, the field of immunization, or vaccination, was born. In the following 200 years of vaccine development, VACV became the vaccinating agent against smallpox (11). Although VACV is indisputably a member of the *Orthopoxvirus* genus, there seems to be no natural host for this virus, and its origin still confounds poxvirologists today (12). It is possible that VACV is actually a hybrid of VARV and CPXV, or it may simply be an extinct virus (11, 12). Nonetheless, VACV is now considered the prototypic poxvirus, as the majority of studies are done in this virus.

1.1.3. Poxvirus Morphology and Genetics. Poxvirus virions are the largest of the animal viruses and have a unique and complex morphology. With dimensions of ~360 $\times$ 270 $\times$ 260 nanometres (nm), their barrel- or brick-shaped virions and

irregular, corrugated surface are just visible by light microscopy (Figure 1.1A) (146). Poxvirus virions come in two infectious forms: the mature virion (MV) and the enveloped virion (EV). The MV is the basic infectious unit comprised of a single lipid membrane, while the EV is a MV surrounded by an additional membrane (146). The outer membranes of the MV and EV contain different sets of viral proteins, rendering the two forms antigenically and functionally distinct (148). Poxviruses also have a complex, asymmetrical internal structure. A dumbbell-shaped nucleoprotein core is flanked by heterogeneous protein aggregates in the concavities called 'lateral bodies' (Fig 1.1B) (146). The core houses the dsDNA genome along with all of the enzymes required for early mRNA transcription (146).

The poxvirus genome is a single linear molecule of covalently closed dsDNA (Figure 1.1C). Poxvirus genomes range in size from 150 kilobase pairs (kbp) in parapoxviruses to 300 kbp in avipoxviruses, which necessitates a physically large virion particle. The overall genome organization is remarkably consistent among the Chordopoxvirus genera (146). The central region consists of highly conserved genes which serve essential functions, including DNA and mRNA synthesis, protein processing, virion assembly, and structural proteins (146). Ninety of these genes are conserved amongst all Chordopoxviruses, 49 of which are also present in Entomopoxviruses (116, 227). In contrast, the two end regions are more variable among genera and species, differing in both gene content and amino acid/nucleic acid sequence (146). These genes are largely involved in virus-host interactions, such as pathogenicity, host range, and immune modulation (116, 137). All poxvirus genomes contain inverted terminal repeats (ITRs) which form hairpin loops to connect the two strands of DNA (146). This region includes a highly conserved sequence responsible for resolution of concatemeric DNA following replication (146). Importantly, poxviruses are highly efficient at homologous recombination, making them amenable to genetic manipulations such as gene insertions, deletions, and mutations (150). A naming

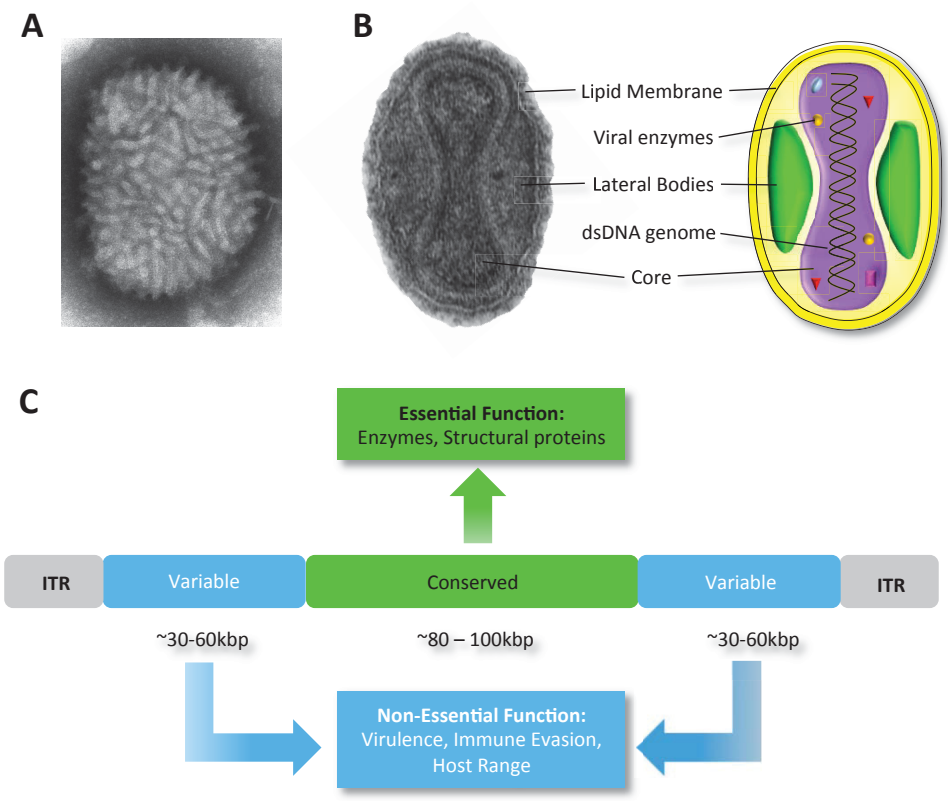

Figure 1.1 Poxvirus morphology and genome organization. All members of the *Poxviridae* family exhibit similar virion morphology and genome organization. **(a)** An electron micrograph image of a Vaccinia virus virion obtained from the Centre for Disease Control and Prevention (CDC) visualizes the irregular, corrugated surface of the virion. **(b)** The poxvirus infectious particle is distinguishable by the dumbbell-shaped core containing a dsDNA genome and enzymes flanked by proteinaceous lateral bodies, all surrounded by 1 or 2 lipid membranes. A transmission electron microscope image visualizes these structures easily (CDC). **(c)** The poxvirus genome contains a central conserved region flanked by variable regions. Genes involved in replication and structure are enriched in the conserved region, while genes responsible for virus-host interactions are found within the termini and vary extensively among poxvirus members. Inverted terminal repeats at the extreme termini encode duplicated genes and are required for genome replication.

convention for VACV genes was created using *Hind*III restriction endonuclease fragment letters, followed by the open reading frame (ORF) number (left to right) within the fragment, then L or R depending on the orientation of the gene. Though a number-based system was introduced recently, this study will only use the former convention.

1.1.4. Poxvirus Life Cycle.

1.1.4.1. Cell Entry. The poxvirus life cycle is rather complex, owing to the cytoplasmic completion of all stages. Although some processes have yet to be fully understood, studies using VACV have elucidated much of the poxvirus life cycle (Figure 1.2). To begin, no single host cell receptor protein has been identified that mediates VACV attachment (148). Studies have shown that MV can bind a variety of surface molecules, including glucosaminoglycans (GAGs), chondroitin sulfate, heparan sulfate, and laminins depending on cell type, virus strain, and experimental condition (14, 35, 44, 46, 94). No surface molecules have been identified that bind EV (148). Following MV attachment, there is a fusion event mediated by an entry-fusion complex of at least 12 virus-encoded proteins within the MV membrane that are conserved among all poxviruses (147). For EV entry, the outermost membrane must first be disrupted in order to expose the entry-fusion complex (148). The location of this event has generated much controversy, as there is evidence to suggest that direct fusion can occur at the plasma membrane or in a pH-dependant manner within endosomes following macropinocytosis of the virion (63, 221).

1.1.4.2. Gene Expression and DNA Replication. Following membrane fusion, the core is released into the cytoplasm of the host cell where transcription and replication can begin (Figure 1.2) (146). The core is transported from the cell periphery to the perinuclear area via microtubules, creating the site of virus transcription and replication, or 'virus factory' (103, 188). Poxvirus genes are

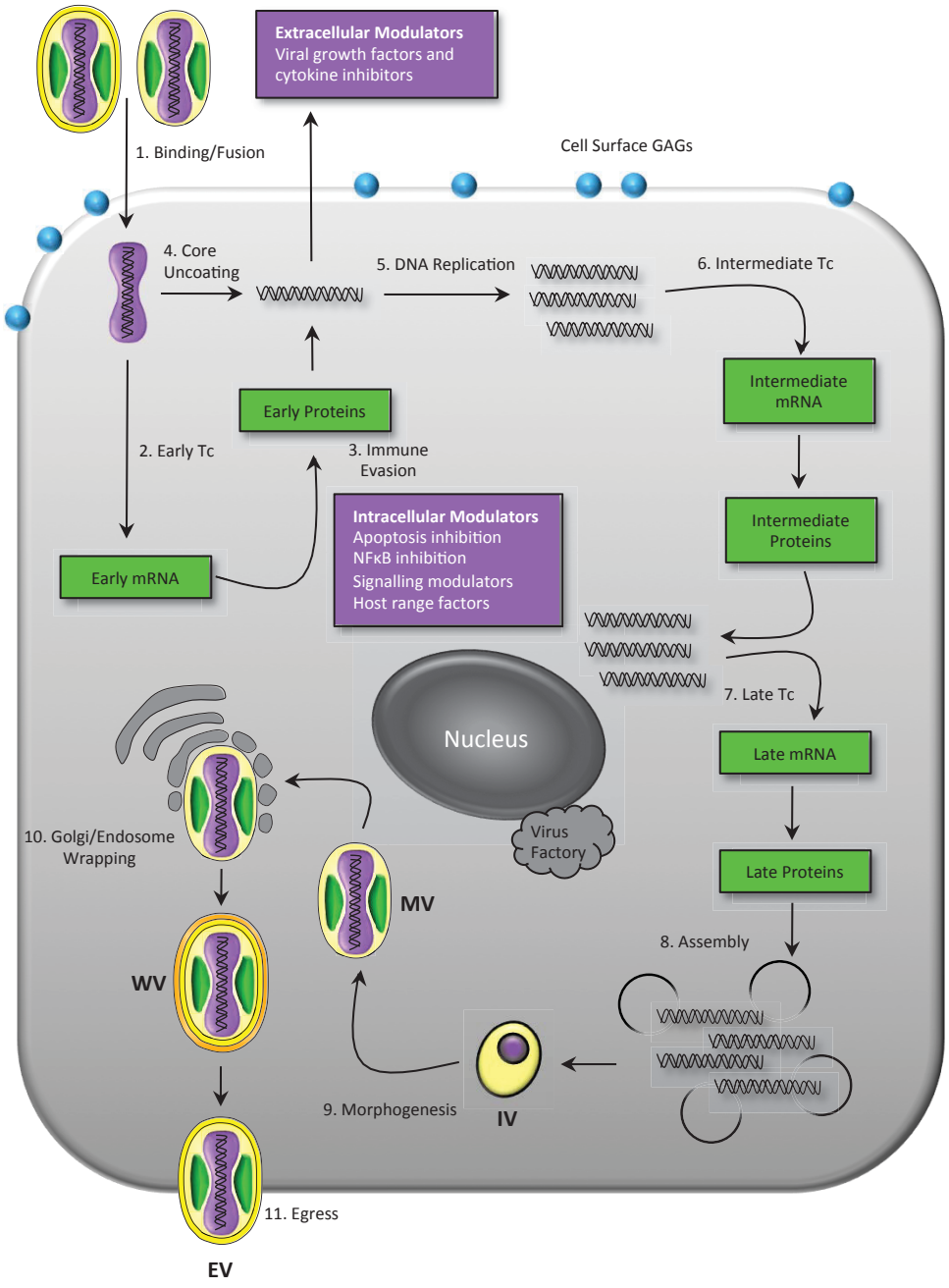
Extracellular Modulators
Viral growth factors and cytokine inhibitors
1. Binding/Fusion
Cell Surface GAGs
4. Core Uncoating
5. DNA Replication
6. Intermediate Tc
Intermediate mRNA
Early Proteins
2. Early Tc
3. Immune Evasion
Intermediate Proteins
Intracellular Modulators
Apoptosis inhibition
NFκB inhibition
Signalling modulators
Host range factors
Early mRNA
7. Late Tc
Nucleus
Late mRNA
Virus Factory
10. Golgi/Endosome Wrapping
MV
Late Proteins
8. Assembly
WV
9. Morphogenesis
IV
11. Egress
EV

Figure 1.2 Poxvirus life cycle. The infectious cycle begins when a virion binds cell surface receptors such as glucosaminoglycans (GAGs) through a fusion complex on the mature virion (MV). Enveloped virions (EV) can initiate infection, however they must first shed their second membrane **(1)**. Early transcription (Tc) begins immediately within the core, generating proteins involved in immune evasion, host range, and intermediate Tc **(2,3)**. Early gene synthesis ceases, coupled with core uncoating **(4)** and subsequent genome replication **(5)** and intermediate Tc **(6)**. Intermediate gene products activate late gene expression, the products of which allow for assembly and morphogenesis of progeny infectious units **(7)**. Genome packaging and assembly of immature virions (IV) from crescent-shaped membranes then occurs **(8)**, followed by morphogenesis into the predominant infectious unit, the MV **(9)**. MVs accumulate within the cell and are released upon cell lysis, or undergo further membrane wrapping to become wrapped virions (WV) **(10)**, which migrate to the cell periphery and egress from the cell as EV **(11)**. Of note, core uncoating, Tc, and DNA replication occur in perinuclear regions known as 'virus factories'. (Adaped from 137)

expressed as a temporal cascade, with early, intermediate, and late classes of genes distinguishable by their promoters (31, 146). Early gene expression begins within the virion core upon cell entry, as it contains the viral RNA polymerase and all necessary enzymes and transcription factors (31). Products of the early class of genes include those involved in DNA replication, such as the viral DNA-dependant DNA polymerase, immune modulation, and intermediate gene transcription. Cessation of early transcription is coupled to uncoating, or dismantling of the core, as it is proposed that the transcriptosome is disrupted by this process (31). DNA replication commences, generating thousands of new genome copies from which intermediate gene transcription can occur (31). Products of the intermediate genes are mostly regulators of late gene expression. Late gene products include those involved in infectious virion assembly and morphogenesis, but they also encode all of the packaged enzymes required for early gene transcription to initiate the next round of infection (51).

1.1.4.3. Virion Assembly and Egress. Poxvirus virion morphogenesis and dissemination is remarkably complex, and has been a source of much controversy in the field of poxvirology (177). At late times of infection, membrane crescents made of lipids and viral core proteins form and are stabilized by a virus scaffold protein (Figure 1.2) (21, 177). The origin of this lipid membrane is unknown, however recent findings suggest that it is derived from the endoplasmic reticulum (ER), allowing viral proteins synthesized at the ER to be added to the crescents, bringing more lipids along with them (98). Once the crescents become fully enclosed around viral core proteins, they are called immature virions (IV). Encapsidation of dsDNA genomes by the IV, followed by proteolytic cleavage of core proteins, transforms the IV into the characteristic brick-shaped MV (177). Morphogenesis ends here for the majority of the infectious virions, which are released by cell lysis and are important for long-range spread from host to host. A fraction of the MVs are transported along microtubules away from the virus factory, where they are further wrapped by

modified trans-golgi cisternae or endosomal membranes, resulting in a wrapped virion (WV) enclosed by three lipid membranes (187). At the cell periphery, the WV fuses with the plasma membrane thereby losing one of the two extra membranes, resulting in a cell-associated EV (CEV) (22). Only a tiny percentage of EVs are released from the cell surface to become extracellular EVs (EEVs) (202). Viral proteins induce the formation of actin projectiles underneath the CEV, propelling them towards neighbouring, uninfected cells (236). This form of infectious virion is important for cell-to-cell spread within an infected host, as it is better able to avoid the host immune system (22).

1.2. POXVIRUS IMMUNE MODULATION

1.2.1. Poxvirus immune evasion. As obligate intracellular pathogens, poxviruses are forced to contend with the multifaceted host immune response. Successful clearance of a poxvirus infection requires both a humoral response and, to a greater extent, a robust cellular immune response mediated by both natural killer (NK) cells and cluster of differentiation 8 (CD8+) T cells (105, 149). Mounting a potent and appropriate adaptive immune response relies upon the concerted efforts of the innate immune pathways, both intrinsic and extrinsic. The importance of innate immunity is underscored by the number of proteins encoded by poxviruses dedicated to subverting these pathways (82, 100, 191, 200). While poxviruses target many of the same pathways, no single immune evasion gene is conserved among all poxviruses, illustrating the intimate co-evolution of poxviruses with their specific hosts (30, 97, 116). Many immunomodulatory proteins share sequence similarity with cellular proteins, suggesting that these genes were acquired from their host via horizontal transmission (116). However, there are a number of orphan genes that seem to lack any obvious cellular, or even viral, counterparts.

One strategy that poxviruses use to circumvent the innate immune system is to express secreted proteins to prevent extracellular signals from reaching infected cells (Table 1-2). The complement system is capable of destroying virions and infected cells, and is countered by poxviral complement control proteins that aid in the cleavage of important factors in the complement cascade (191). Concentration gradients of chemoattractant molecules, or chemokines, are responsible for recruiting leukocytes to sites of poxvirus infection. Both low- and high-affinity chemokine binding proteins secreted by infected cells sequester these molecules, thereby preventing the influx of immune cells (191). Signalling molecules called cytokines, including interferons, interleukins, and tumour necrosis factor-alpha (TNFα), are potent anti-viral molecules that confer an anti-viral state in infected and surrounding cells as well as activate and shape the appropriate Th1 adaptive immune response (2, 163). Poxviruses prevent these molecules from engaging their cognate receptors by secreting receptor homologue decoys or even cytokine mimics (Table 1-2) (2, 24). While highly effective, this strategy cannot prevent every single receptor-ligand interaction, necessitating an intracellular strategy as well.

Poxviruses have numerous strategies to manipulate intracellular signalling of host cells. Should ligands bind their cognate receptors in spite of the numerous secreted viral factors, poxviruses are prepared to interfere with downstream signalling events. Dedicated proteins prevent activation of signal transducers and enzymes which are downstream of interferon receptors (191). MYXV encodes an ER protein that prevents major histocompatibility complex class I (MHC-I) expression on the cell surface, thereby hiding infected cells from circulating immune cells (80). Poxviruses can also evade recognition by infected cells themselves. For example, VACV E3 and K3 can prevent global translational attenuation by protein kinase R (PKR) and 2’,5’-oligoadenylate synthetase (OAS), both of which are activated in the presence of dsRNA - an unintentional by-product of the poxvirus life cycle

Table 1-2. Secreted and intracellular poxviral immune evasion proteins.

Virus	Viral Factor	Mechanism	Source
Secreted Immune Evasion Proteins			
Inhibitors of Complement			
VACV	C21L (VCP)	Complement binding protein	(109, 181)
CPXV	IMP	Complement control protein	(110, 141)
VARV	SPICE	Smallpox inhibitor of complement enzymes	(121)
Inhibitors of Interferons			
MYXV	MT-7	IFNγ receptor homologue	(115, 151)
VACV	B8R	IFNγ receptor homologue	(212)
VACV	B18R	IFNα/β binding protein	(48, 120)
Inhibitors of Chemokines			
MYXV	MT-7	Binds CXC, CC, and C-chemokines	(115, 151)
MYXV	MT-1	CC-chemokine binding protein	(190)
VACV	B29R	CC-chemokine binding protein	(4)
CPXV	vCCI	CC-chemokine binding protein	(33)
MCV	MC148R	Chemokine mimic	(124, 125)
Inhibitors of Cytokines			
MCV	MC54L	IL-18 binding protein	(245)
VACV	D7L	IL-18 binding protein	(67)
MYXV	MT-2	Viral TNF receptor	(189)
CPXV	CrmB, CrmC, CrmD, CrmE	Viral TNF receptor	(96, 122, 183, 199)
TANV	gp38	Multi-cytokine binding protein; binds TNFα, IL-2, IL-5, and IFNγ	(161)
CPXV	B18R	IL-1β receptor decoy	(230)
ORFV	ORFV-IL-10	IL-10 homologue	(38)
VACV	B15R	IL-1 binding protein	(3, 206)
Inhibitors of Inflammation			
MYXV	SERP-1	Serine protease inhibitor; targets plasmin, tissue plasminogen activator, urokinase, and thrombin	(129, 153)
CPXV	SPI-3 (K2L)	Serine protease inhibitor; prevents cell-cell fusion	(225, 226)
Intracellular Immune Evasion Proteins			
Inhibitors of Inflammation			
CPXV	CrmA	Serine protease inhibitor; Prevents cleavage of pro-IL-1β and secretion of mature IL-1β	(172, 218)
MYXV	SERP-2	Serine protease inhibitor; Prevents cleavage of pro-IL-1β and secretion of mature IL-1β	(139, 164)
Inhibitors of Interferons			
VACV	H1L (VH1)	Phosphatase; reverses STAT1 activation by IFNγ	(152)
VACV	E3L	Binds dsRNA; prevents activation of PKR and OAS	(39, 56)
VACV	K3L	eIF2α homologue; PKR pseudosubstrate	(34)
VACV	K7L	Prevents IRF3 activation	(200)
VACV	C16L	Induces hypoxic response in infected cells	(135)
Downregulation of Receptors			
MYXV	M153R	Reduces cell surface MHC-I expression	(80)

(56). A vast number of additional proteins are involved in modulating the NFκB and apoptosis pathways, which are discussed at length in later sections (143, 215).

1.2.2. Apoptosis. Apoptosis is a highly conserved process intrinsic to multicellular organisms to remove damaged, redundant, and pathogen-infected cells (90). It is a complex, tightly regulated process by which cells are dismantled such that minimal damage is incurred by neighbouring cells (64, 217). As originally observed by Kerr *et al* in 1972, apoptotic cells exhibit a number of characteristic morphological changes: Cell rounding and retraction, chromatin condensation, DNA fragmentation, mitochondrial dysfunction, and dynamic plasma membrane blebbing. The final stages of apoptosis result in the formation of intact blebs of cytoplasmic and nuclear contents, called apoptotic bodies, which are taken up by phagocytes and degraded (184). This way the apoptotic cell is safely removed without triggering an unwanted, potentially damaging immune response.

Apoptotic dismantling of a cell is achieved through the actions of cysteine aspartic acid proteases, or caspases, which cleave substrates after aspartic acid residues (197, 217). Caspases themselves require proteolytic cleavage after aspartic acids for activation, as they are synthesized as enzymatically inert pro-caspases (156, 176). Each pro-caspase is comprised of a small and large subunit, as well as pro-domains of either a caspase recruitment domain (CARD) or a death effector domain (DED) (Fig 1.3A). Upon activation, typically by other caspases, the pro-domains are removed and the active caspases form heterotetramers of 2 small and 2 large subunits (217). Initiator caspases (caspases -2, -8, -9, and -10) are activated upon receipt of pro-apoptotic signals, which in turn cleave the executioner caspases (caspases-3, -6, and -7), resulting in a caspase cascade of activation (54). The morphological changes observed during apoptosis are a result of executioner caspases cleaving hundreds of targets, including cytoskeletal components, DNAse inhibitors, and nuclear lamina (220).

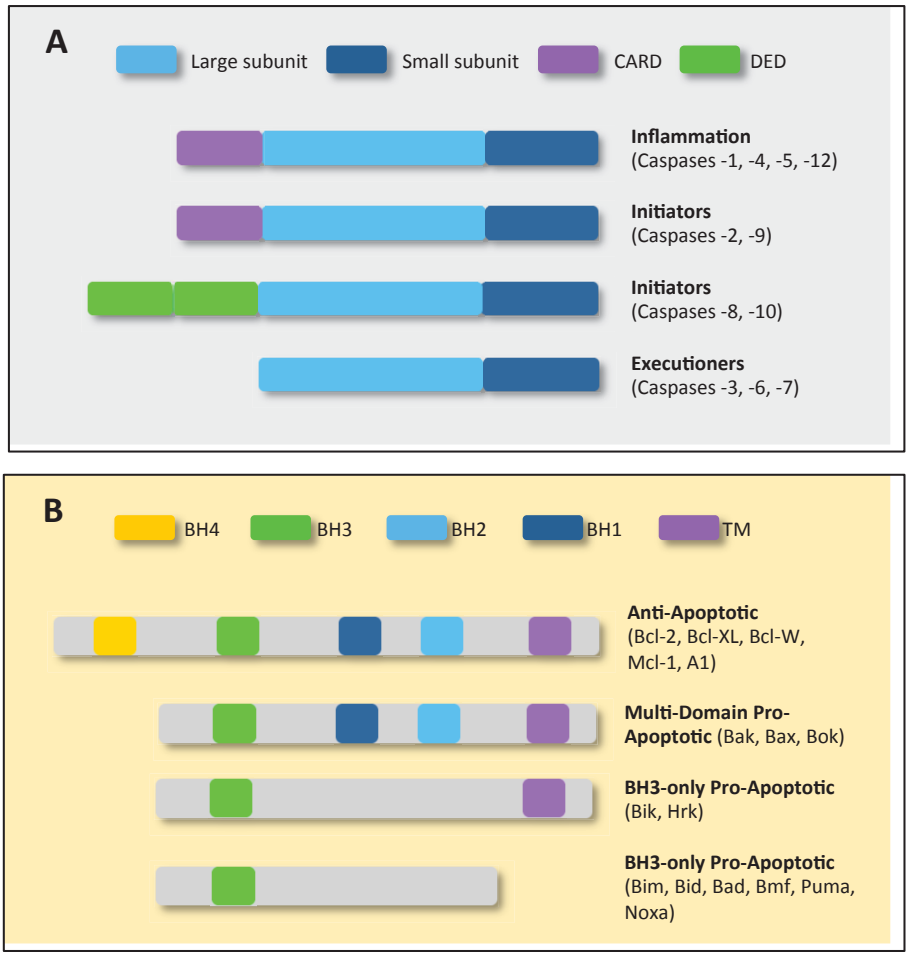

Figure 1.3 Schematic representation of key mediators of apoptosis. (a) The caspase family is comprised of initiators, executioners, and pro-inflammatory caspases. Executioner caspases-3, -5, and -6 contain only a small and large subunit, while initiator caspases-8 and -10 also contain two death effector domains (DED), and pro-inflammatory caspases-1, -4, -5, and -12 and initiator caspases-2 and -9 also contain a caspase recruitment domain (CARD). **(b)** The Bcl-2 family of proteins include pro- and anti-apoptotic members. Anti-apoptotic members contain all four Bcl-2 homology (BH) domains and a C-terminal transmembrane domain. Pro-apoptotic members can be divided into three categories: those with all but the BH4 domain, those with only a BH3 domain and a transmembrane domain, and those with a BH3 domain only. The presence of a BH3 domain in every protein underscores the importance of this domain in requisite protein-protein interactions.

Induction of apoptosis serves as a potent barrier to virus infection. Virus-infected cells are recognized by both NK cells and CD8+ cytotoxic T lymphocytes (CTLs) by a lack of surface MHC expression or presentation of virus-derived peptides, respectively (105, 149). These signals trigger NK cells to engage death receptors, such as Fas or tumour necrosis factor receptor 1 (TNFR1), or CTLs to release granzyme B molecules, both of which culminate in the activation of initiator caspase-8 (Figure 1.4, left) (8, 29). Induction of apoptosis in this way is referred to as the extrinsic pathway. Apoptosis can also be triggered by intracellular signals, including virus infection, a pathway known as the intrinsic or mitochondrial pathway (see 1.2.2.1).

1.2.2.1. The Intrinsic Pathway. The intrinsic apoptotic pathway is also referred to as the mitochondrial pathway owing to the crucial involvement of this organelle (112). The B-cell lymphoma-2 (Bcl-2) protein family is evolutionarily conserved and governs the intrinsic pathway through regulated protein-protein interactions (247). This family is united by the presence of at least one of four Bcl-2 homology (BH) domains which allow for their diverse interactions (Fig 1.3B). Some members also encode transmembrane domains (TMDs) for insertion into the outer mitochondrial membrane (OMM). One class of Bcl-2 proteins inhibit apoptosis and includes Bcl-2, Bcl-XL, Bcl-W, Mcl-1, and A1, while another class promotes apoptosis and includes Bak, Bax, and Bok (247). A third class of proteins, which are also pro-apoptotic, only encode a BH3 domain and includes Bim, Bid, Bad, Bik, Bmf, Puma, Hrk, and Noxa (43, 192, 247). These proteins act as sensors within the cell cytoplasm, promoting apoptosis during growth factor or nutrient deprivation, ultraviolet (UV) exposure, DNA damage, dsRNA, or virus infection (192). The fate of a cell depends on the delicate balance struck by these proteins based on their interactions.

In a healthy cell, Bcl-2-like anti-apoptotic proteins localize to the OMM where they bind and inhibit pro-apoptotic Bak and/or Bax via their BH3 domains

(217). While Bak is constitutively localized to the mitochondria, Bax and the BH3-only proteins are cytoplasmic, however studies suggest that Bax may exist in constant flux between cytoplasmic and mitochondrial localization (247). Upon pro-apoptotic insult, activated BH3-only proteins can directly activate Bak and Bax, or displace Bak/Bax and inhibit anti-apoptotic proteins at the OMM (Figure 1.4) (192). Both Bak and Bax undergo a conformational change, and in the case of Bax, this exposes a TMD and an N-terminal epitope allowing it to localize to the OMM (58, 154). Though the mechanism is not fully understood, studies suggest that Bak and Bax form heterooligomers which form pores in the OMM, resulting in the loss of mitochondrial membrane potential and release of apoptogenic factors from the intermembrane space (57, 247). One factor released is cytochrome *C,* which then binds to apoptosis activating factor-1 (APAF-1), causing it to oligomerize and form a wheel-shaped, heptameric signalling platform called the apoptosome that is responsible for activation of initiator pro-caspase-9 (175). Activated caspase-9 then cleaves pro-caspases-3 and -7, initiating the controlled destruction of the cell. Thus, the mitochondria serves as a crucial checkpoint in determining cell fate, as the loss of the membrane potential and release of cytochrome *C* commits the cell to apoptosis (214). Though the intrinsic and extrinsic pathways are activated by different stimuli, cross-talk is observed between the two via BH3-only protein Bid. Stimulation of the extrinsic pathway results in the activation of caspase-8, which targets and cleaves Bid to its truncated form, tBid (117). tBid then translocates to the OMM and induces Bak/Bax to form the homooligomers responsible for cytochrome *C* release (240).

1.2.2.2. Poxviruses Inhibit Apoptosis. Apoptosis serves as a critical anti-viral response, as it prevents viruses from completing their life cycle and spreading to neighbouring cells and hosts. This form of programmed cell death can be induced by immune cells or by the infected cell itself (217). Not surprisingly, poxviruses are adept at preventing apoptosis through countermeasures targeting

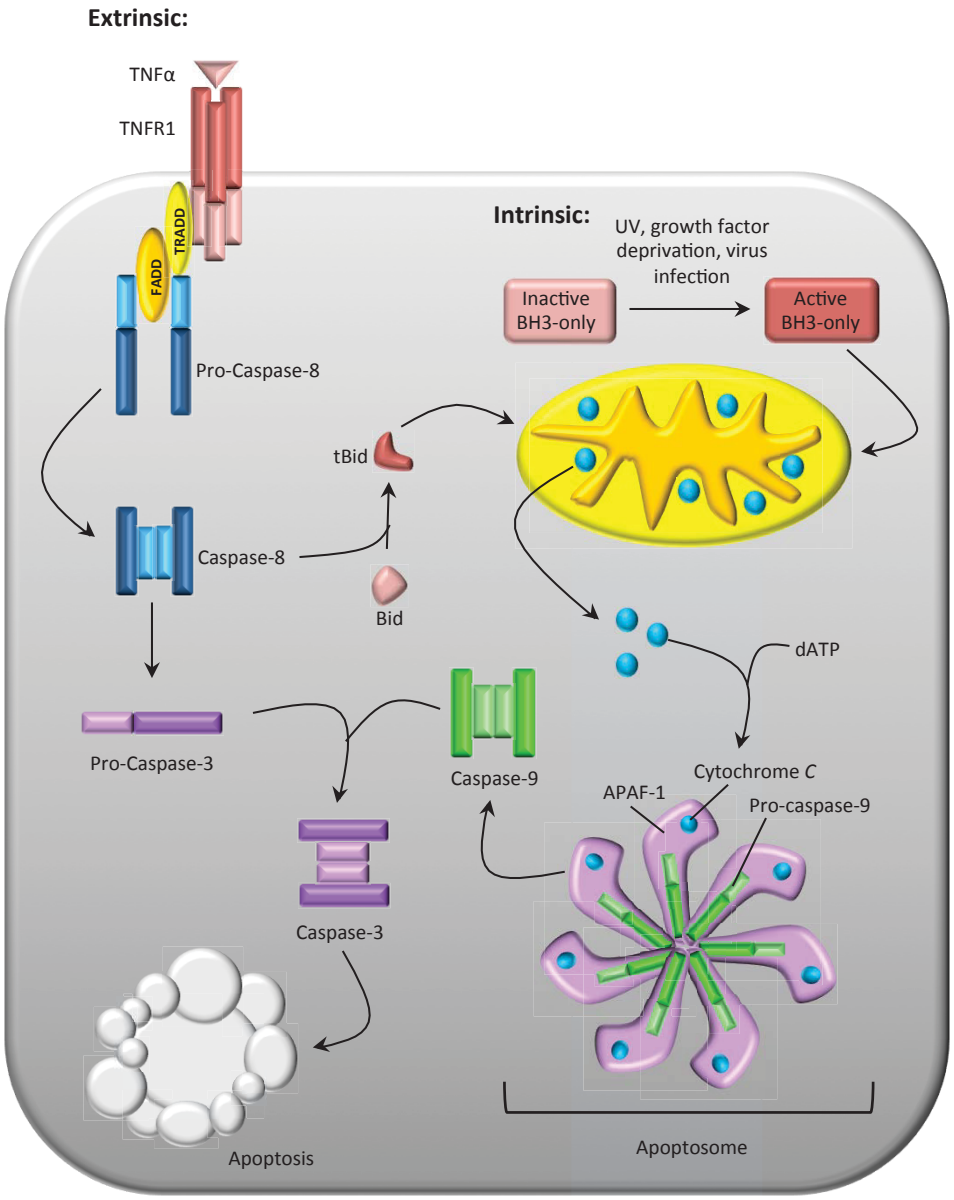
Extrinsic:
TNFα
TNFR1
TRADD
FADD
Pro-Caspase-8
Caspase-8
tBid
Bid
Intrinsic:
UV, growth factor deprivation, virus infection
Inactive BH3-only
Active BH3-only
dATP
Pro-Caspase-3
Caspase-9
Caspase-3
Cytochrome C
APAF-1
Pro-caspase-9
Apoptosis
Apoptosome

Figure 1.4 The extrinsic and intrinsic apoptotic pathways. Activation of apoptosis by TNFα, on the left side, leads to recruitment of pro-caspase-8 to the TNFR1 via TRADD and FADD recruitment proteins, allowing *trans*-activation of initiator caspase-8. Caspase-8 cleaves and activates executioner caspase-3, which culminates in apoptosis. Activation of the intrinsic pathway is through BH3-only proteins sensing stress signals, which culminates in the formation of pores in the outer mitochondrial membrane and release of cytochrome *C.* Cytoplasmic cytochrome *C* recruits apoptosis activating factor-1 (APAF-1) and initiator pro-caspase-9 to form the apoptosome, a signalling platform for activation of caspase-9. Caspase-9 cleaves and activates caspase-3, thus committing the cell to apoptosis. Cross-talk between the pathways is mediated by BH3-only protein Bid. Caspase-8 can cleave Bid to truncated Bid (tBid), which in turn activates the intrinsic pathway.

almost every step of the process (Table 1-3) (68, 215). Virus-infected cells are identified by circulating immune cells when virus-derived peptides are presented on the cell surface in complex with the MHC I molecule (8). To avoid identification, MYXV encodes an ER-resident protein, M153, responsible for downregulating cell surface MHC-I (80). This strategy essentially hides the infected cell from CTL-mediated apoptosis. Activated immune cells such as T cells and macrophages produce inflammatory cytokines, including the potent inducer of anti-viral states and apoptosis, TNFα (198). Poxviruses encode and secrete many TNF receptor decoys which bind to and sequester extracellular TNFα molecules, thus preventing the effects of TNFα on infected and neighbouring cells (68).

Upon infection with a poxvirus, a number of cellular stress signals cause host cells to intrinsically activate the apoptotic pathway, essentially resulting in host cell suicide. In turn, poxviruses encode an arsenal of proteins to inhibit the action of many key players within the apoptotic cascade (68, 215). One strategy exemplified by MoCV is to prevent signal transduction at death receptors, such as the TNFR. Viral FLICE (Fas-associated death domain-like interleukin-1β converting enzyme) inhibitory proteins form complexes with receptors, adaptor proteins, and pro-caspase-8 to prevent caspase-8 activation (196). *Entomopoxvirinae* members encode viral inhibitors of apoptosis (vIAPs) which also prevent activation of caspases (10). Other anti-apoptotic proteins function by acting as pseudosubstrates for caspases thereby interfering with their normal function. These proteins are referred to as serine protease inhibitors, or serpins, of which CPXV cytokine response modifier A (CrmA) is the prototypic example (218). CrmA is capable of interfering with the actions of caspase-1, caspase-8 and even granzyme B (218). There are a number of other inhibitors that function more indirectly and are listed in Table 1-3.

Table 1-3. Poxviral anti-apoptotic proteins.

Protein	Gene	Genus	Mechanism
Downregulation of Receptors	M153R	*Leporipoxvirus*	Downregulates MHC I
TNF Receptor Decoys	MT-2	*Leporipoxvirus*	Sequester TNF
	CrmB, C, D, E	*Orthopoxvirus*	
	TPV-2L	*Tanapoxvirus*	
vIAPS	AMV-IAP	*Betaentomopoxvirus*	Caspase Inhibitor, IBM Inhibitor
	MSV242 and MSV248	*Alphaentomopoxvirus*	
vFLIPS	MC159L, MC160L	*Molluscipoxvirus*	Inhibit Death Receptor Signals
Serpin	CrmA/SPI-2	*Orthopoxvirus*	Inhibit Caspases 1 and 8, Granzyme B
	SPI-1, SPI-3	*Orthopoxvirus*	
	Serp-1, Serp-2	*Leporipoxvirus*	
Anti-Apoptotic E3 Ligases	p28/N1R	*Orthopoxvirus, Leporipoxvirus, Capripoxvirus, Suipoxvirus, Yatapoxvirus*	Unknown
Anti-Apoptotic Inhibitor at the Golgi	vGAAP	*Orthopoxvirus*	Reduce Ca^{2+} Stores
vBcl-2 Proteins	FPV039/CNPV058	*Avipoxvirus*	Inhibit Cytochrome *C* release
Mitochondrial Inhibitors of Apoptosis	DPV022	*Cervidpoxvirus*	Inhibit Cytochrome *C* release
	ORFV125	*Parapoxvirus*	
	M11L	*Leporipoxvirus*	
	F1L	*Orthopoxvirus*	
Others	MC066L	*Molluscipoxvirus*	Protects against UV and H_2O_2
	MT-4	*Leporipoxvirus*	ER resident apoptosis inhibitor
	MT-5	*Leporipoxvirus*	Unknown

Adapted from (68, 215). Tumour necrosis factor, TNF; viral inhibitors of apoptosis, vIAPs; IAP binding motif, IBM; viral FLICE (Fas-associated death-domain-like interleukin-1β converting enzyme) inhibitory protein, vFLIPs; Cytokine response modifier, Crm; serine protease inhibitor, SPI; viral B-cell lymphoma-2 family protein homologue, vBcl-2.

Mitochondria serve as a crucial checkpoint within the apoptotic cascade, and are governed by the Bcl-2 family of proteins. To avoid activation of this intrinsic pathway, poxviruses encode viral Bcl-2 homologous proteins as well as novel mitochondrial inhibitors of apoptosis (215). The *Avipoxvirus* members Fowlpox virus (FPV) and Canarypox virus (CNPV) are the only poxviruses that encode obvious homologues of mammalian Bcl-2 anti-apoptotic proteins (6, 222). Intriguingly, a number of other genera have acquired anti-apoptotic proteins that localize to the mitochondria yet exhibit little to no sequence similarity to their mammalian counterparts. For example, MYXV encodes M11 and VACV encodes F1, both of which localize to the mitochondria where they prevent cytochrome *C* release due to inhibitory interactions with pro-apoptotic proteins (211, 216). Structural studies have revealed that F1 and M11 adopt a Bcl-2-like fold despite the lack of sequence identity, which likely allows for interactions with mammalian pro-apoptotic members (32, 60). The sheer number of anti-apoptotic proteins that poxviruses utilize emphasizes just how immense the selective pressure apoptosis places on these viruses.

1.2.3. The NFκB Pathway. The ability of a cell to rapidly adapt and respond to a fluctuating environment is largely mediated by inducible transcription factors. The nuclear factor kappa-light-chain-enhancer of activated B cells, or NFκB, family of transcription factors serve such a purpose in inflammation and the innate and adaptive immune response (86, 88, 228). For example, in response to virus infection, the NFκB pathway induces the expression of cytokines, chemokines, stress response genes, and apoptosis regulators to remove infected cells (159). This family is very multi-faceted, however, serving roles in development, cell survival, differentiation, and proliferation as well (159). The NFκB pathway integrates signals from a number of different stimuli, including ligand binding to TNFR1, IL-1R, and Toll-like Receptors, as well as B-cell receptor and T-cell receptor engagement (85). Signals are transduced by these receptors

via recruitment of numerous adaptor proteins and kinases which ultimately lead to the translocation of NFκB into the host cell nucleus (85).

The NFκB family is comprised of five members (p65 (RelA), RelB, c-Rel, p100/p52, and p105/p50; Figure 1.5A) that form homo- and heterodimers and function as transcription factors (85). Dimerization is mediated by N-terminal Rel homology domains (RHDs) present in all members. Interestingly, dimers comprised of p50 and p52, which lack transcriptional activation domains (TADs), actually repress the expression of target genes (85). NFκB dimers both repress and induce the expression of hundreds of target genes by binding to DNA at κB sites within promoters and enhancers. As these transcription factors lack enzymatic activity, it is believed that NFκB dimers function by recruiting heterologous co-activators, co-repressors, and enzymes that alter the accessibility of the target genes (85). NFκB dimers themselves undergo post-translational modifications, like phosphorylation, that alter the specific co-regulators recruited by the different dimers (87). With the number of dimer combinations, post-translational modifications, and interactions with a variety of co-regulators, NFκB represents a paradigm of complex and diverse biological transcriptional response programs (85). Research over the past 2 decades has increased our understanding of the complexities of this pathway, however many questions still remain. For the purpose of this study, we focus on the classical, or canonical, NFκB pathway.

1.2.3.1. The Canonical NFκB Pathway. The NFκB pathway integrates a variety of signals and elegantly tailors specific, appropriate transcriptional responses through multiple regulatory mechanisms which are beyond the scope of this study. The canonical pathway has been studied extensively, and while the precise regulatory mechanisms of each step is still controversial, we do have a fairly clear understanding of the general sequence of events (85). In unstimulated cells, NFκB dimers are sequestered in the cytoplasm by members

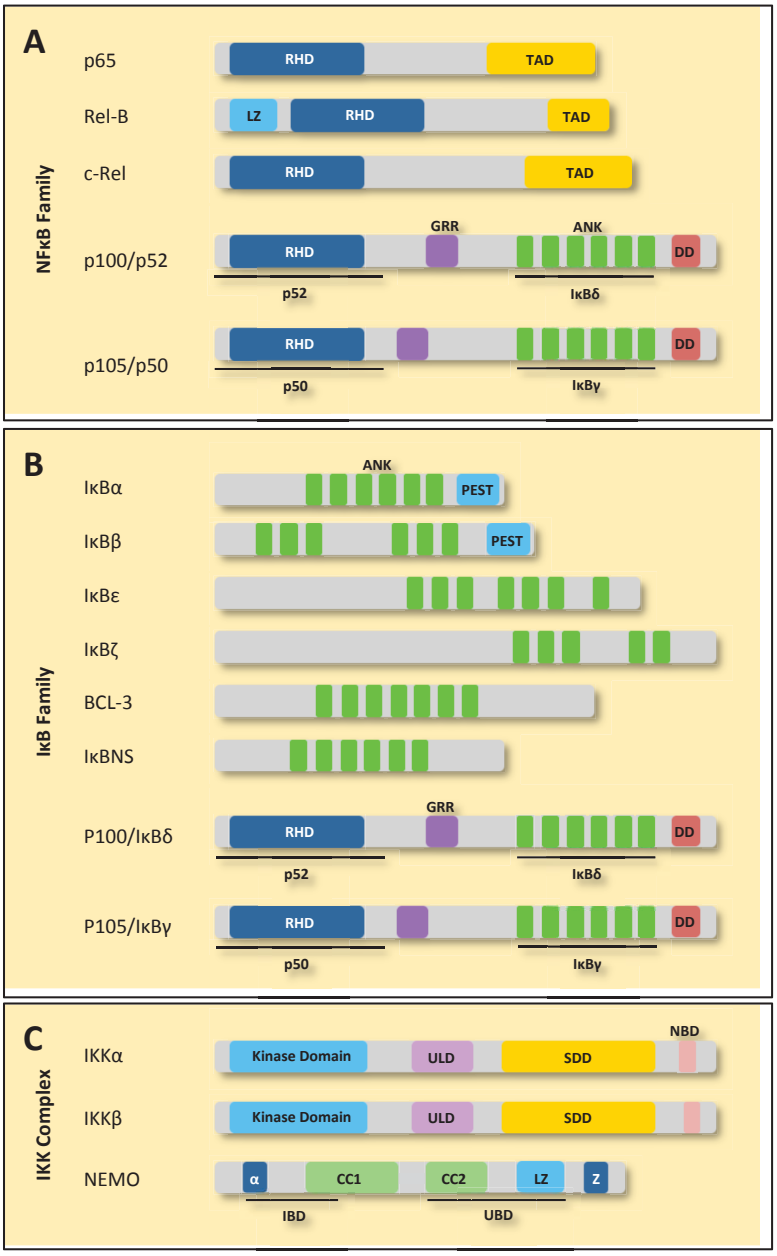
A
NFκB Family
p65
RHD
TAD
Rel-B
LZ
RHD
TAD
c-Rel
RHD
TAD
p100/p52
GRR
ANK
RHD
DD
p52
IκBδ
p105/p50
RHD
DD
p50
IκBγ
B
IκB Family
IκBα
ANK
PEST
IκBβ
PEST
IκBε
IκBζ
BCL-3
IκBNS
P100/IκBδ
GRR
RHD
DD
p52
IκBδ
P105/IκBγ
RHD
DD
p50
IκBγ
C
IKK Complex
IKKα
NBD
Kinase Domain
ULD
SDD
IKKβ
Kinase Domain
ULD
SDD
NEMO
α
CC1
CC2
LZ
Z
IBD
UBD

Figure 1.5 Schematic representation of NFκB signalling proteins. (a) The mammalian NFκB/Rel family includes five members: p65, RelB, c-Rel, p100/p52, and p105/p50. Proteolytic processing of the precursors p100 and p105 gives rise to p52 and p50, respectively. **(b)** The eight members of the IκB family include: IκBα, IκBβ, IκBε, IκBζ, BCL-3, IκBNS, p100 and p105. This family of proteins is characterized by numerous ankyrin repeat domains. **(c)** The IKK complex is comprised of IKKα, IKKβ, and NEMO (IKKγ). All important domains responsible for protein functions are labelled. (RHD) Rel homology domain; (TAD) transactivation domain; (LZ) leucine zipper domain; (GRR) glycine-rich domain; (ANK) ankyrin-repeat domain; (DD) death domain; (PEST) proline-rich, glutamic acid-rich, serine-rich, and threonine-rich; (ULD) ubiquitin-like domain; (SDD) scaffolding and dimerization domain; (NBD) NEMO-binding domain; (α) α-helical domain; (CC) coiled-coil domain; (Z) zinc finger domain; (IBD) IKK binding domain; (UBD) ubiquitin-binding domain. Adapted from (85).

of the inhibitor of κB (IκB) family (Figure 1.5B) (13). The predominant NFκB dimer in the canonical pathway is the p65/p50 dimer, which is primarily sequestered by IκBα (85). The interaction of IκBα with p65/p50 masks the nuclear localization signal within the p65 subunit, thus sequestering it in the cytosol. Other IκB members differ in their expression kinetics and activating signal (85). Another important player in the pathway is the inhibitor of κB kinase (IKK) complex (99). As the name implies, this complex acts as a serine/threonine kinase responsible for phosphorylating IκB, and is comprised of three subunits: IKKα, IKKβ, and the NFκB essential modifier, NEMO (Figure 1.5C) (85). Studies have demonstrated that the IKKβ subunit is responsible for phosphorylating IκBα, not the IKKα (119). NEMO lacks any enzymatic activities, but rather serves a regulatory role in IKK activation (61). In unstimulated cells, the IKK complex remains inactive in the host cell cytoplasm as well.

The canonical pathway can be activated by TNFα, a cytokine produced by activated macrophages and T cells in response to virus infection (Figure 1.6). Interaction of TNFα to TNFR1 results in receptor trimerization and recruitment of the adaptor proteins TNF receptor-associated death domain protein (TRADD) and receptor interacting protein 1 (RIP1) (235). While RIP-1 exhibits E3 ligase activity, it is not known if this activity is required for IKK activation (20). TRADD then recruits TNF receptor associated factor-2 (TRAF2) which in turn recruits cellular inhibitor of apoptosis-1 and -2 (cIAP1/2) (85). cIAP1/2 are E3 ligases that ubiquitinate RIP-1, which acts as a scaffold for recruiting the IKK complex and another kinase complex, TAK1/TAB2/TAB3 (85). Both NEMO and TAB2/3 have ubiquitin-binding motifs, which would explain how these kinase complexes are recruited (102, 169). Two mechanisms have been proposed for IKK activation: By direct phosphorylation by TAK1 or by *trans*-autophosphorylation made possible by induced proximity of IKK complexes (85). Either way, serine residues within the activation loops of IKK become phosphorylated, thus activating the IKK complex.

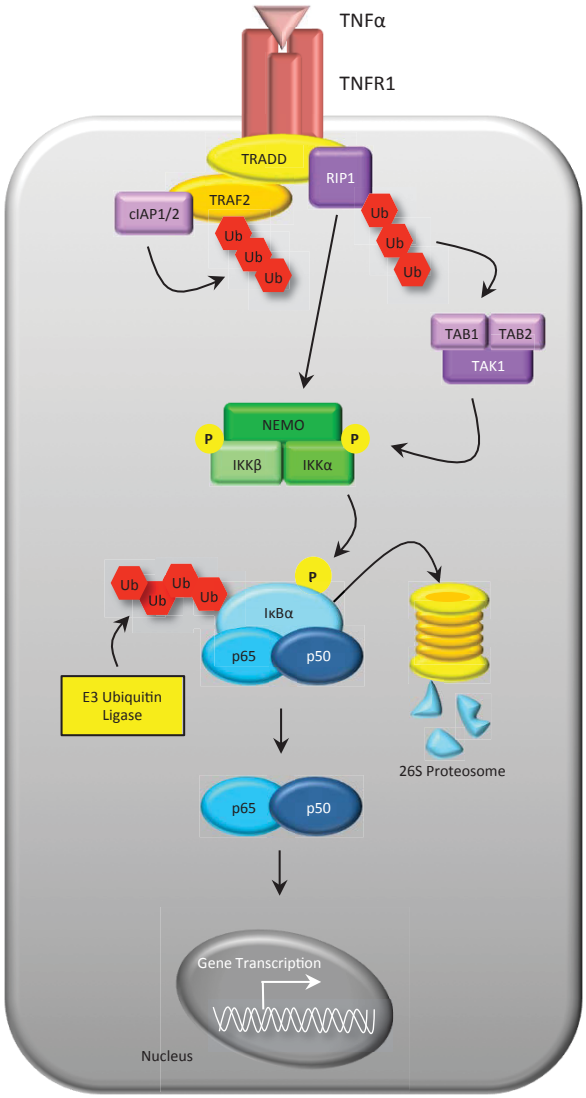

Figure 1.6 The Canonical NFκB Pathway. Ligation of TNFα to TNFR1 results in receptor trimerization and recruitment of adaptor protein TRADD and kinase RIP1. TRADD also recruits TRAF2 which brings in the E3 ligase cIAP1/2. Ubiquitinated TRAF2 and RIP1 act as scaffolds, bringing in both TAK1 kinase via the Tab1/2 ubiquitin-binding domains, and the IKK complex via the NEMO ubiquitin-binding domain. TAK1 kinase phosphorylates and activates the IKK complex (IKKβ subunit) which subsequently phosphorylates IκBα. IκBα is then targeted for ubiquitination and degradation by the 26S proteosome, thus releasing the p65/p50 NFκB dimer which translocates to the nucleus where it induces target gene transcription.

Activated IKK phosphorylates IκBα on target serine residues, which targets the protein for subsequent ubiquitination and degradation by the 26S proteosome (186). This exposes the nuclear localization signal on the unsequestered p65/p50 transcription factor, allowing the dimer to translocate to the nucleus where it regulates genes involved in anti-viral responses (88). This entire process is remarkably fast, with nuclear translocation of p65/p50 seen as early as 10 minutes after TNFα stimulation. Inactivation of the NFκB pathway requires resynthesis of IκBα, inactivation of the IKK complex, and displacement of NFκB and co-regulators from DNA (85). Aberrant activation or deactivation of NFκB signalling has been implicated in many diseases, highlighting the importance of the extensive regulatory mechanisms within this pathway.

1.2.3.2. Poxviruses Manipulate the NFκB Pathway. The integral role of NFκB signalling in response to virus infection makes it a highly attractive target for virus manipulation. Indeed, poxviruses have evolved to interfere with this pathway in a variety of ways (143). The complexity of the pathway lends itself to many points of interference, including direct inhibition of key players within the classical pathway, and preventing indirect activation of the pathway (Table 1-4). As discussed previously, poxviruses encode many secreted receptor homologues to TNFα and IL-1β (191). These sequester the signalling molecules from engaging their cognate receptors and hence prevent initiation of the NFκB signalling cascade. A number of proteins are also dedicated to preventing signal transduction via receptors by binding to adaptor proteins (143). These interactions prevent the formation of signalling complexes, which are crucial for activation of the IKK complex (85).

Intracellular poxviral proteins targeting the IKK complex itself have received much attention, however many of their mechanisms of action remain elusive. Some proteins, such as VACV B14, directly interact with IKK subunits and prevent phosphorylation, while others function in the absence of protein

interactions (40, 131, 243). Intriguingly, VACV-encoded A52, B14, and N1 are NFκB inhibitors that adopt Bcl-2-like folds, however only N1 contains a binding groove for interacting with BH3 domains of Bcl-2 family proteins (52, 77). N1 has been shown to inhibit staurosporine-induced apoptosis in addition to its ability to inhibit NFκB activation (52). Ultimately, poxviral proteins directly targeting the IKK complex prevent the phosphorylation and/or activation of the IKK subunits. Another successful strategy utilized is direct inhibition of NFκB subunits. Select proteins can prevent synthesis of certain subunits, bind and prevent nuclear translocation of certain subunit-containing dimers, or even inhibit dimers within the nucleus (143). Two such proteins, VACV-G1 and CPXV-CP77, interact with NFκB subunits via ankyrin repeats, just like cellular IκB family members (95, 144).

A variety of signalling pathways outside of the classical pathway can activate NFκB. As described previously, VACV-E3 is capable of preventing PKR-induced activation of the IKK complex by binding to and sequestering dsRNA (39). Another VACV protein, M2, is an ER-resident membrane protein that prevents ERK phosphorylation and subsequent NFκB activation (74, 91). Interestingly, M2L mutants that do not localize to the ER are incapable of inhibiting NFκB activation (91). Another important signalling molecule is IL-1β, as it is also capable of triggering the classical NFκB pathway via different adaptor molecules and kinases (85). This molecule forms a positive feedback loop, as it is upregulated by virus-induced NFκB responses and subsequently engages IL-1Rs thereby potentiating the response (85). IL-1β is synthesized in the inactive, pro-IL-1β form and is cleaved by activated caspase-1. Poxviruses interfere with this feedback loop by inhibiting the processing of pro-IL-1β by caspase-1 (107, 170). The fact that poxviruses target both direct and indirect activation of the NFκB pathway illustrates the importance of this pathway in the anti-viral response.

Table 1-4. Poxviral inhibitors of classical NFκB signalling

Function	Gene	Genus	Mechanism
TNF/IL-1 Receptor Decoys	MT-2	*Leporipoxvirus*	Sequesters TNFα
	CrmB-E	*Orthopoxvirus*	
	YTPV-2L	*Yatapoxvirus*	
	B15R	*Orthopoxvirus*	Sequesters IL-1β
Inhibitors of Signalling Platform Formation	K7L	*Orthopoxvirus*	Bind adaptor proteins, preventing receptor attachment and downstream signalling
	A52R	*Orthopoxvirus*	
	A46R	*Orthopoxvirus*	
	MC159L	*Orthopoxvirus*	
Inhibitors of the IKK Complex	B14R	*Orthopoxvirus*	Bind IKKβ, preventing phosphorylation
	N1L	*Orthopoxvirus*	Prevents IKK activation
	K1L	*Orthopoxvirus*	Prevents IκBα degradation
	ORF024	*Parapoxvirus*	Prevents IKKα/β phosphorylation
	MC160L	*Orthopoxvirus*	Reduces IKK subunit phosphorylation
Inhibitors of NFκB Dimers	G1R	*Orthopoxvirus*	Prevents synthesis of p50 subunit
	CP77	*Orthopoxvirus*	Binds p65 subunit, prevents nuclear translocation
	ORF121	*Parapoxvirus*	
	ORF002	*Parapoxvirus*	Binds and inhibits p65 in nucleus
Inhibitors of Other Pathways	E3L	*Orthopoxvirus*	Binds dsRNA, prevents PKR activation of IKK
	M2L	*Orthopoxvirus*	ER-resident; Prevents ERK phosphorylation
	B13R	*Orthopoxvirus*	Inhibits Caspase-1 and pro-IL-1β processing
	M013L	*Leporipoxvirus*	Prevent pro-IL-1β processing and positive feedback loop
	gp013L	*Leporipoxvirus*	

1.3 THE ENDOPLASMIC RETICULUM

1.3.1. The Structure of the ER. The endoplasmic reticulum (ER) is the largest organelle within the eukaryotic cell, comprising >10% of the cell volume (234). The ER forms an extensive network of cisternal sheets and tubules continuous with the nuclear membrane, all with a common lumenal space (Figure 1.7) (76, 234). It is a highly dynamic, multi-functional organelle typically associated with the secretory pathway. However, what makes the ER so unique is its ability to form subdomains within the vast network through enrichment of specific proteins (126). Each subdomain is characterized by a unique set of resident proteins and enzymes required for its particular function (126). Two of the most obvious subdomains are the rough ER (RER), which is visibly studded with ribosomes and mRNA on the cytosolic surface, and the smooth ER (SER), which lacks ribosomes (234). In general, the RER is characterized by a more sheet-like morphology, while the SER is more tubular (234). While the RER is typically found surrounding the nucleus, the SER forms important contacts with many other cellular organelles throughout the cytoplasm, including mitochondria, the golgi apparatus, peroxisomes, and even the plasma membrane (126). These contacts are crucial for the ER to successfully carry out its multi-faceted functions.

Another unique characteristic of the ER is its dynamic plasticity. The relative proportions of RER and SER can change according to the function of the cell (42). For example, when a B-cell is activated and develops into an antibody-producing plasma cell, protein synthesis becomes the dominant function and thus the RER takes over the cytoplasm. In contrast, a hepatocyte working to detoxify the blood of ethanol will expand the SER, which is enriched with detoxifying enzymes. ER tubules are capable of movement in the forms of elongation, retraction, tubule branching, branchpoint sliding, and membrane fusions (76). These movements are dependant on components of the cell cytoskeleton, including microtubules and actin, and utilize dynamin-like motor

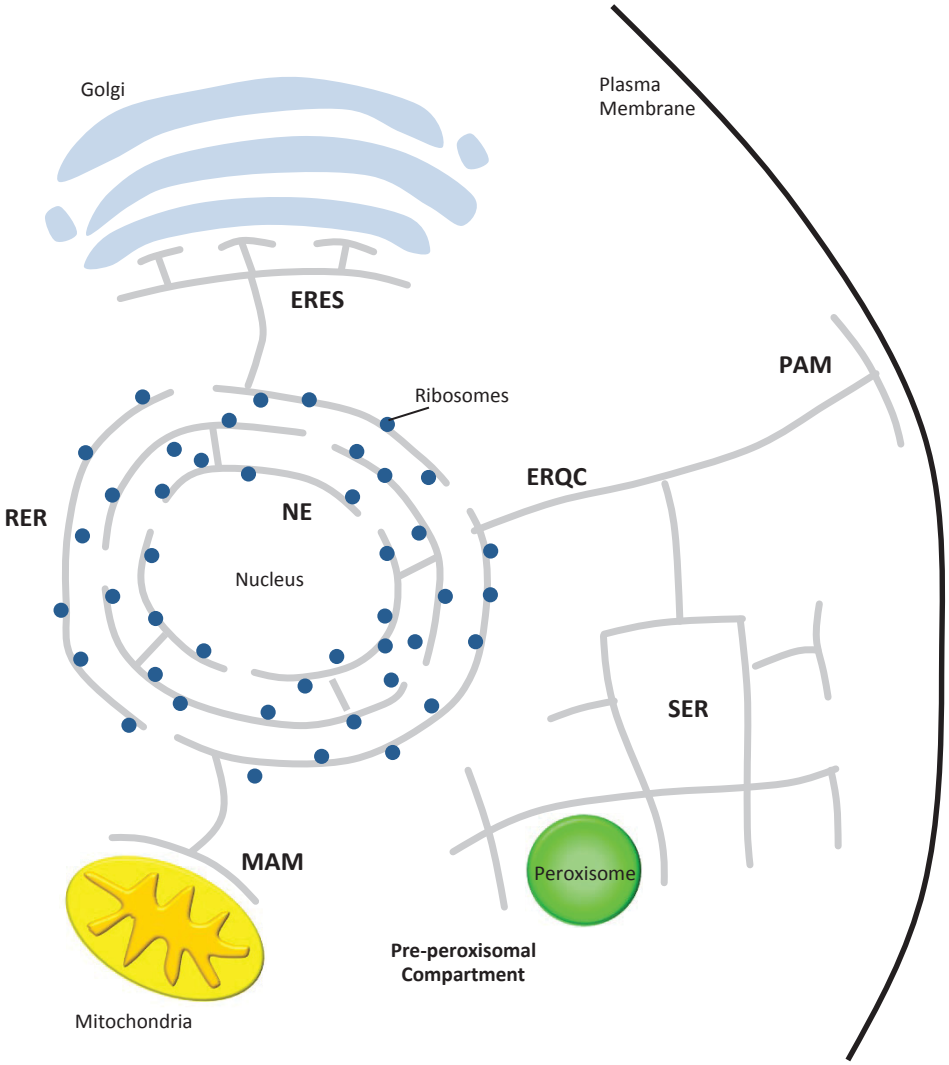

Figure 1.7 ER organization and subdomains. The ER is an extensive, tubular network continuous with the nuclear envelope (NE) that performs a diversity of functions. Sheet-like rough ER (RER) primarily surrounds the nucleus and is studded with ribosomes, while tubular smooth ER (SER) is found in the periphery making contacts with other organelles and consists of numerous subdomains. (ERES) ER exit sites; (PAM) plasma membrane-associated membrane; (ERQC) ER quality control; (MAM) mitochondria-associated membrane.

proteins for movement along microtubules (76). The conversion of ER shape from sheet-like RER to tubular SER requires the reticulon (RTN) and DP1/Yop1p protein family members (41, 59). These proteins contain two TMDs close together, allowing them to form a wedge-like structure that, when inserted in the outer leaflet of the membrane, induces positive curvature (41, 59). As such, these proteins are enriched in areas of high curvature and sharp edges. The ability of the ER to structurally adapt to the requirements of a cell lends itself to the variety of functions it can serve.

1.3.2. Functions of the Rough and Smooth ER. As indicated by the presence of ribosomes and translocation machinery on the RER, and the oxidizing conditions of the lumen, this subdomain's primary role is synthesis and folding of membrane and secretory proteins. The ER lumen is a highly proteinaceous environment (>100 mg/mL), much like the cytoplasm, which poses a challenge for protein folding (108). Though all of the information required for proteins to achieve their native conformations is intrinsic in the amino acid sequence, protein chaperones and foldases allow for more efficient folding (108). In the cytoplasm, members of the heat shock protein (HSP) family fulfill this role, while the ER lumen contains a unique set of chaperones, co-chaperones, and foldases. Chaperones exist as complexes, and different complexes aid folding of different proteins (108). For example, non-glycosylated proteins are often found bound to complexes containing BiP (binding immunoglobulin protein) and the co-chaperone Grp170, while glycosylated proteins are aided by calnexin (CNX) and calreticulin (CRT) in association with ERp57 (113, 149). In conjunction with folding enzymes, many of which are redox-active, chaperones bind to and release substrate proteins in an ATP-dependent manner until the appropriate conformation is achieved and disulfide bonds are formed by protein disulfide isomerase (PDI) (108, 242). Once the correct conformation is attained, folded proteins are released and allowed to exit the ER. If, after numerous cycles of chaperone binding and release, a protein is still misfolded, they are sensed and

targeted for ER-associated degradation (ERAD) (203, 233). These terminally misfolded proteins are retro-translocated to the cytoplasm where they are ubiquitinated and degraded by the 26S proteosome (233). In contrast, misfolded glycoproteins are extracted from the CNX/CRT cycle by α-mannosidase I cleavage of one mannose group, which is recognized by EDEM (ER degradation enhancer, mannosidase α) and targeted for degradation (157). This stringent process of quality control within the ER is crucial, as the ER is responsible for synthesis and release of about one third of all protein within a cell (108).

While the RER is primarily dedicated to protein synthesis, work on SER function has revealed that this subdomain can perform a variety of functions, and is highly cell-type specific (126). In general, the SER is enriched in proteins involved in detoxification, lipid synthesis and transfer, and calcium storage (126). The balance of these functions depends on the cell type: The SER would specialize in detoxification in hepatocytes in the presence of ethanol, while lipid synthesis/transfer proteins would predominate in sterol hormone-producing cells and calcium channel enrichment is crucial in skeletal muscle cells (in this case, the SER is called the sarcoplasmic reticulum or SAR). Also, the SER is responsible for ER contact with other cellular organelles (126). The mitochondria-associated membrane (MAM) is the best characterized of these contacts; not only is it responsible for extensive lipid exchange and synthesis between these two organelles, it also serves as an important calcium release site (78, 171). SER contact with the plasma membrane (PAM) is also important for calcium uptake from the extracellular environment, but also allows for trafficking of sterols to the plasma membrane and synthesis of important lipids such as phosphatidylserine (123, 165). The ER quality control (ERQC) domain is enriched in proteins involved in ERAD, as described earlier, while the ER exit sites (ERES) and ER-golgi intermediate compartment (ERGIC) are responsible for the ER to golgi trafficking of secretory proteins (208, 233). Intriguingly, regions of the SER

are also specialized for organelle biogenesis, including Russell bodies, peroxisomes, and lipid droplets (126).

1.3.3. The ER as a signalling organelle. Calcium signalling is a highly complex and fundamental cellular process that affects muscle contraction, cell growth and proliferation, neuronal excitation, and cell signalling (18). As the primary source of intracellular calcium, it is no surprise that the ER plays a fundamental role in calcium signalling (16). In a resting cell, the ER is constitutively pumping calcium from the cytoplasm into the ER lumen via sarco/endoplasmic reticulum calcium ATPase (SERCA) pumps to maintain a low concentration of calcium in the cytosol (16). Proteins within the ER bind and buffer calcium, thereby maintaining the high lumenal concentration (47, 140). In response to a diverse array of stimuli beyond the scope of this study, inositol-triphosphate (IP3) is generated as a secondary messenger that binds to IP3 receptors (IP3R) in the ER membrane (17). The IP3R is a calcium channel which releases stored calcium upon ligand binding (101). Released calcium can then bind and activate enzymes, cause synaptic release of neurotransmitters, and even potentiate pro-apoptotic signals (16).

The ER must also sense and adapt to accumulations of misfolded and unfolded proteins. This type of ER stress can be caused by aging, glucose deprivation, hypoxia, and even virus infection (36, 130). The unfolded protein response (UPR) is initiated, resulting in an initial adaptation phase followed by recovery or an alarm phase that ultimately leads to cell death (36). The three integral ER stress sensors include double-stranded RNA-activated protein kinase (PKR)-like ER kinase (PERK), activating transcription factor 6 (ATF6), and inisitol-requiring kinase 1 (IRE1) (36, 130). In the presence of hydrophobic regions of unfolded proteins, BiP dissociates from the lumenal domains of the three membrane sensors, allowing for their activation (19). In the case of PERK, BiP dissociation allows for homodimerization and auto-phosphorylation, thereby

activating the serine/threonine kinase activity (36). As the initial pathway activated in the UPR response, PERK phosphorylates eukaryotic initiation factor-2α (eIF2α), causing global attenuation of translation that ultimately reduces the protein folding load on the ER (84). PERK also upregulates the expression of ATF4, a transcription factor that upregulates largely pro-survival targets, however pro-apoptotic C/EBP homologous protein (CHOP) is also upregulated (127). Release of BiP from ATF6 exposes golgi signal sequences, and following translocation, the 50 kDa transcriptional domain of ATF6 is cleaved by dedicated proteases (36, 194). ATF6 increases ER chaperone expression and proteins involved in ERAD in order to increase the folding capacity and decrease the load of the ER (36). Finally, activation of IRE1 leads to dimerization and auto-phosphorylation, thereby activating the kinase and endoribonuclease activity of the protein (36). IRE1 splices the X-box binding protein-1 (XBP1) transcription factor to XBP1s, which also upregulates ER chaperones and ERAD proteins (246). However, IRE1 also upregulates many pro-apoptotic targets, such as CHOP (127). Extensive cross-talk, feedback loops, and regulation mechanisms have been observed among these three pathways (178). Cooperation among these three stress sensors is crucial in determining the fate of the cell in the face of ER stress.

1.3.4. Poxviruses and the ER. Involvement of the ER in the poxvirus life cycle has been studied extensively in the past, with recent findings suggesting a role for this organelle in at least two steps in particular. Electron micrograph and immunofluorescence images have shown that virion cores are transported along microtubules to associate with the cytoplasmic side of the ER (188). This is where virus factories form, and early gene expression and DNA replication occurs (146). Interestingly, viral DNA has been shown to associate with a number of viral factors that are associated with the ER, including I3 and E8 (188). I3 associates with the cytoplasmic side of the ER and binds ssDNA, while E8 is an ER integral protein which binds dsDNA (241). It is proposed that proteins E8 and A40 are responsible for recruiting ER membrane to the viral DNA, resulting in the

wrapping of the virus factory with RER which facilitates DNA replication (188). In the second step following replication, this RER membrane is dismantled and membrane crescents containing viral proteins begin to form. While it was previously believed that these crescent-shaped lipid membranes are synthesized *de novo*, a number of studies have shown that this membrane is actually derived from the SER and relies on viral proteins such as L2, A30.5, and A11 (132, 133, 174). Precisely how these membranes are recruited, how they acquire the viral proteins, and ultimately form the IV, are yet to be determined.

Poxviruses also encode a number of ER-resident immune evasion proteins that may or may not be involved in ER-specific processes. MYXV-M153 is an ER-resident ubiquitin ligase that targets MHC-I and T-cell CD4 co-receptor for lysosomal degradation (80). VACV-M2 is an integral protein responsible for inhibiting the ERK2 pathway of NFκB activation, a function that is contingent on ER localization (91). Also, though an exact function has yet to be ascribed to VACV-B7, initial studies done on this protein has demonstrated that B7 is an ER membrane-associated protein that contributes to virus virulence within the mouse model (166). Taken together, ER-resident poxviral proteins can play a diversity of functions that aren't necessarily involved in ER-related processes.

1.4 TAIL-ANCHORED FAMILY OF PROTEINS

Integral membrane proteins are found in all lipid bilayers of a cell, in all kingdoms of life, and serve a multitude of essential biological functions. One family of integral membrane proteins, the tail-anchored (TA) proteins, is no exception. TA proteins are characterized by an N-terminal cytoplasmic, functional domain and a single C-terminal TMD followed by a polar lumenal tail, typically no longer than 30 amino acids (25, 167). These proteins are found anchored to all lipid membranes within the cell. The location of their TMDs at the C-terminus of the protein poses a unique problem, which has lead to the discovery of another

pathway of membrane protein insertion (193). As with all integral proteins, TA proteins face the challenge of ensuring that their hydrophobic TMDs are efficiently translocated across their target membrane, while avoiding erroneous insertion into other permissive lipid bilayers (26).

1.4.1. Post-translational membrane targeting and insertion. The close proximity of the TMD to the C-terminus in both TA proteins and very small integral proteins means that this hydrophobic domain is not exposed until after ribosomal release (Figure 1.8A). Thus, membrane targeting and insertion occurs via a post-translational pathway that is distinct from the well-characterized co-translational pathway (Figure 1.8B) (26, 193). Studies done in both yeast and mammalian cells have lead to the discovery of 3 modes of biogenesis of ER-targeted TA proteins (167). A subset of TA proteins, including mammalian cytochrome b5, is capable of unassisted insertion into the ER membrane (28). Due to the fact that the TMD is not exposed until after ribosomal release, TA proteins make poor substrates for the ribosome-bound signal recognition particle (SRP) responsible for co-translational insertion (193). Several lines of investigation led to the discovery of an ATP-dependent mode of TA protein integration at the ER called the guided entry of TA proteins (GET) pathway in yeast, or TMD recognition complex of 40 kDa (TRC40) pathway in mammalian systems (Figure 1.8b) (26, 207). When the TMD of a TA protein is being synthesized, a pre-targeting complex is favourably recruited to the ribosome by as yet unknown signals (193). Protein Sgt2 binds and sequesters ER-targeted TMDs as the TMD is released, and through the Get4/Get5 subcomplex, transfers the substrate protein to the Get3 ATPase (193). Sgt2, Get3, Get4, and Get5 form what is called the TRC. Get3 and the substrate protein then dock at the Get1/Get2 ER-resident receptor, where substrate protein release and insertion is orchestrated in an ATP-hydrolysis dependent step of unknown mechanism (193). Thus, the pre-targeting complex efficiently recognizes ER-targeted TMDs and sequesters the hydrophobic domain in an

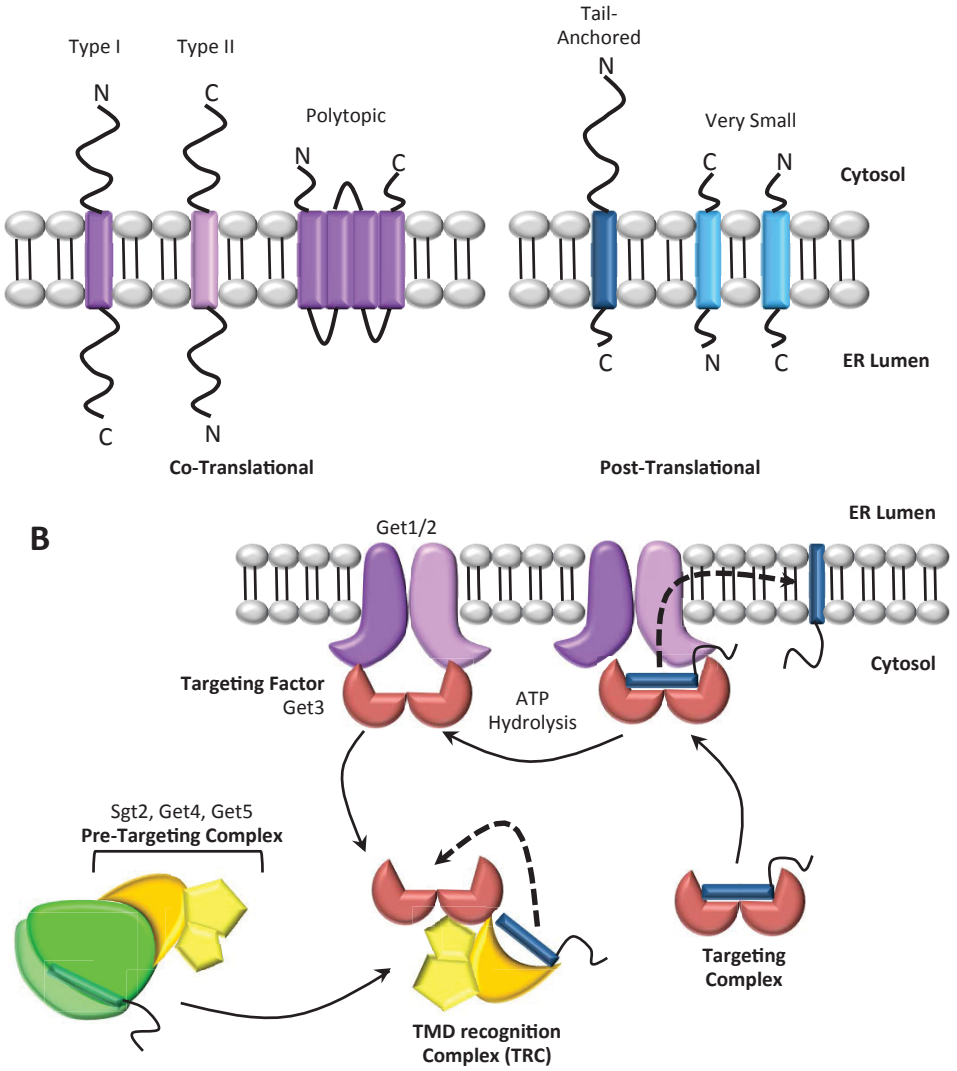

Figure 1.8 Biogenesis of tail-anchored membrane proteins. (a) Type I, II and polytopic integral membrane proteins are inserted in their target membranes co-translationally, while tail-anchored proteins and very small proteins are inserted post-translationally. **(b)** Post-translational insertion of tail-anchored proteins relies on cytoplasmic chaperones and membrane receptors. Pre-targeting complexes (Sgt2, Get4, Get5 in yeast) recognize ribosomes translating C-terminal TMDs, and bind the TMD immediately after ribosomal release. Formation of a TMD recognition complex (pre-targeting complex, substrate protein, Get3) allows transfer of the substrate protein to the targeting factor Get3 ATPase, thus forming the targeting complex. The targeting complex docks on ER membrane integral proteins Get1/2, allowing insertion of the substrate protein into the ER membrane. ATP hydrolysis allows release of Get3 and continued cycling. Adapted from 193.

insertion-competent form, allowing Get3 to target and insert the protein at the ER (193).

TA proteins targeted to the ER, OMM, peroxisome, and chloroplast outer envelope (COE) in plant cells are capable of direct insertion following translation (25). In contrast, organelles downstream of the ER in the secretory pathway acquire TA proteins from the ER via vesicular transport, as they have a higher cholesterol content which is not amenable to direct protein insertion (25, 229). Precisely how different TA proteins are targeted to the appropriate membrane is not fully understood, however a few generalities have been observed. In particular, the hydrophobicity of the TMD and the presence of flanking charges affects which insertion pathway is used and which membrane is targeted (25, 26, 167). Unassisted insertion is attributed to proteins with TMDs of low to moderate hydrophobicity; *in vitro* studies suggest that the Hsc70 ATPase and Hsp40 co-chaperone maintain these proteins in insertion-competent forms and target them to the appropriate site, where they can insert unassisted (167, 168). TMDs of moderate to high hydrophobicities rely on the TRC40 pathway, especially in the case of ER-targeted proteins (167). The ER is the most permissive of intracellular membranes, accommodating TMDs of varying hydrophobicity, length, flanking charges, and polar tail lengths (167). In contrast, OMM-targeted TMDs tend to exhibit moderate hydrophobicity and flanking positive charges (93). There must be additional subtle features, however, as a number of ER-targeted TMDs exhibit these same features (25). Peroxisome TA proteins can be targeted by ER transit, but also through dedicated chaperone Pex26 and receptor Pex19 (83). Peroxisome TMDs are very similar to OMM TMDs, however the presence of signal sequences overrule the potential OMM-localization (26).

At present, our knowledge of the different TA protein biogenesis pathways can explain how these proteins are able to achieve the correct

localization while avoiding insertion into aberrant, permissive membranes along the way (26). Chaperone binding immediately following ribosome release ensures these proteins do not form aggregates within the cytoplasm, and function as targeting proteins in many cases. The complexity and redundancy in TA protein targeting and insertion pathways lends itself to perhaps additional modes of regulation and modulation (167). The importance of TA protein members in lipid homeostasis, intracellular trafficking, protein translocation, and even organelle structure supports the existence of multiple pathways for accurate insertion (193).

1.5 THESIS RATIONALE

In the past, our lab has focused on characterizing strategies used by poxviruses to subvert host immune responses, specifically the apoptotic pathway and the NFκB pathway (69, 209). Early studies suggested that VACV encodes an anti-apoptotic protein that localizes to the mitochondria (239). In search of this anti-apoptotic protein, our lab performed a screen of the VACV genome for proteins with putative TMDs, among which we found the anti-apoptotic protein F1, but also a number of other proteins, including B6. B6 is comprised of 173 amino acids, with a putative TMD at the C-terminus. The gene is located within the B region, which is within the 3' terminus of the VACV genome. Of the many characterized genes encoded within this region, the majority have been shown to perform immune evasion functions. Thus, this work focuses on characterizing B6 and the role it plays during virus infection. We hypothesized that B6 is a TA protein that localizes to the ER, where it plays an immunomodulatory role.

Specific Aims:

1. To assess when and where B6 is expressed during transient transfection and virus infection.
2. To test the role of B6 in modulating the immune pathways most targeted by poxviruses.

Chapter 2

Materials and Methods

2.1 Cell Lines

All cell lines used in this study are listed in table 2-1. Human fibroblast (HeLa), human embryonic kidney (HEK) 293T, baby green monkey kidney (BGMK), African green monkey kidney (CV-1), and HuTK$^{-/-}$-143B cells were all obtained from the American Type Culture Collection (ATCC) and maintained at 37°C and 5% CO_2. HeLa, HEK 293T, CV-1 and HuTK$^{-/-}$-143B cells were cultured in Dulbecco's modified Eagle's Medium (DMEM; Invitrogen) supplemented with 10% heat-inactivated foetal bovine serum (HI-FBS; Invitrogen), 50 U/mL penicillin, 50 µg/mL streptomycin, and 200 µM $_L$-glutamine (Invitrogen). HuTK$^{-/-}$ -143B cell media also contained 25 µg/mL 5-bromo-2'-deoxyuridine (BrdU; Sigma-Aldrich). BGMK cells were cultured in DMEM supplemented with 10% newborn calf serum (NCS; Invitrogen), 50 U/mL penicillin, 50 µg/mL streptomycin, and 200 µM $_L$-glutamine.

2.2 DNA Methodology

2.2.1 Polymerase Chain Reaction. Polymerase chain reactions (PCR) were carried out in 50 µl volumes containing 60 mM Tris-SO_4, 20 mM $(NH_4)_2SO_4$, 2 mM $MgSO_4$, 3% glycerol, 0.06% NP-40, and 0.05% Tween-20 (pH 9.0 at 25°C). Each reaction contained 1 pmole of each primer, 10 mM deoxyribonucleotide triphosphates (dNTPs; Invitrogen), 2.5 units (U) of LongAmp Taq DNA polymerase (New England Biolabs), and either 10 nanograms (ng) of plasmid DNA or 100 ng of viral DNA template. All primers used in this study are listed in table 2-2. Temperature cycles were performed with a C1000 thermal cycler (BioRad) using the following parameters: Initial denaturation for 2 minutes at 95°C followed by 30 cycles of denaturation at 95°C for 30 seconds, primer annealing at 55°C for 30 seconds, and primer elongation at 65°C for 1 minute/kilobase (kb). Alternatively, PCR reactions were done in 50µl volumes containing 200 mM Tris-HCl pH 8.4, 500 mM KCl, 50 mM MgCl, 1 pmole each primer, 10 mM dNTPs, 10 ng template

Table 2-1 Cells and viruses used in this study.

Cell Line	Cell Type	Characteristics	Source*
HEK 293T	Human Embryonic Kidney		ATCC
HeLa	Human Fibroblast		ATCC
BGMK	Baby Green Monkey Kidney		ATCC
CV-1	Monkey Kidney Fibroblast		ATCC
HuTK$^{-/-}$-143B	Human 143B Osterosarcoma	Deficient in Thymidine Kinase	ATCC
Viruses	**Strain**	**Characteristics**	**Source**
VACV	Copenhagen		G. McFadden
VACV-EGFP	Copenhagen	Expresses EGFP in place of TK	G. McFadden
VACV-EGFP-B6R	Copenhagen	Expresses EGFP-B6R in place of TK; Endogenous B6R	This study
VACVΔB6R-EGFP	Copenhagen	Expresses EGFP in place of B6R	This study
ECTV	Moscow		M. Buller

* American Type Culture Collection

DNA, and 2.5 U of Taq DNA polymerase (Invitrogen). Temperature cycles were performed as described above, except that elongations were performed at 72°C.

2.2.2 Agarose Gel Electrophoresis. DNA products of PCR and endonuclease digestion (see 2.2.7) were purified and isolated by agarose gel electrophoresis followed by gel extraction. DNA was suspended in a sample loading dye containing 30% glycerol (Fischer Scientific) and 0.25% bromophenol blue (BioRad). DNA products were separated by gel electrophoresis in gels made of 1% weight per volume (w/v) UltraPure Agarose (Invitrogen) in 1X TAE buffer (40 mM Tris, 20 mM acetic acid, and 1 mM ethylenediaminetetraacetic acid (EDTA)). To visualize DNA bands, SYBR Safe DNA gel stain (Invitrogen) was added to the agarose gels at a 1:100 dilution. Electrophoresis was performed in 1X TAE running buffer in a Mini-Sub Cell GT (BioRad) at 100V. DNA bands were visualized using a Gel Doc EZ Imager (BioRad). Bands of interest were excised and subjected to gel extraction as described in 2.2.3.

2.2.3 Gel Extraction. Gel extraction was performed using a QIAquick gel extraction kit (Qiagen) according to the manufacturer's protocol. In brief, excised DNA bands were suspended in 3 volumes of solubilization buffer per 1 volume of gel (300 µl per 100 mg) and incubated at 50°C for 10 minutes. One gel volume of isopropanol was added and run on a QIAquick DNA column followed by an ethanol wash. Bound DNA was eluted in 30 µl of 10 mM Tris-HCl (pH 8.5). Purity of the extracted DNA was assessed by agarose gel electrophoresis.

2.2.4 DNA Ligation. For ligation into pGEM-T (Promega), PCR was done using LongAmp Taq DNA polymerase to add a single deoxyadenosine to the 3'-end of the fragments. T-A cloning was done in 20 µl reactions containing 2 µl of gel extracted DNA, 50 ng of pGEM-T vector, 3 U of T4 DNA ligase, and 5µl of 2X rapid ligation buffer containing 60mM Tris-HCl (pH 7.8), 20mM $MgCl_2$, 20mM dithiothreitol (DTT), 2mM ATP, and 10% polyethylene glycol. Ligation reactions were incubated at 4°C overnight. For ligation into pCDNA3, pSPUTK, and pSC66,

reactions were done in 20µl volumes containing 4 U T4 DNA ligase (New England Biolabs), 50 mM Tris-HCl (pH 7.5), 10 mM $MgCl_2$, 1 mM ATP, and 10 mM DTT. Vector to insert ratios of 1:3, 1:6 and 1:9 were done and reactions were incubated at 16°C overnight. Ligations were transformed into competent E. coli cells as described in 2.2.5.

2.2.5 Bacterial Transformation. Competent E. coli DH5α cells (Invitrogen) were transformed with ligation reactions using a heat shock method. Fifty µl of competent DH5α cells were incubated with 5 µl of ligation reactions on ice for 30 minutes followed by heat shock at 42°C for 1 minute and a 2 minute recovery on ice. Two hundred fifty µl of SOC media containing 20 mg/mL tryptone, 5 mg/mL yeast extract, 0.5 mg/mL NaCl, and 2.5 mM KCl (pH 7.0) was added and incubated at 37°C for 1 hour. Transformed bacteria were plated on Luria-Bertani (LB) agar plates supplemented with the appropriate antibiotic, either 100 µg/mL ampicillin (Sigma-Aldrich) or 30 µg/mL kanamycin (Sigma-Aldrich). E. coli transformed with pGEM-T plasmids were plated on LB agar plates containing 100 µg/mL ampicillin, 80 µg/mL 5-bromo-4-chloro-3-indolyl-β-D-galactopyranoside (X-gal; Rose Scientific) and 0.5 mM isopropyl β-D-1-thiogalactopyranoside (IPTG; Rose Scientific) to allow for blue/white screening of recombinants.

2.2.6 Plasmid DNA Isolation. Plasmids to be used for cloning were isolated and prepared using the alkaline lysis with SDS minipreparation method (182). E. coli were grown overnight in 5 mL of LB broth containing the appropriate antibiotic (100 µg/mL ampicilin or 60 µg/mL kanamycin) and 2.5 mL were collected and pelleted. The bacterial cells were re-suspended in 100 µl of buffer containing 50 mM glucose, 25 mM Tris (pH 8.0), and 10 µM EDTA (Sigma-Aldrich) followed by lysis in 200 µl of buffer containing 10 mM NaOH and 1% sodium dodecyl sulfate (SDS; Fischer Scientific). Proteins and membranes were precipitated on ice in 150 µl of buffer containing 3M KCH_3COO and 11.5% glacial acetic acid. Following centrifugation (18,000 ×g for 15 minutes), supernatants were collected and 1

volume of equal parts phenol:chloroform were added and centrifuged (18,000 × g for 10 minutes). The aqueous layer was again washed with 1 volume of chloroform. DNA was precipitated in 2.5 volumes of 95% ethanol at -20°C for 1 hour, and pelleted by centrifugation at 18,000 × g for 15 minutes. DNA pellets were typically re-suspended in 30 µl of double distilled (dd)H_20.

To prepare plasmids used for expression in mammalian cells or sequencing, 200 mL of LB broth containing the appropriate antibiotic (100 mg/mL ampicillin or 60 mg/mL kanamycin) was inoculated with E.coli DH5α cells containing the desired plasmid and incubated overnight at 37°C. For low copy plasmids, such as pSC66, cultures were incubated for 8 hours followed by treatment with 170 mg/mL chloramphenicol (Sigma-Aldrich) for another 18 hours. Plasmid DNA was prepared using a Plasmid MaxiPrep kit (Qiagen) according to the manufacturer's protocol. DNA yields and optical densities at 280 nm were determined using a NanoVue Plus spectrophotometer (GE Healthcare).

2.2.7 Endonuclease Digestion. Endonuclease digestions were typically done in 20 µl volumes containing the appropriate buffers, 1 U of enzyme per 1 µg of DNA to be digested, and 10 µg of RNAse (Sigma-Aldrich). Reactions were allowed to incubate at 37°C for 1 hour. In most cases, restriction enzymes were heat-inactivated at 65°C for 20 minutes.

2.2.8 DNA Sequencing and Computer Analysis. Sanger sequencing was performed by either The Applied Genomics Centre (TAGC) in the Faculty of Medicine or the Molecular Biology Service Unit in the department of Biological Sciences, both at the University of Alberta. DNA sequence analyses were performed using the Basic Local Alignment Search Tool (BLAST) provided by the National Centre for Biotechnology Information (NCBI) (5).

2.3 Cloning

2.3.1 Plasmids. All plasmids used in this study are listed in Table 2-3. All T-A cloning was done in the pGEM-T vector (Promega), and the pEGFP-C3 vector (Clonetech) was used to generate all N-terminal enhanced green fluorescent protein (EGFP)-tagged proteins. pEGFP-B6R(1-173), pEGFP-B6R(1-142), and pEGFP-B6R(143-173) were generated previously (S. Wasilenko, unpublished). pCDNA3 was obtained from Invitrogen; pSC66, which contains a synthetic poxviral early/late promoter (pE/L), was provided by Dr. E. Long (National Institute of Allergy and Infectious Disease, Bethesda, MB) (37, 62) and pSPUTK was obtained from Dr. D. Andrews (Sunnybrook Research Institute, Toronto, ON). The pSC66-EGFP-B6R and pSPUTK-B6R vectors were generated previously (unpublished).

2.3.2 Generation of pSC66-FLAG-B6R(1-173) and pSC66-FLAG-B6R(1-142). FLAG-B6R(1-173) and FLAG-B6R(1-142) were generated from VACV genomic DNA as a template using FLAG-B6R *Sal*I forward primer along with the B6R *Not*I or B6R(1-142) *Not*I reverse primer, respectively. The PCR products were ligated into pGEM-T and sub-cloned into pSC66 as *Sal*I/*Not*I fragments to place them under the control of a synthetic poxviral early/late promoter (37, 62).

2.3.3 Generation of pCDNA3-FLAG-B6R(1-173). B6R(1-173) was generated from VACV genomic DNA as a template using FLAG-B6R *Bam*HI forward primer and B6R *Eco*RI reverse primer. The PCR product was ligated into pGEM-T followed by sub-cloning into the pCDNA3 vector as a *Bam*HI/*Eco*RI fragment.

2.3.4 Generation of pSPUTK-B6R(1-142). B6R(1-142) was generated from VACV genomic DNA as a template using primers B6R(1-142) TNT *Eco*RI forward primer and B6R(1-142) TNT BamHI reverse primer. The PCR product was ligated into p-GEM-T and sub-cloned into pSPUTK as an EcoRI/NcoI fragment such that B6R(1-142) was under the control of an SP6 promoter with an intact Kozak consensus

Table 2-2 Plasmids used in this study.

Plasmid	Characteristics	Source
pGEM-T	TA cloning vector; CMV promoter	Promega
pEGFP-C3	Empty EGFP vector with a CMV promoter	Clontech
pEGFP-B6R (1-173)	Full length B6R	S.Wasilenko
pEGFP-B6R (1-142)	B6R lacking the C-terminal transmembrane domain	S.Wasilenko
pEGFP-B6R (143-173)	B6R transmembrane domain only	S.Wasilenko
pSC66	Synthetic poxviral early/late promoter; VACV thymidine kinase sequence flanks LacZ and promoter, and multiple cloning site; Used to generate VACV recombinants	Dr. E. Long (37, 62)
pSC66-EGFP-B6R (1-173)	EGFP-B6R full length	S.Wasilenko
pSC66-FLAG-B6R (1-173)	FLAG-B6R full length	This study
pSC66-FLAG-B6R (1-142)	FLAG-B6R lacking the C-terminal transmembrane domain	This study
pSPUTK	*In vitro* transcription-translation vector; Kozak consensus sequence and SP6 promoter	D. Andrews
pSPUTK-B6R (1-173)	Full length B6R	T. Stewart
pSPUTK-B6R (1-142)	B6R lacking the C-terminal transmembrane domain	This study
pSPUTK-Bcl2-Cyb5	Bcl-2 with the endogenous transmembrane domain replaced with the mammalian Cyb5 transmembrane domain	T. Stewart
pJMT30	Contains EGFP under control of a synthetic poxviral early/late promoter flanked by *Bgl*II cut sites (37)	Taylor, J
pGEM-T-VACVΔB6R-EGFP	Knockout plasmid; Contains EGFP under control of a synthetic poxviral early/late promoter flanked by homologous regions to VACV-B6R	This study

sequence (111). This generated the construct pSPUTK-B6R(1-142) TNT used in the *in vitro* transcription-translation assay described in 2.7.9.

2.3.5 VACVΔB6R-EGFP Knockout Plasmid Generation. To create a VACV devoid of B6R, we replaced ~90% of the ORF with EGFP fluorescent protein under control of a synthetic poxviral early/late promoter (pE/L-EGFP) (37, 237). The knockout plasmid used to generate VACVΔB6R-EGFP was made in the pGEM-T vector (Figure 2.1). To begin, VACV genomic DNA was used as a template to amplify a 356 base pair (bp) homologous region upstream of B6R (Fragment 1, F1) and a 410 bp homologous region downstream of B6R (Fragment 2, F2) using the following primer pairs: B6RkoF1 and B6RkoR1 *Bgl*II to generate F1, and B6RkoF2 *Bgl*II and B6RkoR2 to generate F2. Each fragment contains a *Bgl*II restriction site and a 6 bp complementary linker sequence to allow for overlap PCR. After purifying the DNA fragments by agarose gel electrophoresis and gel extraction, 10 ng of each fragment was used as template for overlap PCR using the B6RkoF1 and B6RkoR2 primers, generating a 772 bp fragment comprised of F1 and F2 separated by a *Bgl*II cut site. This construct was T-A cloned into pGEM-T and designated pGEM-T-VACVΔB6R1-2. A plasmid was previously generated in pGEM-T which contains EGFP under a pE/L promoter (pE/L-EGFP) flanked by *Bgl*II cut sites (pJMT30, Dr. J. Taylor). Both pJMT30 and pGEM-T-VACVΔB6R1-2 were digested with *Bgl*II and separated by agarose gel electrophoresis; the linearized VACVΔB6R1-2 backbone was gel extracted along with the pE/L-EGFP fragment. The two products were ligated together overnight as described in 2.2.4, allowing the pE/L-EGFP fragment to insert between F1 and F2 of the backbone. Successful ligations were chosen based on the excision of an 800 bp fragment (pE/L-EGFP) and a PCR product of 1568 bp when using the B6RkoF1 and B6RkoR2 primers. The resulting plasmid was designated pGEMT-VACVΔB6R-EGFP.

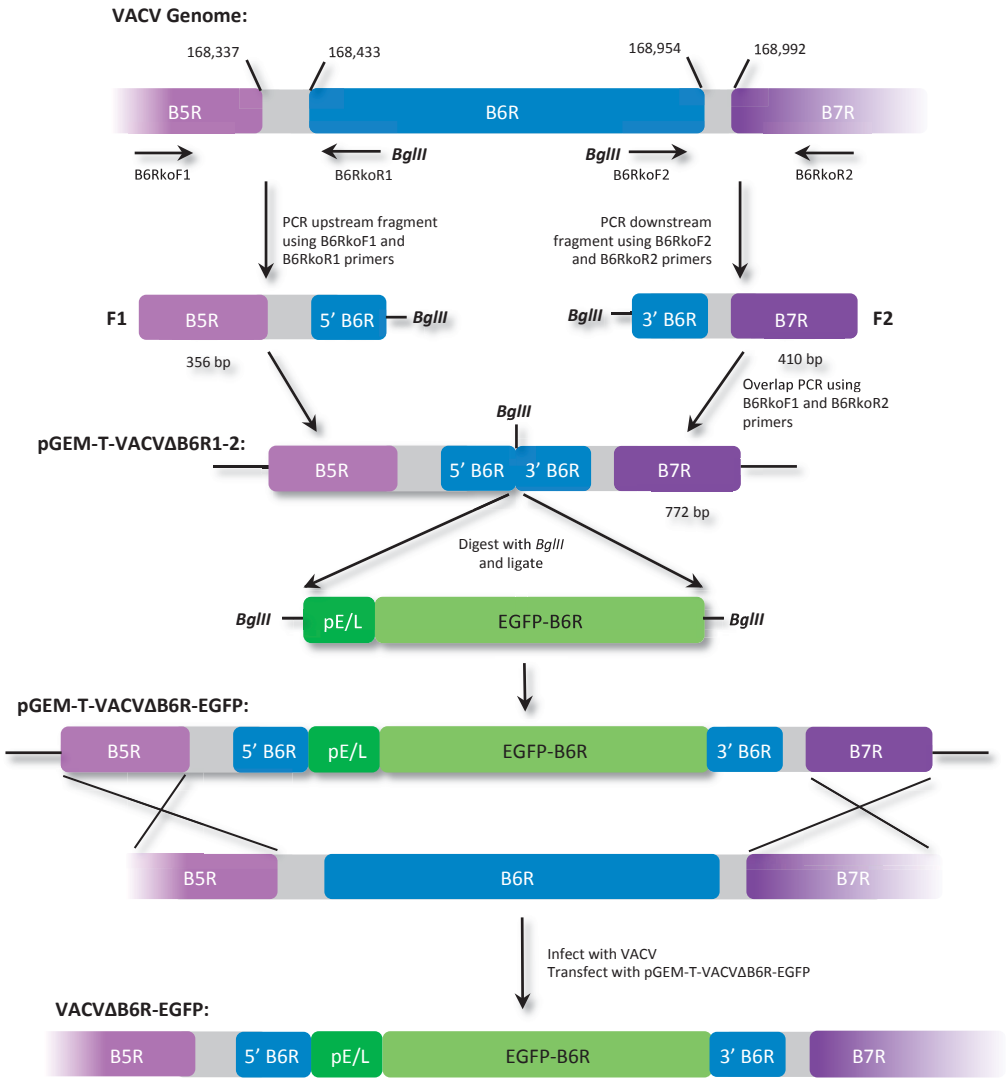

Figure 2.1 Knockout virus generation. To generate the knockout plasmid pGEM-T-VACVΔB6R-EGFP, PCR amplification of homologous fragments 1 and 2 (F1 and F2) upstream and downstream of B6R, respectively, followed by overlap PCR to generate a 772 bp product with fragment 1 and fragment 2 separated by a *Bgl*II cut site (pGEM-T-VACVΔB6R1-2). pGEM-T-VACVΔB6R1-2 and pJMT30 were digested with *Bgl*II to linearize the backbone and excise EGFP fluorescing protein under control of a synthetic poxviral early/late promoter (pE/L), followed by ligation to generate pGEM-T-VACVΔB6R-EGFP knockout plasmid. BGMK cells simultaneously infected with VACV and transfected with pGEM-T-VACVΔB6R-EGFP could undergo homologous recombination, resulting in a knockout VACV devoid of 90% of the B6R ORF that constitutively expresses EGFP.

Table 2-3 Oligonucleotides used in this study.

Primer Name	Primer Sequence (5' – 3')	Rest. Site	Description	Source
B6RkoF1	CCCGACGATGAGACAGATTTGAGC	N/A	Used to generate VACVΔB6R	This study
B6RkoR1 BglII	CGTGCCAGATCTGCCTGAGTAAAAATGCTCTAACCGC	*Bgl*II	Used to generate VACVΔB6R	This study
B6RkoF2 BglII	TCAGGCAGATCTGGCACGATCGCTGGAGGTG	*Bgl*II	Used to generate VACVΔB6R	This study
B6RkoR2	CTACACGTGTGACCTCTGCGTTG	N/A	Used to generate VACVΔB6R	This study
FLAG-B6R BamHI For	GGATCCATG**GACTACAAAGACGATGACGACAAG**CTTCTTCAGTGG	*Bam*HI	Used to generate FLAG-B6R in pCDNA3	This study
B6R EcoRI Rev	GAATTCTTATTTATACAAACTAACTAGATGC	*Eco*RI	Used to generate FLAG-B6R in pCDNA3	This study
B6R(1-142) TNT EcoRI For	GAATTCACCATGGCCATGTCTTCTTCAGTGGAT	*Eco*RI	Used to generate B6R(1-142) in pSPUTK for TNT assay	This study
B6R(1-142) TNT BamHI Rev	GGATCCTTAGTTAATCATATTTCTACG	*Bam*HI	Used to generate B6R(1-142) in pSPUTK for TNT assay	This study
FLAG-B6R SalI For	GTCGACATG**GACTACAAAGACGATGACGACAAG**TCTTCTTCAGTGG	*Sal*I	Used to generate FLAG-B6R in pSC66	This study
B6R NotI Rev	GCGGCCGCTTATTTATACAAACTAACTAGATGC	*Not*I	Used to generate FLAG-B6R in pSC66	This study
FLAG-B6R (143-173) SalI For	GTCGACATG**GACTACAAAGACGATGACGACAAG**AAGTTGTACGGATACGC	*Sal*I	Used to generate FLAG-B6R (143-173) in pSC66	This study
B6R(1-142) NotI Rev	GCGGCCGCTTAGTTAATCATATTTCTACGGATGTATATACCATCGTCG	*Not*I	Used to generate FLAG-B6R (1-142) in pSC66	This study
ECTV161 RTPCR For	GTTTTTCGATTACAATAAAAATAATTCC	N/A	Used for reverse transcription PCR of ECTV-161	This study
ECTV161 RTPCR Rev	TTATTTATACAAACTAACTAGATGCATC	N/A	Used for reverse transcription PCR of ECTV-161	This study
ECTV004 RTPCR For	GTTTAATATCATGAACTGCGACTATCT	N/A	Used for reverse transcription PCR of ECTV-004	Burles, K
ECTV004 RTPCR Rev	TTAATAATACCTAGAAAATATTCCACGAGC	N/A	Used for reverse transcription PCR of ECTV-004	Burles, K
ECTV058 RTPCR For	GAATTCATGGTGGATGCTATAACC	N/A	Used for reverse transcription PCR of ECTV-058	Burles, K
ECTV058 RTPCR Rev	GGATCCACTTTTCATTAATAGGGA	N/A	Used for reverse transcription PCR of ECTV-058	Burles, K
GAPDH RTPCR For	AGCCTTCTCCATGGTGGTGAAGAC	N/A	Used for reverse transcription PCR of GAPDH	Banadyga, L
GAPDH RTPCR Rev	CGGAGTCAACGGATTTGGTCG	N/A	Used for reverse transcription PCR of GAPDH	Banadyga, L

Restriction cut sites are underlined, FLAG sequences are bolded, Rest. – Restriction, For – Forward, Rev – Reverse, N/A – not applicable

2.4 Transfections

2.4.1 General Transfection Protocol. Transfection of 1×10^6 HeLa or 293T cells was accomplished using Lipofectamine 2000 (Invitrogen) according to the manufacturer's specifications. Five µl of Lipofectamine reagent and 0.5-2.5 µg of plasmid DNA were added to separate 500 µl aliquots of OptiMEM (Invitrogen) and incubated for 5 minutes. Lipid and DNA suspensions were gently mixed together and allowed to incubate for another 15 minutes. Following incubation, the DNA-lipid mixture was added to cell monolayers along with another 0.5 mL of OptiMEM for a total of 1 mL. Transfections were incubated at 37°C and 5% CO_2 for 2 hours followed by supplementation with recovery media containing 20% HI-FBS and 2 mM $_L$-glutamine. The cells were incubated at 37°C and 5% CO_2 for an additional 12-16 hours.

2.4.2 General Infection/Transfection Protocol. Twelve hour infection/transfections were performed to express proteins from pSC66 in the context of VACV infection. HeLa cells were infected in 500 µl to 5 mL of OptiMEM with the appropriate virus at a multiplicity of infection (MOI) of 5, rocking every 10 minutes for 1 hour. During this time, 2-5 µg of plasmid DNA and 5-25 µl of Lipofectamine 2000 were incubated in 500 µl to 5 mL of OptiMEM, as described in 2.4.1. Following the 1 hour infection, cells were washed with OptiMEM and the DNA-Lipid mixture was added to the cell monolayer. After 2 hours at 37°C and 5% CO_2, an equal volume of recovery media was added to the existing transfection media, and the cells were maintained at 37°C and 5% CO_2 for another 10 hours.

2.5 Virus Generation and Manipulation.

2.5.1 Viruses. Vaccinia virus strain Copenhagen (VACV) and VACV expressing the EGFP fluorescent protein in place of thymidine kinase (TK) (VACV-EGFP) were kindly provided by Dr. G. McFadden (University of Florida, Gainsville, FL). Ectromelia virus strain Moscow was a gift from Dr. M. Buller (University of St.

Louis, US). A list of all viruses used in this study can be found in Table 2-1. All viruses were stored at -80°C.

2.5.2 General Virus Infection Protocol. Typically, virus stocks were thawed at 37°C and sonicated using a Sonic Dismembrator (Misonix Inc.) for 20 seconds at 0.5 second pulses (on/off cycle) prior to use. To infect cell monolayers in 6-well plates or 12-well plates with 18mm coverslips, 500 µl of appropriate culture media containing the appropriate virus at the indicated MOI was added. The plates were incubated at 37°C and 5% CO_2 for 1 hour with gentle rocking every 10 minutes to allow for virus attachment to cells. An additional 1 mL of culture media was then added for a total of 2 mL. For cell monolayers in 10 cm dishes, 5 mL of culture media containing virus was added to the dishes, incubated at 37°C and 5% CO_2 for 1 hour with gentle rocking every 10 minutes, followed by the addition of 5 mL of cell culture media. Infections were allowed to progress for the indicated amounts of time at 37°C and 5% CO_2.

2.5.3 Generation of VACVΔB6R-EGFP. Removal of the B6R open reading frame (ORF) from VACV was done by replacing it with the EGFP fluorescing protein via homologous recombination (Figure 2.1). BGMK cells (8×10^5) were infected with VACV at an MOI of 0.05 in 500 µl of OptiMEM for 1 hour as described in 2.5.2. During this time, 10 µg of pGEM-T-VACVΔB6R-EGFP (see 2.3.5) and 10 µl of Lipofectamine 2000 were mixed in 200 µl of OptiMEM as described in 2.4.2. The pGEM-T-VACVΔB6R-EGFP plasmid contains EGFP under the control of a synthetic poxviral early/late promoter (pE/L-EGFP) flanked by upstream and downstream regions of homology to VACV-B6R. After one hour, the infection media was removed and replaced with 800 µl of OptiMEM along with the 200 µl DNA-lipid mixture and incubated (37°C and 5% CO_2) for another 5 hours. One mL of recovery media containing 20% NCS and 2 mM $_L$-glucosamine was subsequently added, followed by another 24 hours of incubation. Cells that are both infected and transfected may undergo a double-crossover event within the regions of

homology upstream and downstream of VACV-B6R, thus inserting pE/L-EGFP in place of the B6R ORF within the VACV genome (Figure 2.2). The cells were harvested in standard saline citrate (SSC; 150 mM NaCl, 15 mM tri-sodium citrate), centrifuged at 1000 ×g, and re-suspended in 100 µl of ice-cold swelling buffer (10 mM Tris, pH 8.0, 2 mM $MgCl_2$).

Successful knockout viruses were screened based on the presence of EGFP, as indicated by a green fluorescing plaque. The infected-transfected cells were titered out by serial dilution on BGMK cells, followed by 12-24 hours of infection. Green plaques were visualized under the FITC filter of a fluorescent microscope (Leica) and picked as described in 2.5.5. After 8 rounds of purification, VACVΔB6R-EGFP was amplified on BGMK cells and the absence of B6R was confirmed by PCR analysis of viral genomic DNA (see 2.5.8) using primers B6RkoF1 and B6RkoR2.

2.5.4 Generation of VACV-EGFP-B6R. Recombinant virus VACV-EGFP-B6R that expresses EGFP-B6R in addition to endogenous B6R was generated by homologous recombination into the TK locus (62). BGMK cells were infected with VACV and simultaneously transfected with pSC66-EGFP-B6R. The pSC66 plasmid contains both a *LacZ* gene and EGFP-B6R under control of poxviral promoters flanked by regions of homology to the VACV TK locus (Figure 2.2). Cells that become both infected and transfected may undergo a double-crossover event between the VACV TK locus and flanking regions of homology in pSC66, resulting in a TK negative virus that expresses both EGFP-B6R and β-galactosidase (Figure 2.2). Briefly, BGMK cells (8×10^5) were infected with VACV at an MOI of 0.05 in 500 µl of OptiMEM for 1 hour (see 2.5.2). During this time, 10 µg of pSC66-EGFP-B6R was mixed with 10 µl of Lipofectamine 2000 in 200 µl of OptiMEM as described in 2.4.2. After one hour, the infection media was removed and replaced with 800 µl of OptiMEM along with the 200 µl DNA-Lipid mixture, then allowed to incubate at 37°C and 5% CO_2 for 5 hours. The cells were then

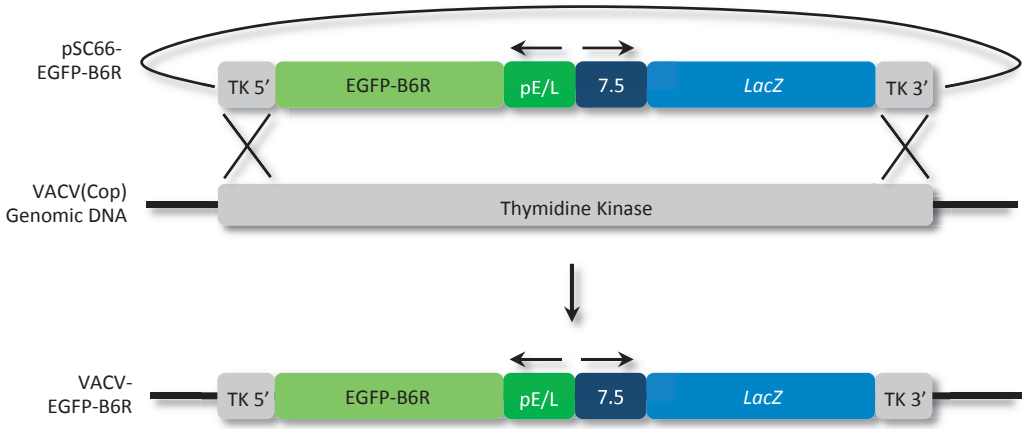

Figure 2.2 Recombinant virus generation. To generate VACV-EGFP-B6R, cells were infected with VACV and simultaneously transfected with the pSC66-EGFP-B6R plasmid. This plasmid contains the *LacZ* gene under a 7.5 poxviral promoter and the gene of interest (EGFP-B6R) under control of a synthetic poxviral early/late promoter (pE/L), both flanked by 5' and 3' regions of homology to the VACV thymidine kinase locus. Cells that are infected and transfected can undergo homologous recombination, resulting in a recombinant virus expressing EGFP-B6R, β-galactosidase, and lacking a functional thymidine kinase.

supplemented with 1 mL of recovery media and incubated for another 24 hours. Cells were harvested in SSC, centrifuged at 1000 ×g, and re-suspended in 100 µl of ice-cold swelling buffer.

Recombinant viruses were selected by titering out serial dilutions on BGMK cells. Twenty-four hours post-infection, cell monolayers were overlaid in the presence of X-gal for 12-16 hours to visualize β-galactosidase-positive viruses indicated by a blue plaque (see 2.5.5). After 4 to 5 purifying rounds in BGMKs as just described, the same screening process was executed in HuTK$^{-/-}$-143B in the presence of 25 µg/mL BrdU. Any virus with an intact TK gene will be unable to grow in the presence of BrdU. Purified viruses were subsequently amplified in BGMK cells and expression of EGFP-B6R was confirmed by western blotting.

2.5.5 Purification of Virus. For selection of recombinant VACV-EGFP-B6R, cell monolayers (1×10^6) infected with serial dilutions of virus were overlaid with 1.5 mL of a low melting point (LMP) agarose mixture containing 2.5 mL of 3% LMP agarose (Invitrogen) in water (w/v), 2.5 mL DMEM, 1 mL NCS, and 100 µl of 100 mg/mL X-gal. The overlay was allowed to solidify at room temperature for 15 minutes, followed by incubation at 37°C and 5% CO_2. Recombinant viruses will express β-galactosidase, the product of the *LacZ* gene, which will hydrolyze X-gal in the overlay and result in a bright blue product. Blue plaques were picked the following day using a pasteur pipette and suspended in 100 µl of ice cold swelling buffer. Plaque picks containing virus-infected cells underwent three freeze-thaw cycles at -80°C and 37°C followed by sonication as described in 2.5.2 to lyse cells and release infectious virus to be used for subsequent purification rounds or amplification.

To purify VACVΔB6R-EGFP, infected cell monolayers (1×10^6) were overlaid with the same agarose mixture described above, but without X-gal. After solidification of the overlay, green fluorescing plaques were visualized under the FITC filter of a fluorescent microscope (Leica) and picked with a Pasteur pipette and

suspended in 100 µl of ice cold swelling buffer. Again, plaques were subjected to 3 freeze-thaws and sonication before subsequent use.

2.5.6 Preparation of Virus Stocks. Viruses were amplified in roller bottles containing 3×10^8 BGMK cells by infecting at an MOI of 5 for 12-24 hours. Infected cells were harvested in SSC, centrifuged at 1000 $\times$g for 5 minutes to pellet the cells, and the pellet was re-suspended in 5 mL of ice cold swelling buffer. The infected cells were lysed by 3 freeze-thaw cycles (see 2.5.5). Virus was isolated by dounce homogenization on ice using a "B" pestle (Bellco Biotechnology) to lyse the cell membranes but not the virus membranes. After 100 strokes, the homogenate was centrifuged (1000 $\times$g, 10 min) to pellet membranes while freed virus remains in the supernatant. After collecting the supernatant, pellets were re-suspended in 10 mL swelling buffer and dounce homogenized again with 60 strokes. After being centrifuged at 1000 $\times$g for 10 minutes, supernatants were pooled and centrifuged at 10,000 $\times$g for 1 hour at 4°C to pellet the virus. Virus pellets were re-suspended in DMEM and viral titres were determined as described in 2.5.7.

2.5.7 Virus Titre Determination. To determine the number of plaque-forming units per mL (PFU/mL) of virus in a stock, serial dilutions were used to infect BGMK monolayers. In brief, 10 µl of the original stock was added to 990 µl of 1X PBS (phosphate-buffered saline) for a 10^{-2} dilution. One hundred µl of this dilution was serially diluted into 900 µl of 1X PBS 6 times for a series of dilutions from 10^{-3} to 10^{-8}. Four hundred µl of each dilution was added to 6-well plates of sub-confluent BGMK monolayers in duplicate, and infections were incubated (37°C and 5% CO_2) for 12-24 hours. Infected wells were then fixed in neutral-buffered formalin (37% (w/v) formaldehyde (Sigma), pH 7.4, 100 mL 10X PBS) and stained with a solution of 0.1% (w/v) crystal violet (Sigma-Aldrich) and 20% (v/v) ethanol. Single infectious virions, or PFU, are seen as visible regions of cell-clearing that can be counted and, with the known dilution of each well, can be

used to calculate the original virus titre. The number of visible PFU multiplied by the reciprocal of the dilution of the well that was counted, divided by the total volume of that dilution added to the well, gives the stock concentration in PFU/mL. The average of the two duplicates was taken as the stock concentration.

To determine what volume was required for a given MOI, the following calculation was performed: the number of cells to be infected was multiplied by the desired MOI to give the total number of PFU required. This value was then divided by the stock concentration to give the volume of virus stock which contains the desired number of PFU.

2.5.8 Preparation of Virus Genomic DNA. To extract and prepare viral genomic DNA for PCR reactions, SDS lysis and phenol:chloroform extraction was performed. BGMK cells (1×10^6) were infected with the desired virus at an MOI of 5 for 16 hours. The infection media was then replaced with cell lysis buffer (1.2% SDS, 50 mM Tris-HCl (pH 8.0), 4 mM EDTA, 4 mM $CaCl_2$, 0.2 mg/mL proteinase K) to lyse the cells and incubated overnight (37°C and 5% CO_2). The lysate was collected in a microfuge tube and DNA was extracted in half a volume of phenol:chloroform (1:1) by vigorous vortexing. After centrifugation, the aqueous layer was collected and 50 µl of 3M $NaCH_3COO$ and 2.5 volumes of 95% ethanol were added and incubated at -70°C for 10 minutes to precipitate the DNA. The DNA was pelleted by centrifugation (9000 ×g, 10 minutes) and re-suspended in 50 µl ddH_2O.

2.6 Protein Methodology

2.6.1 Antibodies. All antibodies used in this study are listed in table 2-4, along with the source and working concentration for each assay. All antibodies used for western blots were suspended in 5% skim milk (w/v) in tris-buffered saline plus Tween-20 (TBST).

2.6.2 Immunoprecipitation to Detect Interacting Proteins. To identify any proteins that interact with VACV-B6R, immunoprecipitation (IP) of EGFP-B6R or FLAG-B6R in the context of virus infection was utilized. HeLa cells (4×10^6) seeded in 10 cm dishes were infected with VACV-EGFP-B6R at an MOI of 5 or infected/transfected with VACV at an MOI of 5 and 2 µg pSC66-FLAG-B6R(1-173) or pSC66-FLAG-B6R(1-142) for 12 hours. After one wash with 5 mL of 1X PBS, the infected HeLa cells were lysed in 1% NP-40 lysis buffer containing 1% (v/v) NP-40 (Sigma-Aldrich), 150 mM NaCl, 50 mM Tris-HCl pH 8.0, and EDTA-free protease inhibitor cocktail (Roche). Mechanical lysis of cell membranes was done by douncing the lysates 6 times with a 22G needle (BD) and 1 mL syringe (BD). Lysis was allowed to occur while rocking for 1.5 hours at 4°C. Membranes were pelleted by centrifugation at $9000 \times g$ for 10 minutes, and 10% of the supernatant was collected for acetone precipitation (see 2.6.3) while the remaining 90% was used to IP. Three µl of goat anti-EGFP or mouse anti-FLAG M2 was added to the IP sample and rocked at 4°C for 2 hours to bind EGFP-B6R or FLAG-B6R constructs. Thirty µl of a 1:1 mixture of lysis buffer to protein G-conjugated sepharose beads (GE Healthcare) was added to the IP samples, and immune complexes were allowed to form for 1 hour at 4°C. Immune complexes were pelleted by centrifugation (300 $\times g$, 30 seconds) and washed three times with 200 µl of lysis buffer. After the supernatant was carefully removed, the beads were suspended in 60 µl of SDS sample loading buffer (see 2.6.5).

2.6.3 Acetone Precipitation of Cell Lysates. Ten percent of supernatants from immunoprecipitations were subjected to acetone precipitation to precipitate whole cell lysate proteins. Five volumes of ice-cold acetone (Fisher Scientific) were added to supernatants and protein precipitation was allowed to occur at -20°C for at least 1 hour. Proteins were isolated by centrifugation at 10,000 $\times g$ for 10 minutes, air-dried, and re-suspended in 100 µl of SDS sample loading buffer.

2.6.4 Silver Staining and Coomassie Staining. To assess interacting partners, anti-EGFP or anti-FLAG IP samples were subjected to SDS-PAGE on a Hoefer electrophoresis unit SE 600 series (GE Healthcare). Proteins were visualized by silver staining using an adapted protocol (23, 195). First the gel was fixed in 50% methanol and 5% acetic acid for 15 minutes, then washed in 50% methanol for 25 minutes and washed 5 times for a total of 25 minutes. All washes were done with milli-Q water. To sensitize the gel, 0.02% sodium thiosulfate was added for 1 minute followed by two 1 minute washes. Protein bands were stained with 0.1% cold silver nitrate for 25 minutes and washed twice for 1 minute. To develop, the gel was incubated in 2% sodium carbonate anhydrous and 37% formaldehyde for 10 minutes, and stopped with 5% acetic acid for 20 minutes. Gels were washed twice and stored in milli-Q water.

Protein bands were also visualized using a high sensitivity coomassie staining protocol (Dr. R. Fahlman, University of Alberta, Canada). The gel was first fixed in a 50% methanol, 2% phosphoric acid solution for 1 hour. After two 20 minute washes in milli-Q water, a staining solution comprised of 20% methanol, 10% phosphoric acid, 1.4 mM coomassie brilliant blue G-250, and 0.8 M ammonium sulfate was added to the gel and incubated overnight at 4°C. The gel was washed and stored in milli-Q water.

2.6.5 SDS Polyacrylamide Gel Electrophoresis. Protein samples were resolved by sodium dodecyl sulfate polyacrylamide electrophoresis (SDS-PAGE). Protein samples were suspended in SDS sample loading buffer comprised of 6.26 mM Tris, pH 6.8, 2% SDS (Fisher Scientific), 32% glycerol (Anachemia), 0.05M beta-mercaptoethanol (Bioshop), and 0.005% bromophenol blue. Prior to separation by gel electrophoresis, samples were boiled at 100°C for 15 minutes. In general, 10-15 µl of boiled protein samples were loaded on 10-15% acrylamide gels (1.5 millimetre (mm)) and run in a Mini-PROTEAN Cell system (BioRad) at 150-200V along with 7.5 µl of pre-stained low molecular weight protein markers

(Fermentas). Gels were run in 1X SDS running buffer containing 190 nM glycine, 25 mM Tris, and 3.5 mM SDS. To resolve radiolabelled proteins, 10% acrylamide, 0.75 mm gels were utilized to allow for subsequent gel drying (see 2.6.6).

2.6.6 Semi-Dry Transfer and Gel Drying. Proteins resolved by SDS-PAGE were transferred to polyvinylidene difluoride (PVDF) membranes for 2 hours at 450 mA with a semi-dry transfer apparatus (Tyler Research). Membranes were blocked in 5% skim milk (w/v) in TBST at room temperature for at least 1 hour or overnight at 4°C. In contrast, gels used to resolve radiolabelled proteins were dried and immediately exposed to film. Gels were placed on 2 sheets of water-soaked filter paper, covered with plastic wrap, and placed on the Drygel Sr. slab gel drier (Hoefer Scientific Instruments). The gels were dried under vacuum suction at 70°C for ~1.5 h and exposed to film at -80°C for at least 4 hours.

2.6.7 Western Blotting. To detect proteins of interest, membranes were probed with primary antibodies according to the dilutions listed in Table 2-4 for either 2 hours at room temperature or overnight at 4°C. Three 15 minute washes with TBST removed any excess primary antibodies from membranes. Secondary antibodies were added (Table 2-4) for 1 hour at room temperature, followed by four 15 minute TBST washes to remove any excess. Proteins were visualized by enhanced chemiluminescence (ECL; GE Healthcare) according to the manufacturer's protocol.

2.6.8 Protein Sequence Analysis. To determine VACV-B6R homologues, position-specific iterated (PSI) BLAST analysis was performed using the non-redundant protein sequence database. Protein sequences were obtained from NCBI and the Poxvirus Bioinformatics Resource. Protein sequence alignments were generated using the tCoffee multiple sequence alignment program and edited in Genedoc. The presence of a transmembrane domain(s) within VACV-B6R was identified by the TMpred transmembrane domain prediction software (92).

Table 2-4 Antibodies used in this study.

Antibody	Dilution	Source
Immunoprecipitation		
Goat anti-EGFP	2 µl	L. Berthiaume
Microscopy		
Rabbit anti-PDI	1:200	Cell Signalling Technology
Rabbit anti-p65	1:200	Santa Cruz Biotechnology
Mouse anti-FLAG M2	1:200	Sigma-Aldrich
Goat anti-rabbit Alexafluor 546	1:400	Invitrogen
Goat anti-mouse Alexafluor 488	1:400	Invitrogen
Western Blotting		
Mouse anti-FLAG M2	1:10,000	Sigma-Aldrich
Mouse anti-EGFP	1:10,000	Covance
Donkey anti-mouse-HRP	1:25,000	Jackson Immunoresearch
Donkey anti-rabbit-HRP	1:25,000	Jackson Immunoresearch

EGFP – enhanced green fluorescent protein, PDI – protein disulfide isomerase, HRP – horseradish peroxidase

2.7 Assays

2.7.1 Growth Curves. Single-step growth curves were generated by infecting BGMK cells (1×10^6) with the indicated viruses at an MOI of 10. After 1 hour incubation (37°C and 5% CO_2) with gentle rocking every 10 minutes, the infecting media was removed, the cell monolayer was washed with 1 mL 1X PBS, and 2 mL of culture media was added back. At 0, 4, 8, 12, 24, and 48 hours post-infection (hpi), the cells and media were harvested in SSC, centrifuged at $300 \times g$ for 5 minutes, and the pellet was suspended in 100 µl of ice cold swelling buffer. The experiment was performed in triplicate, and the time points were titered as described in 2.5.7. The mean viral titre and standard deviation for each timepoint were determined and represented graphically using GraphPad Prism version 5 (GraphPad Software, La Jolla California USA, www.graphpad.com). Likewise, multi-step growth curves were generated by infecting BGMK cells with the indicated viruses at an MOI of 0.01 and harvesting at 0, 12, 24, 48, and 72 hpi. There was no wash step following the 1 hour infection: Fresh media was added directly to the infecting media.

2.7.2 Reverse Transcription PCR to Detect Virus Gene Expression. To determine the temporal expression of VACV-B6R, reverse transcription PCR (RT-PCR) was performed with RNA extracts from infected CV-1 cells. CV-1 cells (1×10^6) were infected or mock infected with ECTV at an MOI of 5 for 1 hour as in 2.5.2. After washing once with culture media, infected cells were supplemented with 1 mL of culture media with or without 80 µg/mL of β-D-arabinofuranoside hydrochloride (AraC; Sigma-Aldrich), an inhibitor of DNA replication and subsequent intermediate and late gene synthesis. After 4, 12, and 24 hours of infection, cells were harvested in 1 mL of TRIZOL (Invitrogen) and stored at -80°C. A mock infected sample was collected at 12 hpi. RNA was extracted according to the manufacturer's directions. Two hundred µl of chloroform was added to the Trizol suspensions, vigorously shaken for 15 seconds, incubated at room temperature

for 3 minutes, and centrifuged at 10,000 ×g for 10 minutes at 4°C. The aqueous layer containing the RNA was collected in a new centrifuge tube and 0.5 mL of isopropanol was added and incubated at room temperature for 10 minutes. Precipitated RNA was isolated by centrifugation at 10,000 ×g for 10 minutes at 4°C. The supernatant was carefully removed and the RNA pellets were washed with 70% ethanol (v/v) made in diethylpyrocarbonate (DEPC)-treated water followed by centrifugation at 7500 ×g. The RNA pellets were allowed to air dry and re-suspended in 50 µl of DEPC-treated water, followed by a 10 minute incubation on ice and another 10 minute incubation at 55°C. The RNA concentration and purity was determined using a NanoVue Plus spectrophotometer (GE Healthcare). Only RNA extracts exhibiting an A260/280 of ≥ 1.7 were used.

Two µg of RNA was treated with 1 U/mL of RQ1 RNAse-free DNAse (Promega) to remove any contaminating dsDNA. After 1 hour incubation at 37°C, 2 µl of stop-solution was added and the DNAse was inactivated at 65°C for 10 minutes. cDNA was then generated by first-strand synthesis. Two µl of Oligo(dt)$_{12\text{-}18}$ primer (Invitrogen) and 2 µl of 10 mM RNA-free dNTPs were added to 20 µl of DNAse-treated RNA for 5 minutes at 65°C to allow primer annealing. Reverse transcription was performed by adding 8 µl of 5X first-strand buffer, 4 µl of DTT, and 2 µl of DEPC-treated water to the mixture and incubated for 2 minutes at 42°C. Four hundred U of SuperScript II RT (Invitrogen) was subsequently added, followed by incubation at 42°C for 50 minutes then at 70°C for 15 minutes to generate cDNA. Parental RNA was then degraded by treatment with 2 µl of RNAse H (Invitrogen) at 37°C for 20 minutes. To assess RNA transcript levels, PCR reactions were performed using Taq polymerase as described in 2.2.1. Five µl of cDNA was used as a template and gene-specific primers (Table 2-3) were used to amplify the 3'-most 250 nucleotides (nt) of each gene.

2.7.3 Confocal Microscopy

2.7.3.1 Live Cell Imaging to Assess Intracellular Localization. HeLa cells (2×10^5) seeded in collagen-coated 35 mm glass bottom dishes (MatTek Corp.) were transfected with the indicated plasmids or infected with the indicated virus at an MOI of 5. Twelve hours post-infection or transfection, 100 nM ER Tracker Blue-White DPX (Molecular Probes) made in culture media was added to the cells for 30 minutes. Staining solution was removed and cells were washed with 1 mL 1X PBS and replaced with 2 mL of culture media. Images were taken on a WaveFX spinning disc microscope at 405 nm to detect ER tracker fluorescence and 491 nm to detect EGFP fluorescence.

2.7.3.2 Fixed Cell Imaging. HeLa cells (2×10^5) were seeded in 12-well plates on 18 mm coverslips 24 hours prior to treatment. The cells were then infected with the indicated virus at an MOI of 5 or transfected with the indicated plasmid. Following infection or transfection, the cells were fixed for 10 minutes in 500 µL of 4% (w/v) paraformaldehyde (PFA; Sigma-Aldrich) made in 1X PBS. The cells were generally permeabilized with 800 µL of 1% NP-40 (v/v) in 1X PBS for 5 minutes. To prevent non-specific background staining, the cells were subsequently blocked with 30% goat serum (Invitrogen) for 1 hour at room temperature. Primary antibodies were used at the dilutions listed in Table 2.4: rabbit anti-protein disulfide isomerase (PDI; Cell Signalling) or mouse anti-FLAG M2 (Sigma-Aldrich). Primary staining was done for 1 hour, followed by secondary staining for 1 hour with goat anti-mouse Alexafluor 488 or goat anti-rabbit Alexafluor 546. Washes were performed between each step with 1% (v/v) FBS in 1X PBS. Nuclei were stained last with 4',6'-diamidino-2-phenylindole (DAPI) for 2 minutes and rinsed in double-distilled H_20. Coverslips were then mounted using 50% (v/v) glycerol and 4 mg/mL N-propyl-gallate (Sigma-Aldrich). Cells were visualized on a WaveFX spinning disc microscope at 405 nm to detect DAPI fluorescence, 491 nm to detect EGFP fluorescence, and 561 nm to detect red PDI fluorescence.

2.7.3.3 Infection Time Course. To assess the localization of B6R throughout the course of infection, fixed cell imaging was performed at sequential timepoints during infection. HeLa cells (2×10^5) were seeded onto 18mm coverslips 24 hours prior to infection. HeLa cells were then either mock infected or infected with VACV, VACV-EGFP-B6R, or VACVΔB6R-EGFP at an MOI of 5. The cells were fixed at 2, 4, 6, 8, 12, and 24 hours post-infection for each virus, followed by permeabilization, blocking, and staining as described in 2.7.2.2. Cells were visualized on a WaveFX spinning disc microscope at 405 nm to detect DAPI fluorescence, 491 nm to detect EGFP fluorescence, and 561 nm to detect red PDI fluorescence.

2.7.4 *In vitro* Transcription-Translation. To study the membrane insertion of VACV-B6R, an *in vitro* transcription-translation (TNT) assay was done using the TNT SP6 coupled reticulocyte lysate system (Promega). Reactions included: 25 µl rabbit reticulocyte lysate, 2 µl reaction buffer, 1 µl SP6 RNA polymerase, 1 µl amino acid mixture minus methionine, 1 µl [^{35}S]methionine (Perkin-Elmer), 40 U RNasin ribonuclease inhibitor (Promega), 1 µg pSPUTK template plasmid (as indicated), and 17 µl DEPC-treated water. Reactions were incubated at 30°C for 90 minutes. Ten µg cycloheximide (CHX; ICN Biomedicals Inc.) was added and incubated at room temperature for 5 minutes to terminate the reactions. Five µl of canine pancreatic microsomal membranes (CPMM; Dr. D. Andrews, McMaster University, Hamilton, ON) were added to simulate ER membrane either prior to the 90 minute incubation or after CHX termination to observe co-translational and post-translational insertion, respectively. Microsomes were isolated by centrifugation at 10,000 ×g for 20 minutes at 4°C, and supernatants were collected in separate tubes. The pellets were washed twice with 200 µl of 1X PBS, and finally suspended in 50 µl of 1X PBS.

The nature and topology of membrane association was assessed by subjecting the microsomes to a Na_2CO_3 wash, trypsin treatment, or proteinase K

treatment. Reactions were carried out as described above with 5 µl of CPMMs present during transcription-translation. Following termination, microsomes and integral proteins were isolated by centrifugation (10,000 ×g, 20 minutes, 4°C) and the supernatants were collected in separate tubes. One microsomal pellet was washed with 200 µl of 0.1 M Na_2CO_3, pH 11, another pellet was treated with 0.1 mg trypsin (Sigma-Aldrich) for 30 minutes at 30°C, and the last pellet was treated with 0.1 mg proteinase K (Roche) for 30 minutes at 30°C. Following treatments, the microsomes were isolated by centrifugation (10,000 ×g, 20 minutes, 4°C), washed twice with 200 µl 1X PBS, and finally suspended in 50 µl 1X PBS. Supernatant and pellet fractions were resolved by SDS PAGE as described in 2.6.5. Five µl of samples were added to 25 µl of SDS sample loading buffer, boiled for 15 minutes, and 5 µl of each sample was loaded onto the gels. The gels were dried and exposed to film at -80°C.

2.7.5 Selective Permeabilization to Determine Membrane Topology. HeLa cells (2×10^5) seeded on 18 mm coverslips in a 12-well plate were infected with VACVΔB6R-EGFP at an MOI of 5 and transfected with pSC66-FLAG-B6R(1-173) as described in 2.5.2. After 8 hours, the cells were fixed in 4% PFA (see 2.7.2.2). To permeabilize both the cell membrane and organelle membranes, 1% NP-40 was used as described in 2.7.2.2. To selectively permeabilize the plasma membrane while retaining organelle membrane integrity, the cells were treated with 1 U/mL streptolysin O (SLO) for 1 minute at 37°C or with 0.025% digitonin (Sigma-Aldrich) in 1X PBS for 2 minutes at room temperature. Blocking, staining, and mounting was performed as described in 2.2.7.2 with DAPI, mouse anti-FLAG M2 (goat anti-mouse Alexafluor 488) and rabbit anti-PDI (goat anti-rabbit Alexafluor 546). The cells were imaged on a WaveFX spinning disc microscope at 405 nm to detect DAPI fluorescence, 491 nm to detect green FLAG fluorescence, and 561 nm to detect red PDI fluorescence.

2.7.6 Measurement of Mitochondrial Membrane Potential Loss by Flow Cytometry. To assess any potential role of VACV-B6R in the apoptotic pathway, the loss of mitochondrial membrane potential was measured by flow cytometry. In brief, 2 sets of HeLa cells (7×10^5) were first transfected with 0.25 µg pEGFP-C3, 2 µg pEGFP-Bcl-2, 2 µg pEGFP-F1L, 2.5 µg pEGFP-B6R(1-173), 2.5 µg pEGFP-B6R(1-142), or 2.5 µg pEGFP-B6R(143-173) for 12 hours (see 2.4.1). One set of transfected cells were then treated with 10 ng/mL of tumor necrosis factor-alpha (TNFα; Roche) and 5 µg/mL CHX in culture media for 4 hours to induce apoptosis, while simply replacing the culture media of the other set. After 4 hours the cells were washed with 1X PBS and stained with 0.2 µM tetramethylrhodamine ethyl ester (TMRE; Invitrogen Life Technologies) in culture media for 30 minutes at 37°C and 5% CO_2 (185). Cells were harvested and re-suspended in 1% FBS (v/v) in 1X PBS and analyzed by two-colour flow cytometry (FACScalibur; Becton Dickinson). The EGFP fluorescence was measured through the FL-1 channel equipped with a 489 nm filter (42 nm band pass) while TMRE fluorescence was measured through the FL-2 channel equipped with a 585 nm filter (42 nm band pass). Data were acquired on 20,000 cells per sample with fluorescent signals at logarithmic gain, and analysis was performed using CellQuest software. All subsequent calculations took into account the cytotoxicity caused by the transfection process. The percentage of apoptotic cells was calculated by dividing the number of EGFP-positive, TMRE-negative cells in a sample by the total number of EGFP-positive cells. The amount of apoptosis induced by TNFα was calculated by subtracting the percentage of apoptotic cells in untreated samples from the percentage of apoptotic cells in the treated counterparts. Apoptosis induction was determined by averaging the result of at least three separate experiments.

2.7.7 Detection of NFκB Activation by Immunofluorescence Microscopy. To assess the activation of the NFκB pathway, immunofluorescence microscopy was used to visualize nuclear translocation of the NFκB transcription factor subunit,

p65. First, HeLa cells (3.5×10^5) seeded on 18 mm coverslips were mock transfected or transfected with 2.5 μg pEGFP-B6R(1-173) as described in 2.4.1. After 14 hours of transfection, the cells were treated with or without 10 ng/mL TNFα for 20 minutes. The cells were fixed, permeabilized, blocked, stained, and mounted as described in 2.7.2 with DAPI and rabbit anti-p65 (Santa Cruz Biotechnology) (goat anti-rabbit AlexaFluor 546) to visualize p65. The cells were visualized with the 40X oil immersion lens of a Zeiss Axiovert 200M fluorescent microscope equipped with an ApoTome 10 optical sectioning device (Carl Zeiss, Inc). Representative images of at least 3 separate experiments are shown.

CHAPTER 3:

Vaccinia virus B6 is an ER Resident Tail-Anchored Protein

Three of the constructs used in this study were generated previously by graduate student Shawn Wasilenko: pEGFP-B6R(1-173), pEGFP-B6R(1-142), and pEGFP-B6R(1-173). Both pSPUTK-Bcl-2-Cyb5 and pSPUTK-B6R(1-173) were generated previously by graduate student Tara Stewart. All experimental work presented in this study was completed by R. Burton. The written work was done entirely by R. Burton, with an editorial contribution from Dr. Michele Barry.

Poxviruses are characterized by their large, brick-shaped virions and dumbbell-shaped core which houses a large dsDNA genome (55). Members of this family are tailored to infect insects and vertebrates, with some species exhibiting broad host ranges and others very narrow (55). A core set of 49 genes are conserved among all poxviruses, as they encode all of the machinery required for their uniquely cytoplasmic life cycle (116, 227). These conserved genes tend to be located within the central region of the genome, while genes within the termini vary greatly between members, as they dictate host-specific interactions such as host range, cellular modulation, and immune evasion (55). The most notorious member is VARV, the causative agent of smallpox. Though VARV was successfully eradicated from the human population in the 1970's, research efforts have continued in characterizing a number of other poxviruses, particularly the virus used as the smallpox vaccinating agent, VACV (11, 12, 71). Though the natural host of VACV remains unknown, research over the past few decades has lead to a greater understanding of the complex interactions and the co-evolution between poxviruses and their specific hosts (11, 12, 70).

Poxviruses are capable of interfering with a variety of normal cellular processes, making them highly successful intracellular pathogens (137). In response to virus infection, host organisms elicit immune responses involving both circulating immune cells and intrinsic cellular anti-viral processes (105, 149). Poxviruses, like VACV, encode an arsenal of proteins dedicated to manipulating and evading essentially every aspect of the host immune response (191, 200). Research efforts have lead to an understanding of the precise mechanism of action of an impressive number of these proteins; however, many still have yet to be characterized. Importantly, these immunomodulatory poxviral strategies and proteins have been exploited for medical use, including oncolytic therapies, recombinant gene therapies, and vaccines . Thus, at least a portion of the current work with poxviruses is focused on elucidating the function of previously uncharacterized proteins, with the intention of gaining a deeper understanding

of the complex virus-host interactions associated with these viruses and their potential use in therapeutics.

Research in our lab over the past decade has focused on the ability of poxviruses, primarily VACV and ECTV, to inhibit two critical immune response pathways: the apoptotic pathway, and the NFκB pathway (69, 209, 215). Early studies suggested that VACV encodes a mitochondrial protein whose function was to prevent virus infection-induced apoptosis (238). An initial screen of VACV proteins containing putative transmembrane domains identified the anti-apoptotic protein of interest, F1, in addition to the uncharacterized protein B6 (239). While very preliminary studies had been performed with B6 and its putative transmembrane domain, we sought to refocus on characterizing B6 and the function it serves during virus infection. The present study provides an initial characterization of VACV strain Copenhagen protein B6 along with preliminary functional studies, with the working hypothesis that it is an ER resident protein that may play an immunomodulatory role.

3.1 Homologues of B6R are confined to a subset of Orthopoxviruses. The conservation of a gene among poxvirus members is indicative of the type of function it may serve (79, 146). Highly conserved genes tend to be those that serve essential functions, while species-specific genes are typically confined to certain species or even strains (79, 146). A number of these host-specific genes have been evolutionarily acquired by poxviruses through horizontal gene transfer events with host cells, viruses, and even bacteria (97, 158). As such, we sought to determine the conservation of the B6R gene and identify any viral, cellular, or bacterial homologues by performing a position-specific iterated (PSI)-BLAST of the VACV-B6R amino acid sequence (5). Interestingly, the only significant hits obtained (E<3e-07) were genes encoded by certain orthopoxvirus members. The hits obtained show remarkably strong sequence identity ranging from 88-100%. One exception is the homologue encoded by the distantly related

Yoka poxvirus, with only 27% identity. Yoka poxvirus was discovered in a mosquito pool in the Central African Republic, and based on genomic studies, has been proposed to comprise an entirely new genus that is most closely related to the *Orthopoxvirinae* (249). A striking observation can be made from a sequence alignment of representative orthopoxvirus members: VARV strains encode a number of different truncated versions of B6R (Figure 3.1). For example, both highly virulent (VARV Bangladesh) and attenuated (VARV Garcia) strains have only retained the C-terminal 64 amino acids. Examination of the VARV nucleotide sequence revealed numerous insertion-deletion mutations within the N-terminus of the B6R ORF. Interestingly, the homologue encoded by VARV Bangladesh is annotated as a protein, while that encoded by VARV Garcia is annotated as a pseudogene. It is possible that among the dozens of VARV strains, some may still express truncated versions of B6R while others have lost expression entirely. The alignment also shows that the B6R ORF in horsepox virus (HSPV) has undergone fragmentation (HSPV-183a and HSPV-183b), an occurrence that is not uncommon for this virus (223). Both of these fragments are annotated as proteins rather than pseudogenes, suggesting that both may still be expressed during virus infection.

Unfortunately none of the homologues revealed by the BLAST search have been ascribed a function, however a number of them are annotated as 'ankyrin-like proteins'. An ankyrin repeat consists of a 33 residue motif that forms a characteristic alpha-helical structure (118). These domains are found in proteins of all forms of life, including a significant number in poxviruses, and mediate protein-protein interactions (27, 204). Another interesting observation made from the sequence alignment is that the N-terminus (aa 1-60 of B6R) and C-terminus (aa 114-173 of B6R) display strong sequence similarity among homologues, while the central region (aa 61-113 of B6R) appears to have undergone a number of mutations, insertions, and deletions. A possible explanation for this could be that B6R contains two functional domains

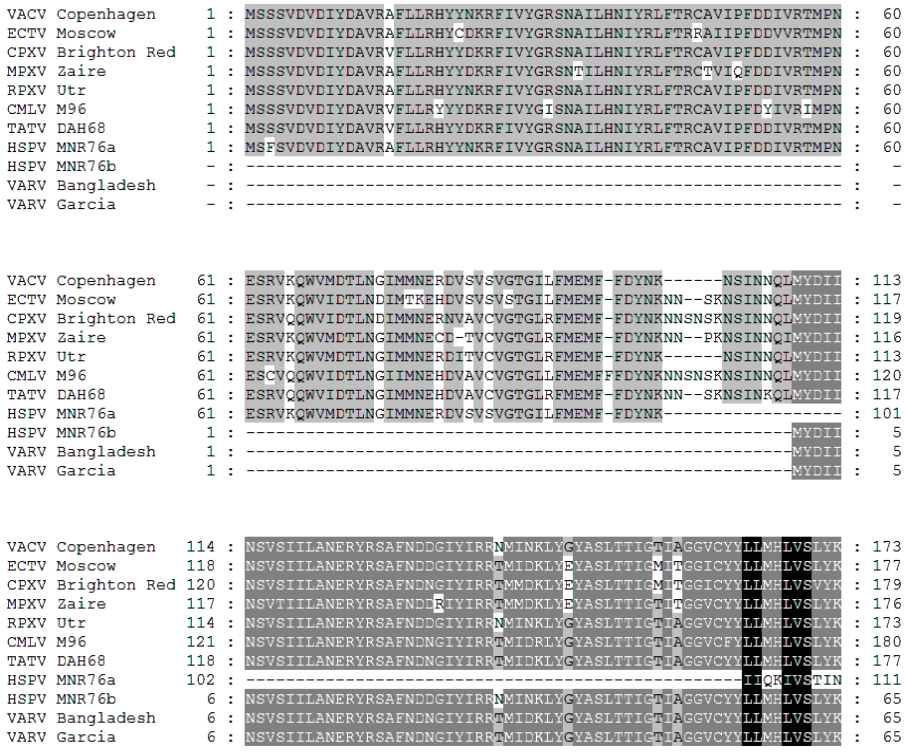

Figure 3.1 VACV-B6R homologues are confined to members of the *Orthopoxviridae*. Sequence alignment of VACV-B6R homologues encoded by representative *Orthopoxviridae* species: Vaccinia virus (VACV), Ectromelia virus (ECTV), Cowpox virus (CPXV), Monkeypox virus (MPXV), Rabbitpox virus (RPXV), Camelpox virus (CMLV), Taterapox virus (TATV), Horsepox virus (HSPV), and Variola virus (VARV). Homologues of VACV protein B6R were found using position-specific iterated basic local alignment search tool (PSI-BLAST; NCBI) based on the primary sequence. An alignment was generated using the tCoffee multiple sequence alignment program and edited in GeneDoc.

separated by a linker region which is under less evolutionary pressure and thus has mutated freely. Taken together, it seems that B6R homologues have been retained by certain members of the *Orthopoxvirinae*, some of which have undergone mutation and fragmentation across evolution.

3.2 B6R and homologues are actively expressed early during virus infection. With the observation that at least some VARV isolates encode B6R homologues that have become pseudogenes across evolution, we next wanted to assess whether the B6R gene is actively expressed during virus infection, and if so, when. The temporal expression pattern of a protein can shed light on its function, with host manipulation and immune evasion genes typically expressed early, while structural proteins are expressed late (31, 146). Because VACV-B6R and ECTV161 exhibit 88% sequence identity, and the intergenic spaces flanking these genes are also ~95% identical, we utilized ECTV with the assumption that these homologues will exhibit the same expression patterns. CV-1 cells were infected with ECTV in the presence or absence of 80 μg/mL of AraC, a DNA replication inhibitor that also prevents late gene expression. At 4, 12, and 24 hours post-infection (hpi), RNA was extracted from infected cells and subjected to first-strand reverse transcription-PCR (RT-PCR), allowing us to assess gene expression by PCR analysis using gene-specific primers. ECTV058 is a virion membrane protein that was used as a late gene control which, as seen in Figure 3.2, was not expressed until 12 hpi and was not expressed at all in the presence of AraC (205). ECTV004, a BTB domain-containing protein of unknown function, is an early gene control that was expressed as early as 4 hpi and was unaffected by AraC, and GAPDH served as a loading control (155, 244). Interestingly, ECTV161 was detected at all time points tested, even in the presence of AraC. This suggests that ECTV161, and VACV-B6R, are actively expressed during virus infection, and likely fall in the early temporal class of genes. While there appears to be a decrease in mRNA levels at 12 hpi in the presence of AraC, this experiment is qualitative and can only be used to assess the presence or absence

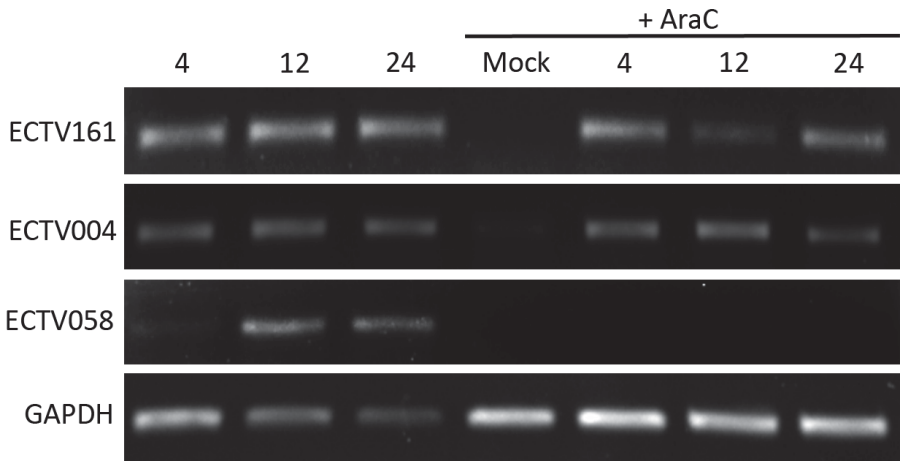

Figure 3.2 ECTV161, a VACV-B6R homologue, is expressed early during virus infection. Reverse transcription PCR was performed to determine when ECTV161, a VACV-B6R homologue, is expressed. CV-1 cells were infected with ectromelia virus at an MOI of 5 in the presence or absence of 80 µg/mL cytosine arabinoside (AraC). RNA was extracted at 4, 12, and 24 hpi and gene expression was assessed using gene-specific primers. ECTV004 is a BTB domain-containing protein of unknown function used as an early gene control, ECTV058 is a virion membrane protein used as a late gene control, and GAPDH is a ubiquitously expressed cellular protein used as a loading control.

of gene expression. This provides support for our hypothesis that B6 functions in either host modulation or immune evasion.

3.3 Vaccinia virus B6 is not required for virus growth *in vitro*. The B region of over 20 genes is located within the 3' terminus of the VACV genome, approximately half of which have been at least partially characterized (146). Many of these proteins serve to modulate host cell processes, including immune responses (146). One notable exception would be B5R, a structural membrane protein required for formation of EVs (30, 104). Interestingly, B5R contains four domains similar to complement regulatory domains; however, a complement control function has yet to be attributed to this protein (30, 191). It is therefore important not to assume that all genes found within the more variable regions of the genome are involved in host modulation and immune evasion. To this end, we initially sought to determine if B6 plays a role in essential processes like replication or structure.

If B6 is involved in essential processes, we would expect the growth of a VACV devoid of B6R to be affected. To test this, we compared the growth patterns of VACV and VACVΔB6R-EGFP, a knockout virus in which 90% of the B6R ORF was replaced with the EGFP gene, under both high and low MOI conditions (Figure 3.3) (237). BGMK cells infected with VACV or VACVΔB6R-EGFP at an MOI of 10 were harvested at 4, 8, 12, 24, and 48 hours post-infection (hpi) and titres were determined on BGMK cells to generate a single-step growth curve. Under these conditions, both viruses exhibited the same eclipse of infectious virions at 4 hpi, followed by the same drastic increase up to 24 hpi, where it levelled off to the final 48 hpi time point (Figure 3.3B). A slight difference in viral titres was observed at 8 hpi, however this difference is not significant ($p=0.2842$). BGMK cells infected with the same viruses at an MOI of 0.01 were harvested at 12, 24, 48, and 72 hpi and titres were again determined on BGMK cells to generate multi-step growth curves. Despite the half-log difference seen at only the 24

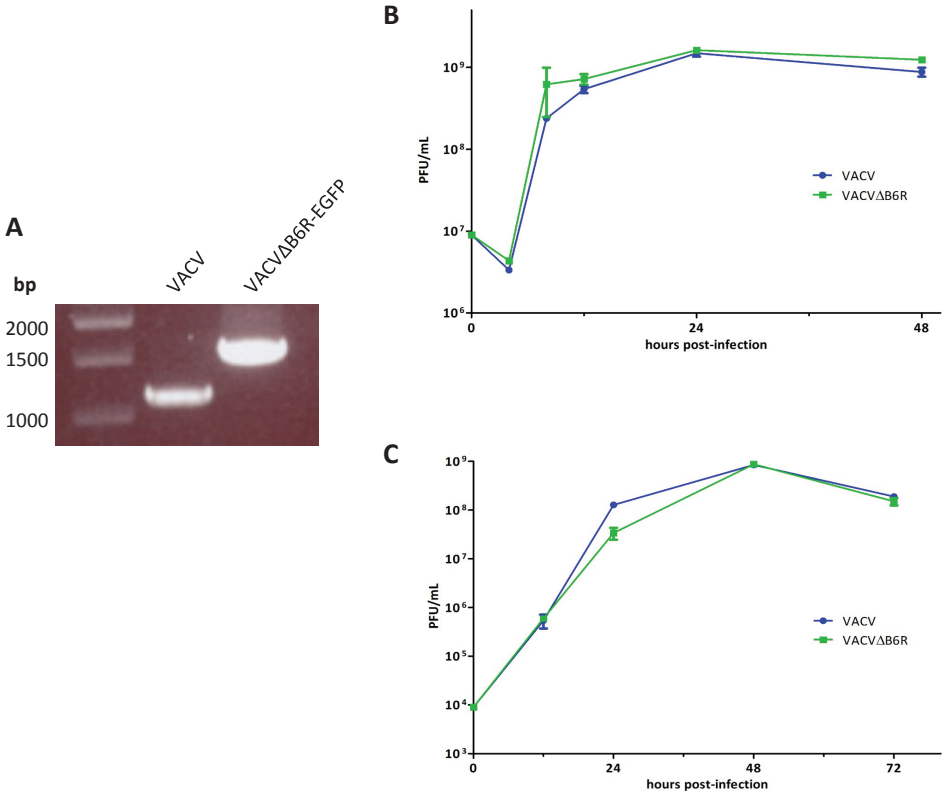

Figure 3.3 VACV devoid of the B6R gene exhibits the same replicative success as VACV *in vitro*. (A) PCR analysis of VACV and VACVΔB6R-EGFP genomes to confirm successful deletion of the B6R ORF using primers B6RkoF1 and B6RkoR2. **(B)** Single-step growth curves were performed to assess virus replication. BGMK cells were infected with VACV or VACVΔB6R-EGFP at an MOI of 10, with one PBS wash after 1 hour of infection. Cells and supernatants were harvested at 4, 8, 12, 24, and 48 hpi. **(C)** Multi-step growth curves were performed to assess virus growth under low MOI conditions. BGMK cells were infected with VACV or VACVΔB6R-EGFP at an MOI of 0.01 with no wash step. Cells and supernatants were collected at 12, 24, 48, and 72 hpi. All virus titres of each time point were determined on BGMK cells in triplicate. Graphed viral titres represent the average and S.D. of three separate experiments.

hour time point, the two viruses exhibited the same growth pattern under low MOI conditions at all other time points (Figure 3.3C). There was also no obvious difference in plaque size between the two viruses, so measurements were not deemed necessary for the purpose of this study. These results imply that, in tissue culture conditions, the absence of B6 does not affect the ability of VACV to replicate and produce infectious progeny at both high and low MOI. These results are typical for genes involved in virulence and pathogenicity, as the effects of their absence are only obvious in an immune competent environment.

3.4 The C-terminal 30 amino acids of B6 are responsible for ER localization. To begin studying VACV-B6R, we turned to bioinformatics to glean as much information from the protein sequence as possible. According to the NCBI, B6 is a 173 aa protein (522 nucleotides) of approximately 20 kDa that has a pI of 8.50 (5). To gain further insight as to the structure and function of B6, we turned to prediction software programs to analyze the amino acid sequence. A BLAST search of the B6 primary sequence reveals that full-length homologues contain a domain of unknown function 1500 (DUF1500), which is located in the N-terminus of B6 (5). We also utilized PSIpred server to predict the secondary structure of B6, which revealed that this protein is predominantly comprised of alpha helices, with four short beta sheets (Figure 3.4A) (138). This prediction was further corroborated by the I-TASSER protein structure prediction program, which presented 5 potential models, all of which contained primarily alpha-helices (Figure 3.4B) (248). The abundance of alpha-helices predicted in the B6 structure supports the finding that a number of B6R homologues are annotated as ankyrin-like proteins. Further structural analyses would be needed to corroborate this, however, as the predicted model given by I-TASSER does not resemble that of a typical ankyrin domain.

The primary sequence of B6 was predicted to contain at least one putative transmembrane domain, as illustrated by the hydrophobicity plot

A

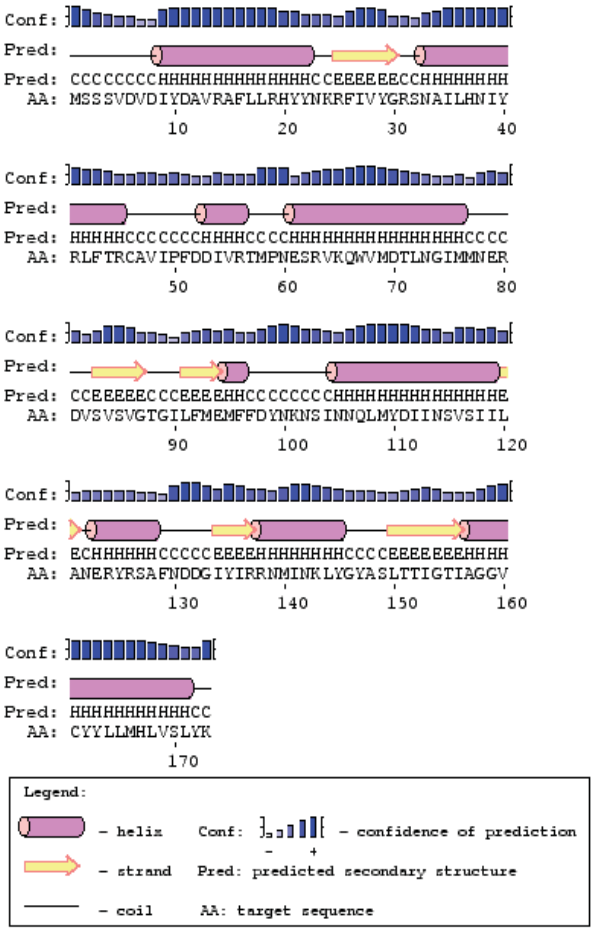

B

Figure 3.4 Secondary structure of B6 is predicted to be rich in alpha-helices. **(A)** Prediction of the secondary structure of B6 using PSIpred. Alpha helices are depicted as pink cylinders, beta sheets as yellow arrows, and coils as black lines. **(B)** Structural and functional prediction of B6 using I-TASSER. Based on the primary sequence of B6, I-TASSER proposes five models of the structure of B6, with the strongest one shown here. Alpha helices are pink, beta sheets are blue, and coils are grey.

generated by the TMpred program (Figure 3.5) (92). One model proposed that there are two transmembrane domains (TMDs) (Figure 3.5, light grey), one spanning aa 80 – 100, and another from aa 143-166, however the central hydrophobic region just barely reaches the significant value of 500. The other more promising model (Figure 3.5, black) suggested a single TMD at the C-terminus, again spanning amino acids 143-166 (Figure 3.4, red box). A TMD of this length is typical for ER-localized proteins, however B6 does not contain the signature lysine-asparagine-glutamine-leucine (KDEL) ER-retention signal (26, 210). Aside from the N-terminal DUF1500 and C-terminal TMD, the amino acid sequence does not contain any other obvious signal or retention sequences, post-translational modification sites, or structural/functional domains. This information reveals little as to the function of B6, however it is possible that it localizes to a membrane, such as the ER, via at least amino acids 143-166.

To determine the sub-cellular localization of B6 and the potential role of amino acids 143-166, we made use of three constructs generated previously in the lab by S. Wasilenko (Figure 3.6). N-terminal EGFP tags were appended to full length B6 (pEGFP-B6R(1-173)), B6 missing the C-terminal 30 amino acids (pEGFP-B6R(1-142)), and the C-terminal 30 amino acids alone (pEGFP-B6R(143-173)). HeLa cells were transiently transfected with these constructs, along with EGFP alone as a control, and the ER was stained using ER tracker. Live cell images of mock-transfected cells showed ER staining that was strong around the nucleus and spread throughout the cytoplasm in a tubular fashion, a typical distribution of the ER (Figure 3.7 a-c). EGFP alone was found diffuse throughout the cytoplasm and nucleus, with very little overlap with ER tracker (Figure 3.7 d-f). In contrast, full-length B6 appeared to accumulate around the nucleus and spread through the cytoplasm in a tubular pattern that is reminiscent of ER (Figure 3.7 g). While ER tracker did not look as tubular as it usually does, there was still a moderate amount of overlap between EGFP-B6(1-173) and ER tracker, as indicated by the yellow color in the merge image, especially near the nucleus

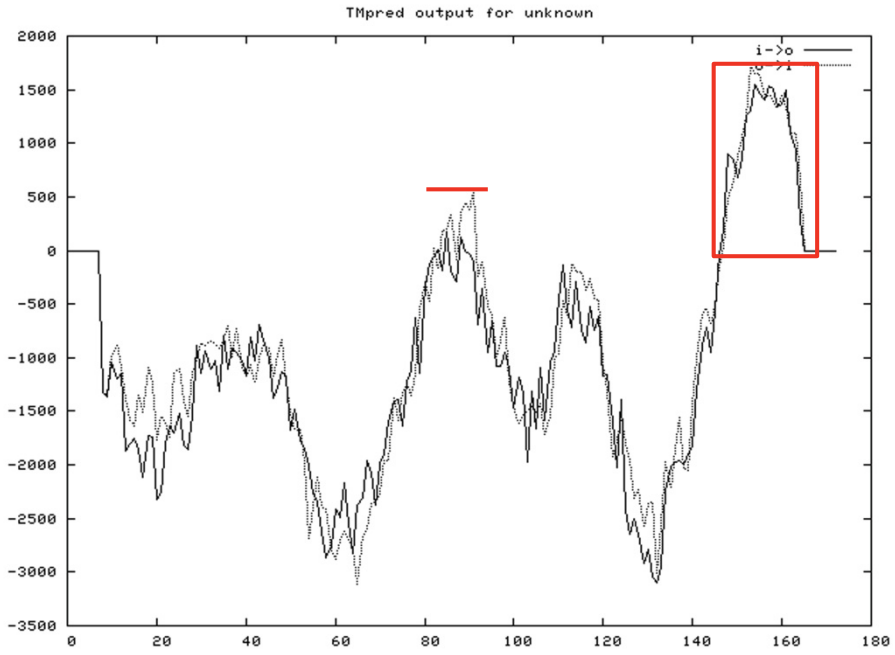

5’ –YIRRNMINKLYGYASLTTIGTIAGGVCYYLLMHLVSLYK – 3’

Figure 3.5 B6 contains a putative transmembrane domain. Analysis of the primary sequence of B6 using the TMpred program predicts two possible models indicated by the light grey and black lines in the hydrophobicity plot. A slightly hydrophobic region is found spanning amino acids 82 to 100, indicated by the red line, and a more hydrophobic region from amino acids 143-166 indicated by the red box. One model suggests two transmembrane domains while the other suggests a single transmembrane domain, however both agree that the N-terminus faces the cytosol. The amino acid sequence of B6 shown below the hydrophobicity plot highlights amino acids 143-166 in blue and flanking residues in black.

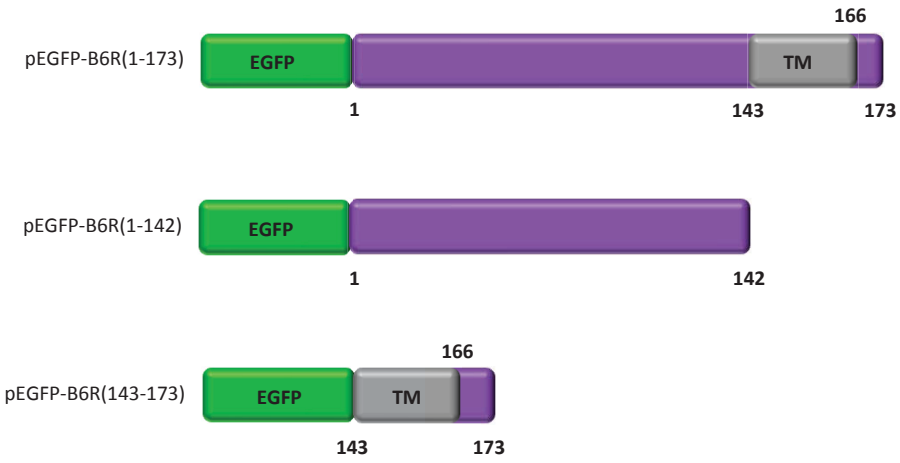

Figure 3.6 Schematic of recombinant proteins used in this study. B6 contains a putative transmembrane domain spanning amino acids 143-166. To assess the sub-cellular localization of B6, full-length B6R was N-terminally tagged with EGFP. To assess the role of the transmembrane domain, two N-terminal EGFP-tagged mutants were generated: B6R(1-142), which lacks the C-terminal 30 amino acids and putative transmembrane domain, and B6R(143-173) which consists of the C-terminal 30 amino acids of B6R alone.

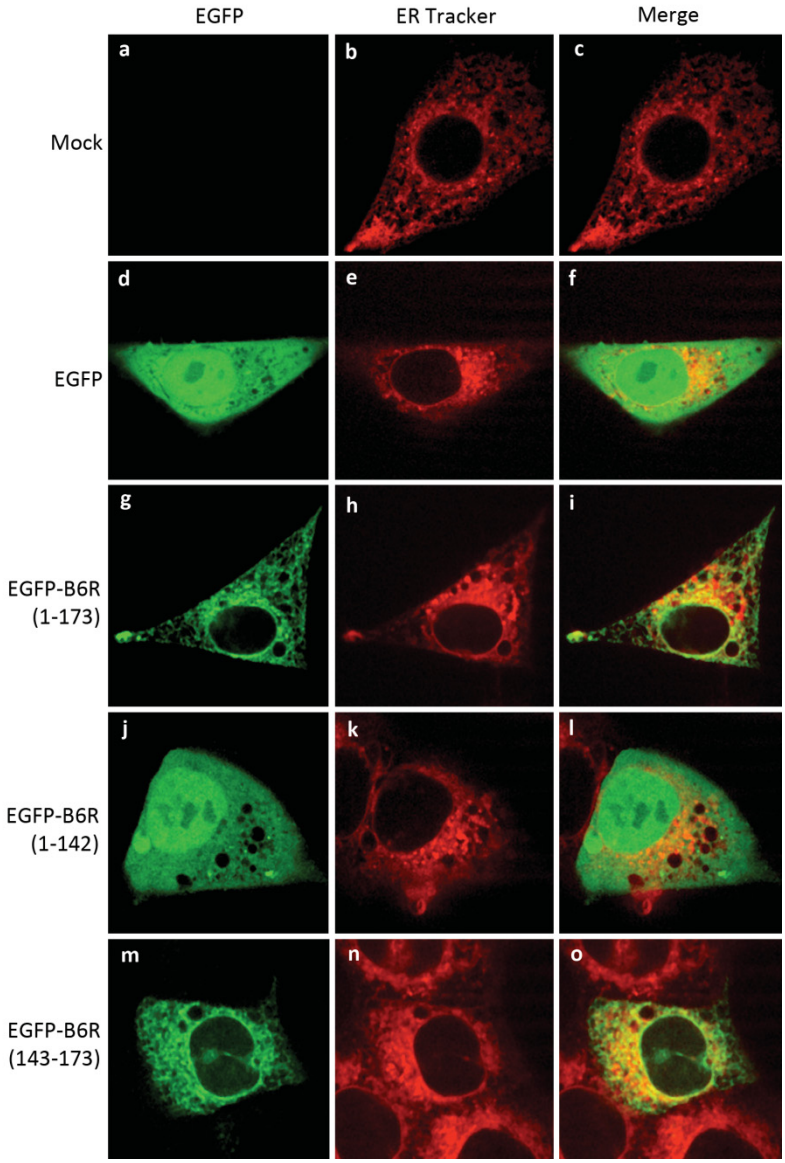

Figure 3.7 Transiently expressed B6 exhibits an ER-like distribution with moderate co-localization with ER tracker. Live cell imaging was utilized to assess the sub-cellular localization of B6 during transient transfection. HeLa cells were mock transfected (a-c) or transiently transfected with pEGFP (d-f), pEGFP-B6R(1-173) (g-i), pEGFP-B6R(1-142) (j-l), or pEGFP-B6R(143-173) (m-o) for 16 hours. B6 constructs were visualized by EGFP fluorescence and cells were stained with 100 nM ER tracker for 30 minutes to visualize the ER.

(Figure 3.7 g-i). B6 devoid of the C-terminal 30 amino acids exhibited the same distribution pattern as EGFP alone, with very little overlap with ER tracker (Figure 3.7 j-l). The B6 construct with only the C-terminal 30 amino acids again exhibited a typical ER-like distribution, which overlaps with ER tracker in the perinuclear region (Figure 3.7 m-o). Thus, it seems that B6 localizes to at least a portion of the ER when expressed exogenously, and that this localization is dependent on the C-terminal 30 amino acids.

To corroborate these findings in the context of VACV infection, we imaged live infected HeLa cells at 6 hpi, again staining for the ER with ER tracker. As expected, mock-infected cells displayed typical ER staining (Figure 3.8 a-c). Cells infected with VACV showed no green fluorescence, as expected, and while the cells were rounded up, the ER tracker was still visible around the nucleus and enriched on one side of the cell (Figure 3.8 d-f). The ER of cells infected with VACV-EGFP displayed the same pattern as VACV, with EGFP throughout the nucleus and cytoplasm with minimal overlap with ER tracker (Figure 3.8 g-i). To observe B6 localization in the context of infection, we utilized a recombinant VACV that over-expresses EGFP-B6(1-173) in addition to the endogenous B6. Some of the cells infected with this virus appeared rounded up with EGFP-B6(1-173) surrounding the nucleus and accumulating to one side, with modest co-localization with ER tracker (Figure 3.8 j-l). Intriguingly, other rounded up cells stained similarly with ER tracker within the cell, however there were also ER tracker-positive blebs surrounding the cells, which was the sole location of EGFP-B6(1-173) (Figure 3.8 m-o). Oddly, the two phenotypes were observed in equal proportions within a sample. Taken together, these data agree with the transfection localization data in Figure 3.7, however it seems that the over-expression of EGFP-B6(1-173) in the context of infection can cause dramatic ER morphological changes.

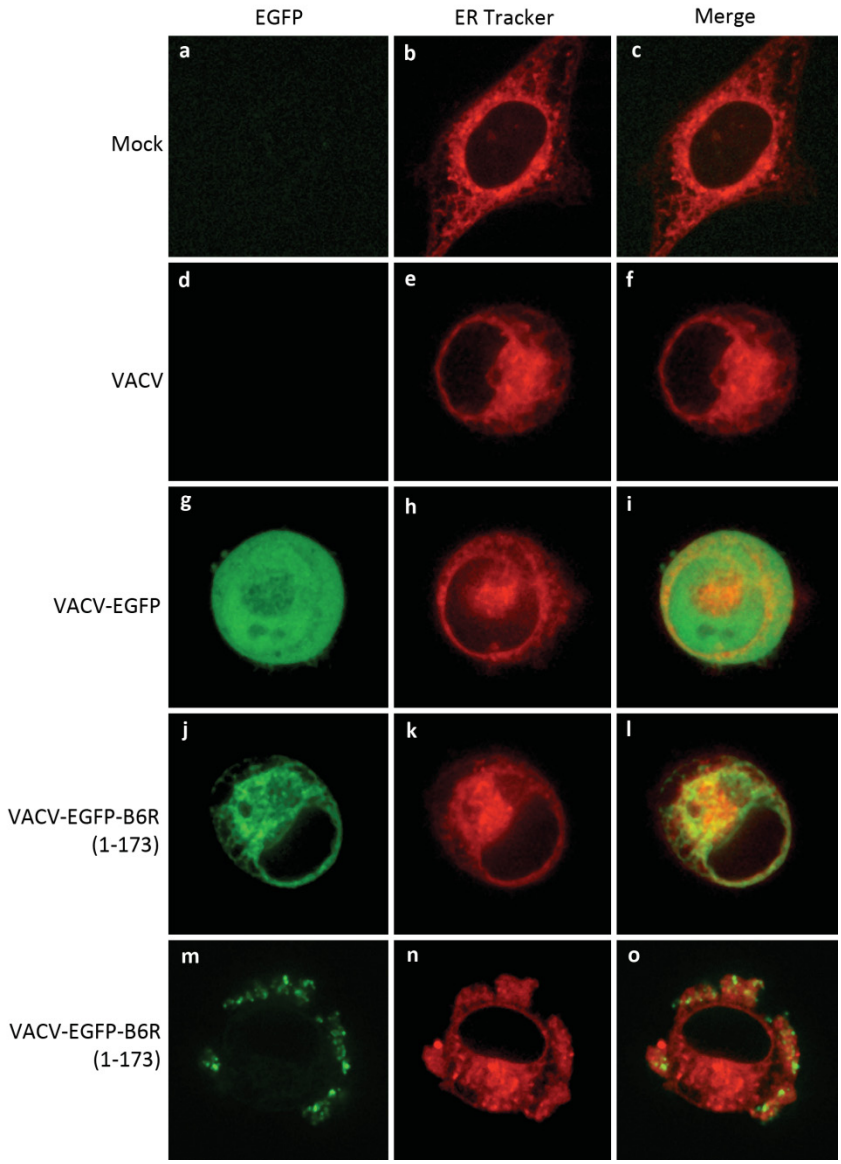

Figure 3.8 B6 exhibits two distinct distribution patterns during vaccinia virus infection. Live cell imaging was utilized to determine the sub-cellular localization of B6 in the context of infection. HeLa cells were mock infected (a-c) or infected with VACV (d-f), VACV-EGFP (g-i), or VACV-EGFP-B6R(1-173) (j-o) at an MOI of 5 for 6 hours. B6 was visualized by EGFP fluorescence and cells were stained with 100 nM ER tracker for 30 minutes to visualize the ER.

3.5 Over-expression of B6 induces unique ER morphological changes at early times of infection. The live cell images discussed previously suggest that B6 localizes to at least some portion of the ER via the C-terminal 30 amino acids, however the co-localization of B6 with ER tracker was far from absolute. The ER is the initial compartment of the secretory pathway, and is known for the many important contact points it makes with other organelles, such as the golgi apparatus, mitochondria, and plasma membrane (42, 126). With this in mind, we next sought to investigate the possibility that B6 localizes to additional intracellular membranes, especially considering it does not have a signature KDEL ER-retention signal. To this end, HeLa cells were again infected with VACV-EGFP-B6R(1-173) and fixed at the indicated times post-infection (Figure 3.9). To visualize the ER, an antibody to the ER lumenal enzyme protein disulfide isomerase (PDI) was used, and nuclei and virus factories were stained with DAPI (242). As expected, in the absence of infection, PDI was localized throughout the cytoplasm, though the characteristic ER tubular pattern was not obvious (Figure 3.9 a-d). At 2, 4, and 6 hpi, PDI was unexpectedly found in both the cytosol and nucleus of the cell, and within the same unique ER structures surrounding the cells seen in Figure 3.8 (Figure 3.9 e-p). EGFP-B6(1-173) was also found exclusively within these surrounding ER structures up until 6 hpi (Figure 3.9 e-p). Virus factories were not visible at these early time points, however this could be due to the orientation of the cells that were imaged. At 8 hpi, PDI was less concentrated within the nucleus, and the surrounding ER structures were no longer present (Figure 3.9 q-t). At this time, EGFP-B6(1-173) was found within the cytoplasm of the cell, accumulating mostly around the nucleus where it exhibited the strongest co-localization with PDI (Figure 3.9 q-t). A virus factory was just visible on the upper left side of the nucleus at this time (Figure 3.9 q). Similar distributions were seen at 12 and 24 hpi, however both PDI and EGFP-B6(1-173) accumulated in perinuclear areas that overlap with the virus factory, as seen by the DAPI staining (Figure 3.9 u-bb). Overall, co-localization of B6 and

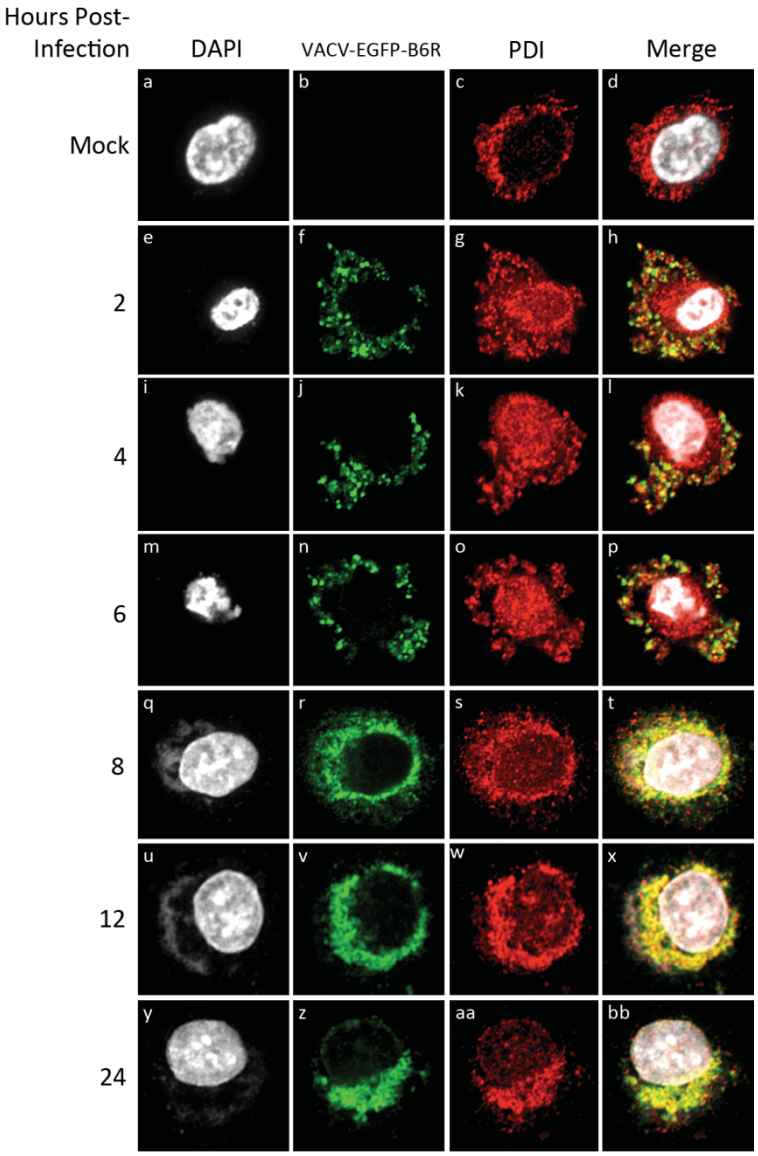

Figure 3.9 B6 localizes to unique ER structures at early times of infection. Fixed cell microscopy was utilized to observe the sub-cellular localization of B6 throughout the course of VACV infection. HeLa cells were infected with VACV-EGFP-B6R at an MOI of 5 and prepped for visualization at sequential time points from 2 to 24 hpi. B6 was visualized by EGFP fluorescence, nuclei were visualized by DAPI, and anti-PDI (protein disulfide isomerase) to used to visualize the ER.

PDI was fairly strong from 8-12 hpi, but it still appears that B6 is localizing to additional regions devoid of PDI. Likewise, B6 found within the surface ER blebs at early time points exhibits very little overlap with PDI staining.

The PDI- and B6-containing structures seen at early time points of infection have never been observed before in the context of VACV infection, making it tempting to propose that these structures are induced by the over-expression of B6. We performed the same experiment using VACV to test if these structures form when B6 is only expressed at endogenous levels (Figure 3.10). In this case, DAPI staining visualized a virus factory at 6 hpi and all subsequent time points (Figure 3.10 j, m, p, s). A slight accumulation of nuclear PDI was visible at 4 hpi, was most concentrated at 6 hpi, and decreased slightly from 8-24 hpi (Figure 3.10 h, k, n, q, t). The most striking observation was the lack of unique cell surface blebs from 2-6 hpi; there were some small blebs of PDI-positive structures at 8 hpi, however it was not nearly as pronounced as those observed with VACV-EGFP-B6R(1-173) infections (Figure 3.10 m-o). At 24 hpi, PDI staining appeared to accumulate around the nucleus, albeit to a lesser degree than in VACV-EGFP-B6R(1-173) infections, where the virus factory was located (Figure 3.10 s-u). These data support our initial prediction that it is the over-expression of B6 that is causing the ER morphological changes at early time points.

If B6 is responsible, at least in part, for the morphological changes in the ER, then this phenotype should be ablated in the absence of B6. To test this, we performed the same time-course experiment using VACVΔB6R-EGFP (Figure 3.11). DAPI staining revealed virus factory formation by 6 hpi, similar to that of VACV infection (Figure 3.11 m-p), and EGFP was found diffusely distributed throughout the nucleus and cytoplasm of infected cells at all time points, as expected (Figure 3.11 b, f, j, n, r, v, z). Interestingly, only a slight accumulation of PDI within the nucleus was observed up until 6 hpi, when comparable amounts of PDI was seen in the nucleus as seen with VACV infection. At 8 hpi, PDI was

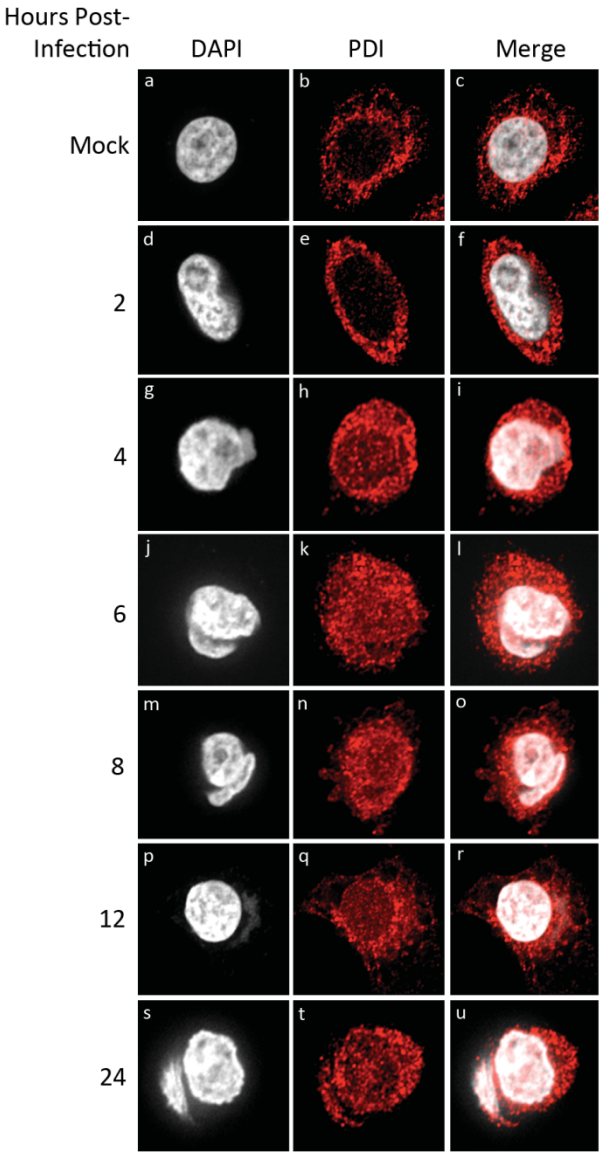

Figure 3.10 Infection with vaccinia virus does not induce ER morphological changes. Fixed cell microscopy was utilized to observe the morphology of the ER throughout the course of VACV infection. HeLa cells were infected with VACV at an MOI of 5 and prepped for visualization at sequential time points from 2 to 24 hpi. Cells were stained with DAPI to visualize nuclei and anti-PDI (protein disulfide isomerase) to visualize the ER.

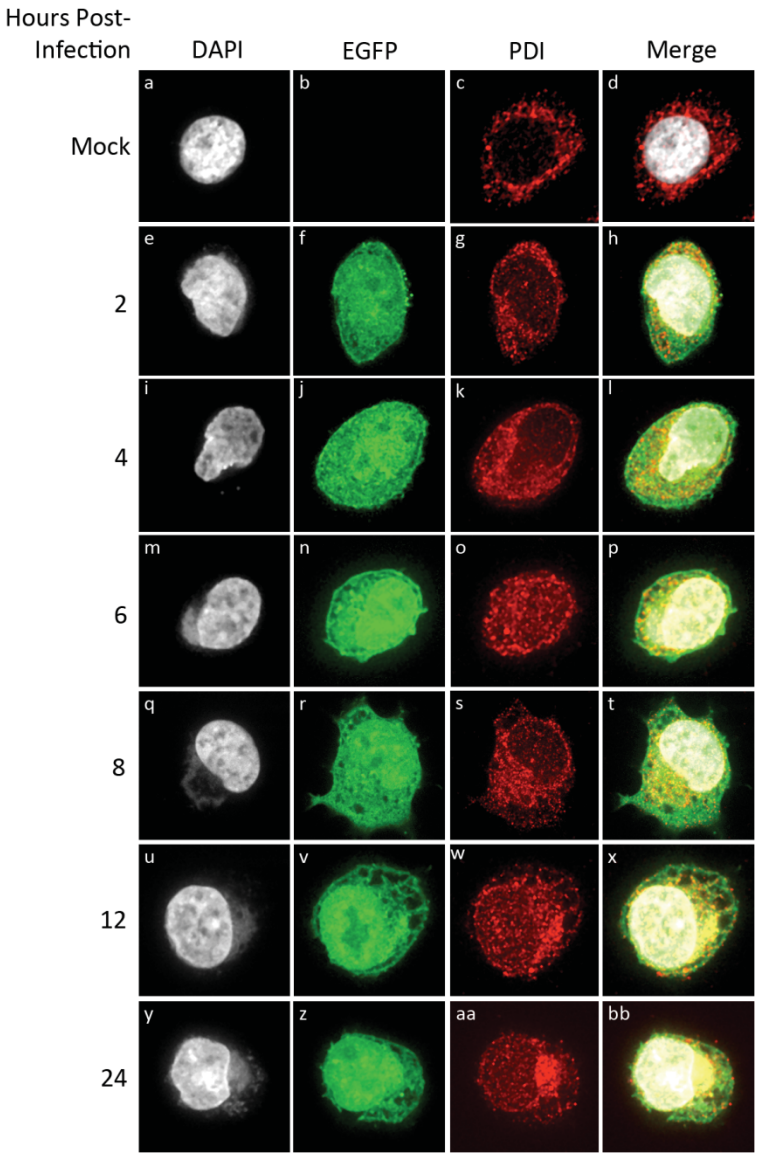

Figure 3.11 Cells infected with VACV devoid of B6 do not appear to undergo ER morphological changes. Fixed cell microscopy was utilized to observe ER morphology throughout the course of infection with VACVΔB6R-EGFP. HeLa cells were infected with VACVΔB6R-EGFP at an MOI of 5 and fixed at the indicated time points from 2-24 hpi. Cells were stained with DAPI to visualize nuclei and anti-PDI (protein disulfide isomerase) to visualize the ER.

concentrated in the perinuclear region with a visible accumulation where the DAPI-positive virus factory was seen (Figure 3.11 q-t). After 12 and 24 hpi, there again appeared to be a small increase in nuclear PDI, however it was still slightly concentrated in regions corresponding to the virus factories (Figure 3.11 u-bb). In general, cells infected with VACVΔB6R-EGFP showed similar morphological changes as that of VACV; however, the cells appeared to be spread out at approximately 8-12 hpi rather than rounded up. Most notably, none of the cells infected with VACV devoid of B6 underwent ER morphological changes like that seen in VACV-EGFP-B6R(1-173) infection. It seems, then, that the expression level of B6 can affect the overall ER morphology at early times of infection, and may serve to enhance the recruitment of ER, along with PDI, to virus factories at late times of infection. In addition, the localization of PDI may be affected by B6 expression levels, as there is a reduced amount of nuclear PDI during knockout VACV infection.

3.6 B6 behaves like a tail-anchored protein *in vitro*. The B6 TMD is located at the extreme C-terminus, followed by a very short polar tail, and we have shown that this domain is necessary for intracellular membrane localization (Figure 3.7). These observations suggest that B6 is potentially another tail-anchored protein. This class of proteins is characterized by post-translational insertion into their target membrane such that the functional N-terminus faces the cytosol (26, 167). First we addressed the ability of B6 to insert into microsomal membranes both co- and post-translationally using an *in vitro* transcription-translation (TNT) system. Full length B6 was cloned into the pSPUTK vector to allow for efficient translation in the presence of [^{35}S]methionine. A chimera of the Bcl-2 N-terminus with the Cyb5 TMD, which is known to localize to the ER via unassisted membrane insertion, was used as a positive control, and a B6(1-142) construct was also tested to assess the role of the B6 TMD in membrane insertion. Canine pancreatic microsomal membranes (CPMM) were either not added, added during the TNT reaction, or added after translation was terminated with CHX

(Figure 3.12A). The CPMMs were pelleted by centrifugation and radio-labelled proteins from pellet and supernatant fractions were visualized by autoradiography. As expected, in the absence of any CPMMs all [^{35}S]-labelled protein was found exclusively in the supernatant fractions (Figure 3.12A lanes 1 and 2). When CPMMs were present during the reaction, a small amount of [^{35}S]Bcl-2-Cyb5 was found in the pellet fraction, and when the CPMMs were added after reaction termination, there was a slight increase in [^{35}S]Bcl-2-Cyb5 in the pellet fraction (Figure 3.12A compare lanes 4 to 6). Compared to Bcl-2-Cyb5, there was a larger amount of [^{35}S]B6(1-173) detectable in the co-translational pellet fraction (Figure 3.12A lane 4), while there were comparable levels of [^{35}S]B6(1-173) and [^{35}S]Bcl-2-Cyb5 in pellet fractions under post-translational insertion conditions (Figure 3.12A lane 6). Interestingly, [^{35}S]B6(1-142) was found in the pellet fractions under both conditions, an unexpected result as this protein does not contain the putative TMD (Figure 3.12A lanes 4 and 6).These results suggest that full-length B6 is capable of post-translational insertion into microsomal membranes much like the Cyb5 control. The fact that B6 devoid of the putative TMD was still found in the pellet fractions could be due to the slightly hydrophobic region in the central region (aa 80-100), however further testing would need to be done to confirm this possibility. Though this data shows that all 3 proteins could insert into CPMMs present during the TNT reaction, we cannot discount the possibility that they are still inserting after ribosomal release under these experimental conditions.

Next, we utilized the same *in vitro* TNT system to investigate whether B6 is an integral membrane protein, and if so, with what topology does B6 insert. [^{35}S]B6(1-173) was generated in the presence of CPMMs and the pellet fractions were subjected to three different treatments (Figure 3.12B). First, one pellet was washed with a 0.1M Na_2CO_3, pH 11 solution which would remove loosely associated proteins. [^{35}S]B6(1-173) was still present in the pellet fraction after this wash, suggesting that B6 is not loosely associated, but rather is an integral

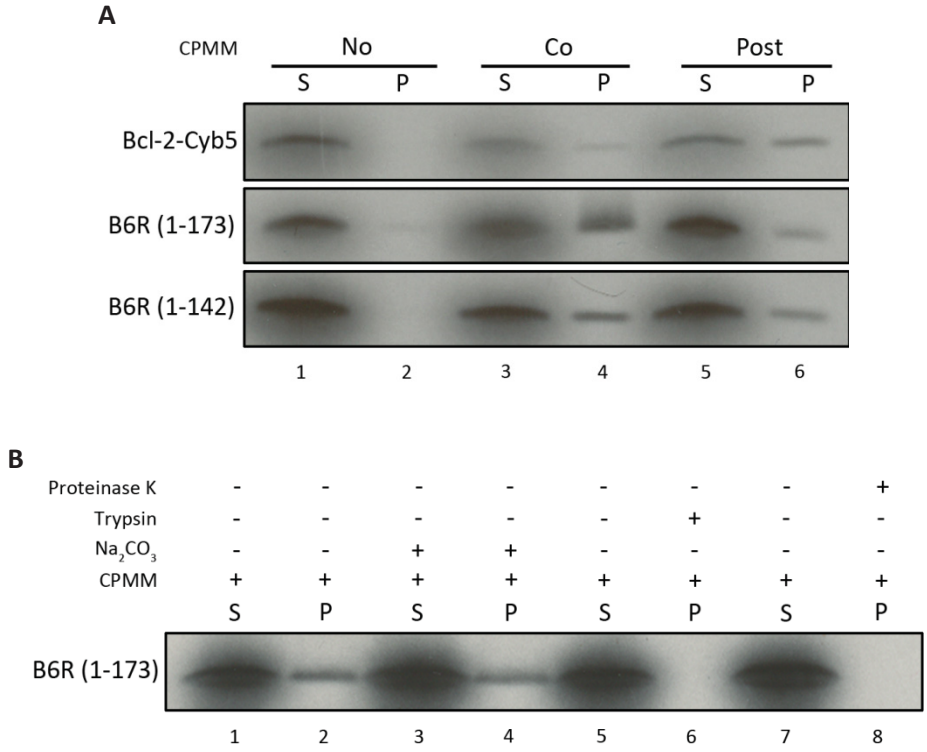

Figure 3.12 B6 behaves like a tail-anchored protein *in vitro*. (A) B6 inserts into canine pancreatic microsomal membranes (CPMM) both co- and post-translationally. TNT-generated [^{35}S]-labelled B6R(1-173), B6R(1-142), and positive control Bcl-2-Cyb5 were not exposed (lanes 1 and 2) or exposed to CPMMs during (lanes 3 and 4) or after termination (lanes 5 and 6) of the TNT reaction. Supernatant (S) and CPMM pellet (P) fractions were separated by centrifugation, resolved by SDS-PAGE, and visualized by autoradiography. **(B)** B6 is an integral protein that inserts with the N-terminus on the outside of the CPMMs. Microsomal pellets of [^{35}S]B6R(1-173) generated in the presence of CPMM were washed with 200 µl of 0.1 M Na_2CO_3, pH 11 to remove loosely associated proteins (lanes 3 and 4), treated with 0.1 mg trypsin for 30 minutes at 30°C (lanes 5 and 6), or treated with 0.1 mg proteinase K (lanes 7 and 8) for 30 minutes at 30°C to assess orientation. Proteins were resolved by SDS-PAGE and visualized by autoradiography.

membrane protein (Figure 3.12B lane 4). Next, to assess the topology of B6, pellet fractions were treated with either trypsin or proteinase K, both of which are broad-spectrum serine proteases. Any protein located on the outside of the microsomes, thus facing the cytosol within a cell, would be exposed to these enzymes and be degraded. Pellets treated with both trypsin and proteinase K no longer contained [^{35}S]B6(1-173), suggesting that the protein was exposed to the enzymes and was degraded (Figure 3.12B lanes 6 and 8). The absence of [^{35}S]B6(1-173) in the pellets was not due to an unsuccessful TNT reaction, as there was [^{35}S]-labelled protein found in the supernatant fractions (Figure 3.12B lanes 5 and 7).

To investigate the relevance of this *in vitro* topology data within the context of infection, we selectively permeabilized cells and visualized them by confocal microscopy. First, HeLa cells were infected with VACV and simultaneously transfected with a plasmid that expresses N-terminally FLAG-tagged B6(1-173) in infected cells only. Following fixation, three different permeabilization methods were performed: 1% NP-40 was used to permeabilize both the plasma membrane and organelle membranes, and 0.025% digitonin or 1 U/mL streptolysin O was used to only permeabilize the plasma membrane. B6 was stained using an anti-FLAG antibody, and ER lumenal PDI was stained using anti-PDI. Both FLAG-B6(1-173) and PDI epitopes were accessible to the corresponding antibodies when the cells were permeabilized with 1% NP-40, as indicated by the successful staining of both proteins (Figure 3.13 a-d). In contrast, PDI was not visible after both digitonin and streptolysin O permeabilization, indicating that the ER membrane was not permeable to the probing antibody (Figure 3.13 g, k). However, the N-terminal FLAG-tag on B6(1-173) was still accessible to the FLAG antibody, meaning that this epitope was within the cytosol of the cell (Figure 3.13 f, j). This data serves to confirm our topology data within the context of infection, and further supports that B6 is a tail-anchored protein.

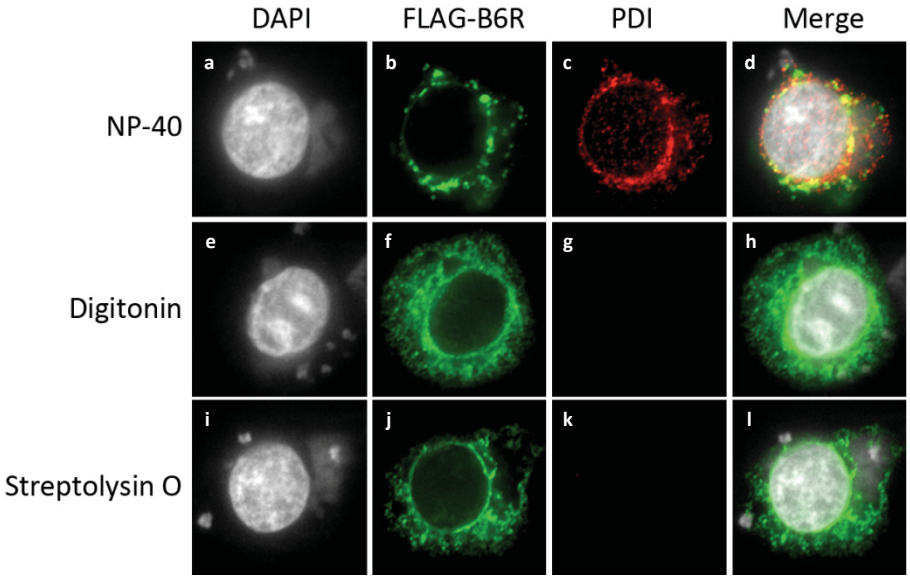

Figure 3.13 The topology of B6 during virus infection corroborates *in vitro* data. Selective permeabilization of infected/transfected HeLa cells was done to assess the membrane orientation of B6 during VACV infection. HeLa cells were infected with VACV at an MOI of 5 and simultaneously transfected with pSC66-FLAG-B6R for 12 hours. Only infected cells will express FLAG-B6R(1-173). Cells were fixed and permeabilized with 1% NP-40 in PBS (a-d), 0.025% digitonin in PBS (e-h), or 1 U/mL streptolysin O (i-l) followed by staining with DAPI to visualize nuclei, anti-FLAG to visualize B6, and anti-PDI to visualize the ER lumen.

3.8 Identification of potential B6 interacting partners. In light of the fact that a number of B6R homologues are annotated as ankyrin-like proteins, it is possible that the function of B6 has to do with some form of protein-protein interaction (118). If we could identify any interacting partners of B6, this would provide key information as to the function of this protein. To do this, we planned to immunoprecipitate (IP) B6 and any potential interacting proteins from infected cell lysates and identify them by mass spectrometry. As we do not have a B6-specific antibody, we chose to generate FLAG-tagged B6 constructs to avoid erroneous protein interactions that are common with EGFP tags. Unfortunately, appending an N-terminal FLAG-tag to the three B6 constructs had an unforeseen problem in terms of protein expression. First we cloned FLAG-B6R(1-173), FLAG-B6R(1-142), and FLAG-B6R(143-173) into the pCDNA3 vector for expression in mammalian cells by transient transfection. To assess the expression of these proteins, 293T cells were transfected with pCDNA3-FLAG-F1L as a positive control along with the three plasmids for 16 hours and whole cell lysates were western blotted for FLAG. While full-length FLAG-B6 was capable of being expressed from this plasmid, we were never able to achieve expression of FLAG-B6(1-142) or FLAG-B6(143-173) (Figure 3.14A). We also sought to generate a recombinant VACV that over-expresses N-terminally FLAG-tagged B6 constructs in place of the TK locus (Figure 2.2). After generating pSC66-FLAG-B6R(1-173) and pSC66-FLAG-B6R(1-142), we used these plasmids for recombinant virus generation in the VACV background (see section 2.5.4). Following purification and amplification, we infected HeLa cells with VACV-FLAG-B6R(1-173) and VACV-FLAG-B6R(1-142) for 12 hours and whole cell lysates were western blotted for FLAG to assess protein expression (Figure 3.14B). While the positive control VACV-FLAG-F1L protein was expressed as expected, there was essentially no expression of FLAG-B6(1-173) (Figure 3.14B). In addition, FLAG-B6(1-142) was found to run at the expected size of 18 kDa, however an additional band was found running at 22-23 kDa (Figure 3.14B). To ensure that the loss of expression

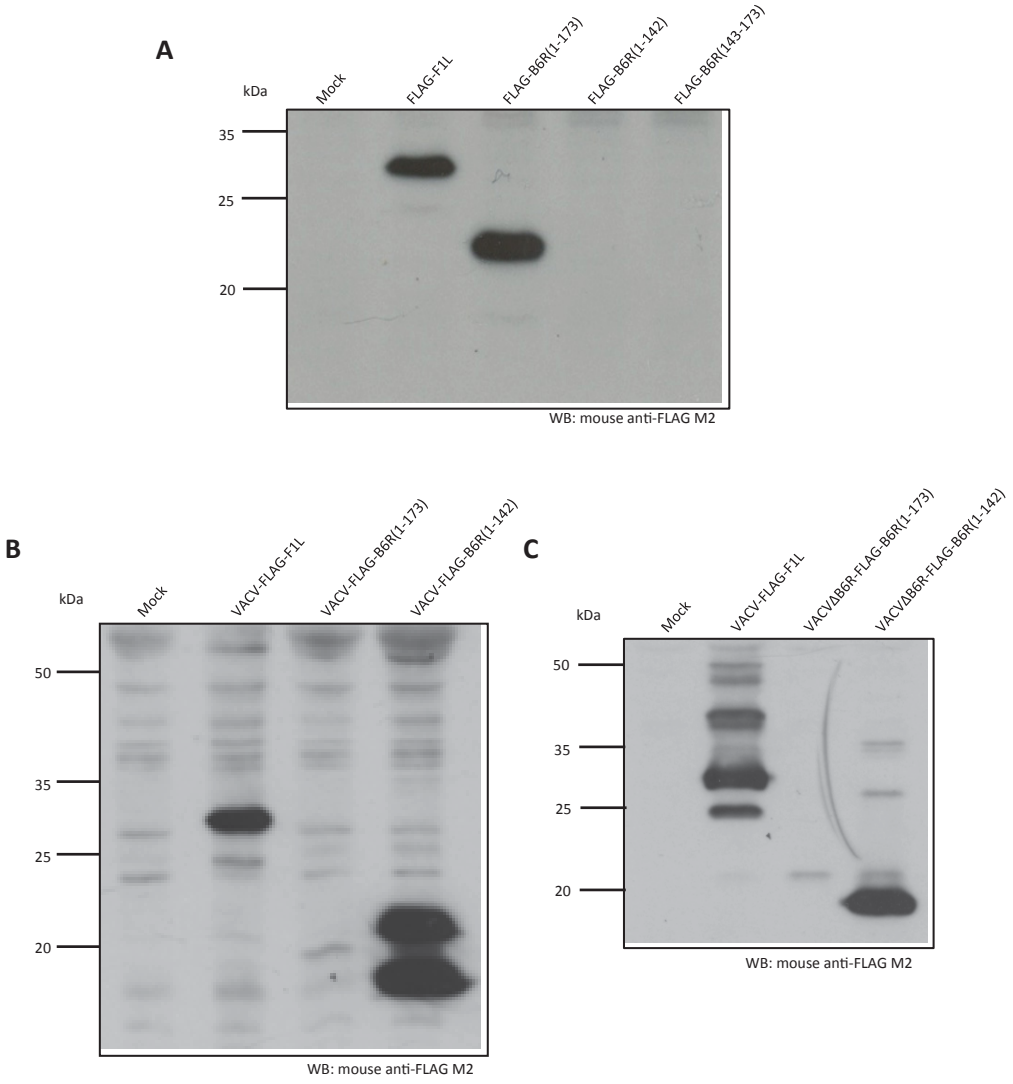

Figure 3.14 Expression of FLAG-tagged B6 constructs during transfection and recombinant VACV infection. (A) 293T cells were mock transfected or transfected with pCDNA3-FLAG-F1L as a positive control, pCDNA3-FLAG-B6R(1-173), pCDNA3-FLAG-B6R(1-142), or pCDNA3-FLAG-B6R(143-173). **(B)** HeLa cells were mock infected or infected for 12 hours with VACV-FLAG-F1L as a positive control, VACV-FLAG-B6R(1-173), or VACV-FLAG-B6R(1-142). **(C)** HeLa cells were mock infected or infected for 12 hours with VACV-FLAG-F1L as a positive control, VACVΔB6R-FLAG-B6R(1-173), or VACVΔB6R-FLAG-B6R(1-142). In all cases, whole cell lysates were resolved by SDS-PAGE and western blotted with mouse anti-FLAG M2.

of FLAG-B6(1-173) was not due to homologous recombination between the FLAG-tagged B6R and the endogenous B6R gene, we next attempted to insert FLAG-B6R(1-173) into the TK locus of the VACVΔB6R-EGFP background. Unfortunately this resulted in the same loss of expression after virus amplification (Figure 3.14C). As such, we moved forward with the mass spectrometry experiment using EGFP-tagged B6.

To identify interacting partners, HeLa cells were mock infected or infected with VACV, VACV-EGFP, or VACV-EGFP-B6R(1-173) for 12 hours. The infected cells were lysed in 1% NP-40 lysis buffer and immunoprecipitated with anti-EGFP. Immune complexes were run on a Hoefer gel to allow maximum separation of bands and stained with "Blue-Silver" G-250 coomassie to visualize all protein bands (Figure 3.15A) (Dr. R. Fahlman, University of Alberta). Antibody heavy and light chains were visible in all samples lanes, but there was no visible band that would correspond to EGFP at ~32 kDa in the VACV-EGFP lane, which may be due to insufficient IP or an issue with EGFP expression from this virus (Figure 3.15A). There was a distinct band running just below the heavy chain in the VACV-EGFP-B6R(1-173) lane, which likely corresponds to the EGFP-B6(1-173) protein (Figure 3.15A). Interestingly, there is another band just below this (~45 kDa) that appears to be unique to the VACV-EGFP-B6R(1-173) lane. We repeated this experiment and instead performed silver staining, which is more sensitive and may visualize weaker protein bands. Again, EGFP did not seem to be detectable, there was a strong band seen where EGFP-B6(1-173) would run, and the same unique bad was visible just below it (Figure 3.15B). Unfortunately this same band can be seen in all of the other lanes, albeit to a much lesser extent, which suggests that it may not be a unique interacting partner of B6.

3.9 Expression of B6 does not affect activation of the classical NFκB pathway. Poxviruses are known for their redundancy in immunomodulatory proteins, and proteins targeting the NFκB pathway are no exception (143, 191). VACV encodes

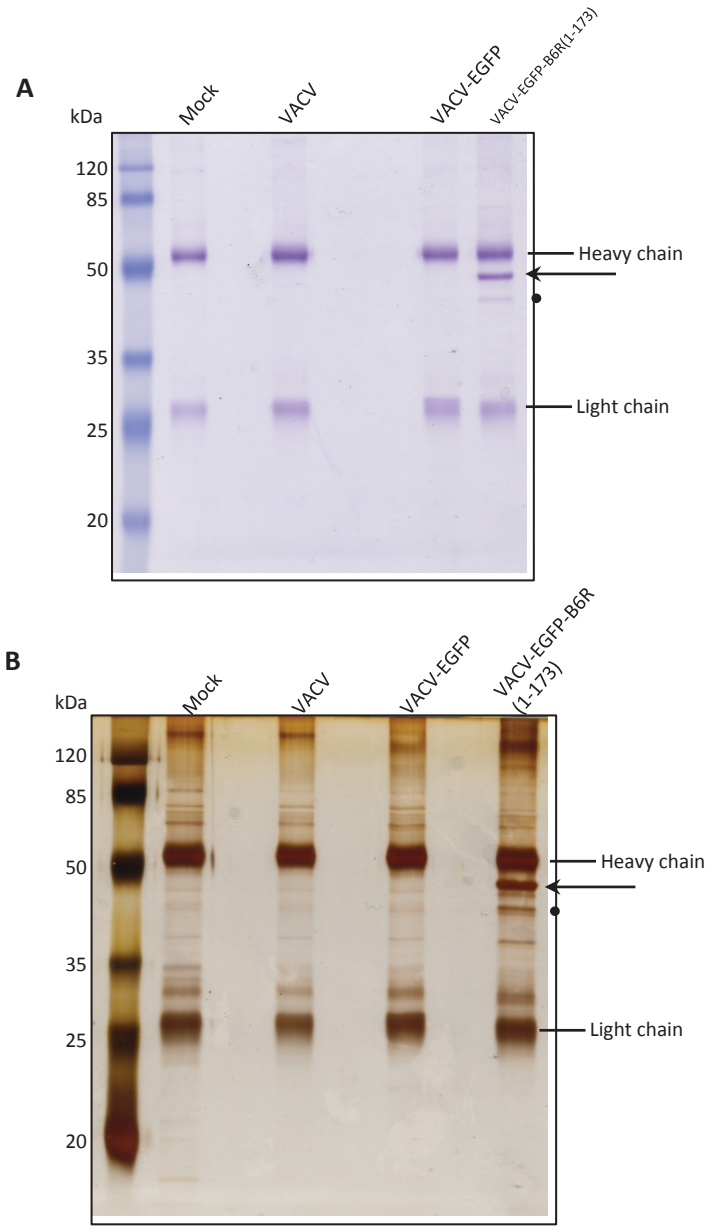

Figure 3.15 Identification of interacting proteins of B6. HeLa cells ($5X10^6$) were mock infected or infected with VACV, VACV-EGFP, or VACV-EGFP-B6R(1-173) at an MOI of 5 for 12 hours, and lysates were immunoprecipitated for EGFP. IP samples were run on a hoefer gel followed by "Blue-Silver" G-250 coomassie staining **(**A) or by silver staining **(**B) to visualize all protein bands. EGFP-B6R(1-173) is indicated by an arrow, potentially distinct bands are designated by a circle, and heavy and light chain are labelled.

four ankyrin/F-box proteins which inhibit the NFκB pathway, although the mechanism has yet to be determined (unpublished, our lab). These proteins contain a variable numbers of ankyrin repeats, as do members of the IκB family, which lead us to investigate whether B6 also functions within this pathway (85). To this end, HeLa cells were mock-transfected or transfected with pEGFP-B6R(1-173) for 12 hours, followed by TNFα stimulation for 20 minutes to activate the classical NFκB pathway. The final step of the pathway, nuclear translocation of the p65 subunit, was observed by immunofluorescence microscopy (Figure 3.16). Mock transfected cells retained p65 within the cytoplasm (Figure 3.16 a-c), and after TNFα stimulation, the cells showed obvious nuclear accumulation of p65 as expected (Figure 3.14 d-f). In the absence of stimulation, cells expressing exogenous EGFP-B6(1-173) displayed p65 solely within the cytoplasm, and upon TNFα stimulation, p65 was found to accumulate in the nucleus in both B6-expressing and non-expressing cells (Figure 3.14 g-l). This data suggests that TNFα stimulation of the classical NFκB pathway, as indicated by the last step of the pathway, is not affected by the expression of B6 in tissue culture conditions.

3.10 Expression of B6 may directly or indirectly affect mitochondrial membrane potential. Though the Bcl-2 family of proteins are typically regarded as mitochondria-associated, it has long been known that members can also localize to the ER where they affect calcium signalling, apoptosis, UPR, and even autophagy (179, 213). With the understanding that apoptosis serves as a potent barrier to virus infection, it seems plausible that VACV may encode an ER-resident protein that serves to inhibit ER-dependent apoptosis induction. Loss of mitochondrial membrane potential ($\Delta\Psi_m$) precedes the release of cytochrome *C*, which ultimately commits the cell to programmed cell death (75, 217). Mitochondrial membrane potential can be measured using TMRE, a cell permeant, positively-charged dye that is readily accumulated within healthy, respiring mitochondria (185). Loss of $\Delta\Psi_m$ leads to the loss of negative charge, thus leading to a decrease in TMRE uptake (185). To investigate the possibility

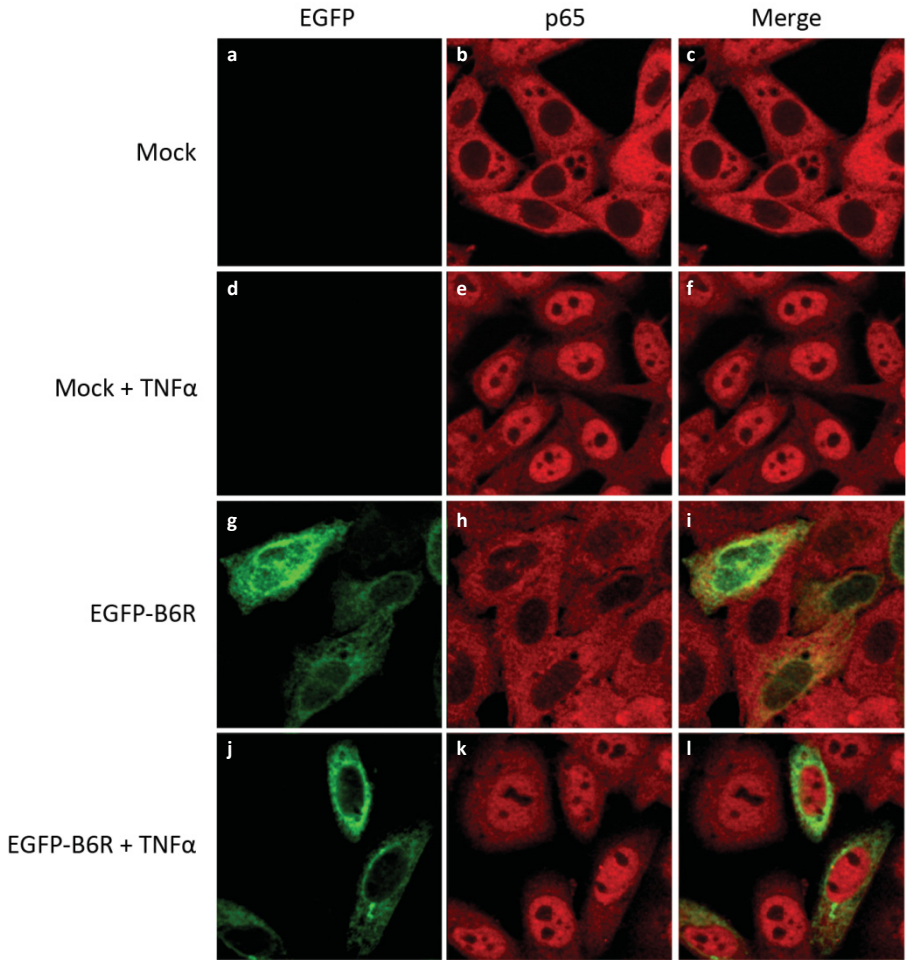

Figure 3.16 Transient expression of B6 does not prevent p65 nuclear translocation upon TNFα stimulation. TNFα-induced p65 nuclear translocation was visualized by immunofluorescence microscopy. HeLa cells were mock transfected (a-f) or transfected with pEGFP-B6R(1-173) (g-l) for 16 hours followed by mock treatment (a-c, g-i) or treatment (d-f, j-l) with 10 ng/mL of TNFα for 20 minutes. Cells were fixed and stained with anti-p65 to visualize NFκB dimers containing this subunit, and B6 was visualized by EGFP fluorescence. The data shown is representative of at least three separate experiments.

that B6 plays a modulatory role in the apoptotic pathway, we examined the levels of TMRE within cells expressing exogenous EGFP-tagged constructs with and without TNFα treatment using flow cytometry.

First we assessed the proportion of TMRE-low cells, which would suggest an effect on $\Delta\Psi_{m,}$ in cells transfected with EGFP alone as a negative control, EGFP-Bcl-2 and EGFP-F1L as anti-apoptotic controls, and the three different EGFP-tagged B6R constructs. Within the same samples, we also assessed the proportions of TMRE-low cells in EGFP-negative cell populations (Figure 3.17). Overall, cells from the EGFP and EGFP-F1L samples had less TMRE-low cells compared to cells expressing EGFP-Bcl-2 or the three B6 constructs. Nonetheless, cells with very low to no EGFP fluorescence, designated the EGFP-negative population, exhibited fairly consistent proportions of TMRE-low cells among the different constructs, ranging from approximately 15-30%, as seen by the black bars in Figure 3.17. The slight variance could be due to cells with very low EGFP expression, which may alter TMRE levels. In contrast, cells expressing the indicated EGFP constructs exhibited varying proportions of TMRE-low cells, depending on the construct involved (Figure 3.17, grey chequered bars). Ten to twenty percent of cells expressing EGFP alone exhibited low TMRE levels, while only 2-8% of those expressing EGFP-F1L showed low TMRE uptake, which supports the role of F1L as an anti-apoptotic protein. Intriguingly, 35-45% of cells expressing EGFP-Bcl-2 demonstrated low TMRE levels; when comparing EGFP-positive and EGFP-negative counterparts, only the EGFP-Bcl-2 populations displayed significantly different proportions of TMRE-low cells based on t-test analysis ($p=0.0341$). Notably, cells expressing the three different B6 constructs showed similar TMRE-low proportions in both EGFP-negative and EGFP-positive populations; however, the range was similar to that of EGFP-Bcl-2-expressing cells. It seems, then, that expression of B6 may be causing the same phenomenon as Bcl-2.

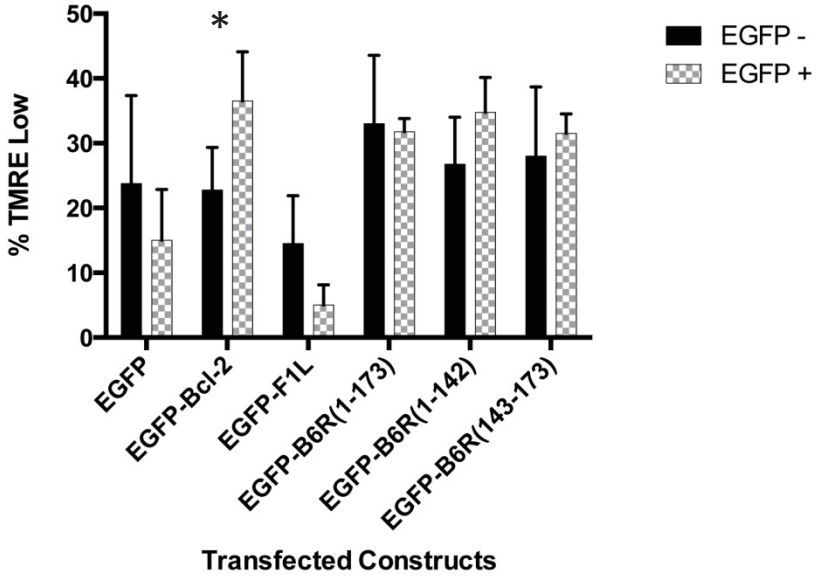

Figure 3.17 Differences in mitochondrial membrane potential in unstimulated cells. Comparison of the percentage of cells exhibiting low TMRE levels, indicative of a loss in mitochondrial membrane potential, in the absence of treatment. Black bars represent cells with very low to no expression of EGFP constructs while grey chequered bars represent cells expressing the indicated EGFP construct. Percentages were calculated as number of TMRE low cells divided by total number of EGFP negative or EGFP positive cells. Significant differences between EGFP negative and EGFP positive cells are denoted by an asterisk (*). Values used to generate this histogram are from at least three separate experiments.

Next we sought to determine if the expression of the three B6 constructs affected the loss of $\Delta\Psi_m$ upon treatment with TNFα. To this end, HeLa cells transiently transfected with the EGFP plasmids for 12 hours were treated with or without 10 ng/mL of TNFα along with 5 μg/mL of CHX to prevent translation of pro-survival genes. The cells were stained with TMRE and quantified by flow cytometry (Figure 3.18). Prior to TNFα treatment, 84% of cells expressing EGFP alone were also TMRE-high, which decreased to 25% after TNFα treatment (Figure 3.18 a, b, upper right quadrant). In the case of EGFP-Bcl-2 expressing cells, there appears to be two different EGFP-positive populations: the low-expressing cells which appear to exhibit very few TMRE-low members, and the high-expressing cells which include many TMRE-low cells (Figure 3.18 c, lower right quadrant). This pattern was also seen in cells treated with TNFα, but with only a 10% decrease in EGFP-positive, TMRE-high cells (Figure 3.18 d). While very few cells expressing EGFP-F1L had low TMRE levels both before and after TNFα treatment, a 12% decrease in TMRE high cells was seen in EGFP-F1L expressing cells. However, it appears that the loss in TMRE was mostly confined to cells with lower expression of EGFP-F1L (Figure 3.18 e, f). These results are typical of anti-apoptotic proteins such as Bcl-2 and F1L. Again, cells expressing EGFP-B6(1-173) somewhat mimic the effects of EGFP-Bcl-2, in that in the absence of TNFα, there was a large population of high EGFP-expressing cells that had low TMRE levels (Figure 3.18 g lower right quadrant). Upon TNFα stimulation, there was a 47% decrease in EGFP-positive, TMRE-high cells, suggesting that the expression of B6 did not interfere with the loss of $\Delta\Psi_m$ (Figure 3.18 g, h). Cells expressing EGFP-B6(1-142) showed a large number of TMRE-low cells, with a slight increase in TMRE levels in the higher EGFP-expressing cells (Figure 3.18 i, lower right quadrant). With TNFα treatment, there was a decrease of 40% in TMRE-high cells in the EGFP-B6(1-142)-expressing cells. Similar results were seen in cells expressing EGFP-B6(143-173), with only 71% TMRE-high cells in the absence of TNFα, and a reduction of 50% TMRE-high cells upon treatment with TNFα (Figure

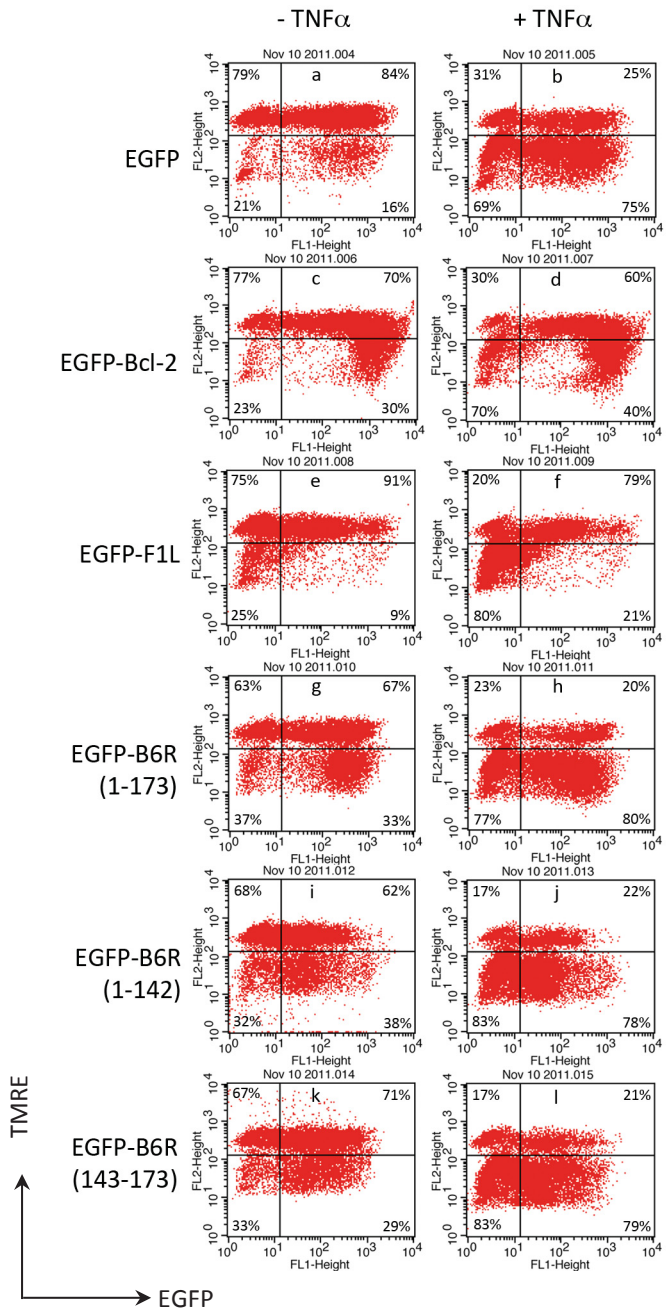
- TNFα
+ TNFα
EGFP
EGFP-Bcl-2
EGFP-F1L
EGFP-B6R (1-173)
EGFP-B6R (1-142)
EGFP-B6R (143-173)
TMRE
EGFP
FL1-Height
FL2-Height
Nov 10 2011.004
Nov 10 2011.005
Nov 10 2011.006
Nov 10 2011.007
Nov 10 2011.008
Nov 10 2011.009
Nov 10 2011.010
Nov 10 2011.011
Nov 10 2011.012
Nov 10 2011.013
Nov 10 2011.014
Nov 10 2011.015
79% a 84%
21% 16%
31% b 25%
69% 75%
77% c 70%
23% 30%
30% d 60%
70% 40%
75% e 91%
25% 9%
20% f 79%
80% 21%
63% g 67%
37% 33%
23% h 20%
77% 80%
68% i 62%
32% 38%
17% j 22%
83% 78%
67% k 71%
33% 29%
17% l 21%
83% 79%

Figure 3.18 TNFα induces loss of mitochondrial membrane potential in cells expressing B6. HeLa cells were transfected with pEGFP (a,b), pEGFP-Bcl-2 (c, d), pEGFP-F1L (e, f), pEGFP-B6R(1-173) (g, h), pEGFP-B6R(1-142) (i, j), or pEGFP-B6R(143-173) (k, l) for 14 hours, and subsequently mock-treated (a, c, e, g, I, k) or treated (b, d, f, h, j, l) with 10 ng/mL TNFα and 5 µg/mL CHX for 4 hours to induce apoptosis. Differences in mitochondrial membrane potential were assessed by flow cytometry as measured by the loss in TMRE. Percentages represent the number of TMRE high (upper quadrants) or TMRE low (lower quadrants) cells out of the total EGFP-positive (right quadrants) or EGFP-negative (left quadrants) populations. Data were acquired on 20,000 cells and analyzed using CellQuest software. The data shown is representative of at least three separate experiments.

3.18 k, l). Overall, it seems as though cells expressing the three B6 constructs still undergo TNFα-induced loss of $\Delta\Psi_m$, however there may be a correlation between expression levels and $\Delta\Psi_m$ like that exhibited by Bcl-2-expressing samples.

After performing the experiment described above (Figure 3.18) four times, the data were compiled to allow us to compare the effects of TNFα stimulation on both non-transfected and transfected cells. To ensure that the TNFα treatment was consistently effective in each of the samples, we calculated the loss of TMRE-high cells with very little to no EGFP expression (Figure 3.19A). One-way ANOVA analysis of these results confirmed that there were no significant differences among these losses, which supports that the efficacy of the TNFα treatment in each sample was consistent (Figure 3.19A). In contrast, the loss of TMRE-high cells in EGFP-positive populations was significantly different among the different constructs, as indicated by a p-value of <0.0001 based on one-way ANOVA analysis (Figure 3.19B). Cells expressing EGFP alone displayed up to 65% loss in TMRE-high cells, while those expressing EGFP-Bcl-2 or EGFP-F1L only underwent up to a 10% loss. Interestingly, all three of the B6 constructs showed the same levels of TMRE-high loss, which was approximately 35-40%. This somewhat intermediate loss compared to EGFP alone and EGFP-Bcl-2/EGFP-F1L suggests that both full-length B6 as well as the two mutant constructs confer mild protection from loss of $\Delta\Psi_m$ induced by TNFα. This may be a direct or indirect effect of the primary role that B6 plays.

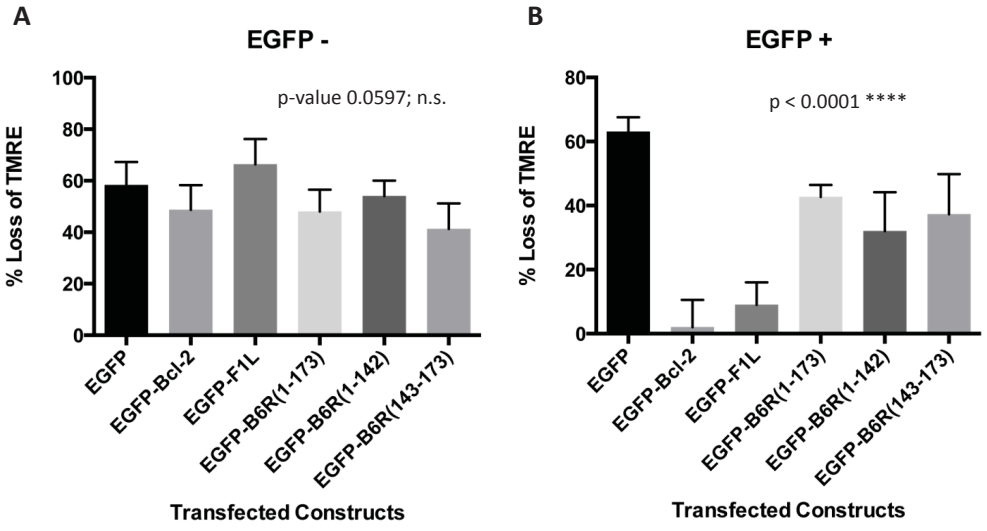

Figure 3.19 Ectopic expression of B6 confers mild protection from TNFα-induced TMRE loss. To assess the induction of apoptosis as indicated by a loss of TMRE, the percentage of TMRE-positive cells in TNFα-stimulated cells was subtracted from the percentage of TMRE-positive cells in unstimulated cells for both EGFP negative **(A)** and EGFP positive **(B)** populations. One-way ANOVA analysis was performed to compare TMRE loss among the different constructs for each population and p-values are listed above the histograms. Not significant, n.s., very significant, ****.

Chapter 4

Discussion

Historically, poxviruses have greatly impacted the lives of humans for both the good and the bad. VARV, the causative agent of smallpox, is responsible for killing more people than all other infectious diseases combined (71). The silver lining to this story is that the work done by Edward Jenner and William Woodville with VARV paved the way for modern day vaccination (11, 71). The global eradication of VARV from the human population in the 1970s through the dedicated efforts of the WHO marks one of the greatest achievements of the medical field (71, 201). Today we still benefit from scientific research done with poxviruses in the form of recombinant gene vectors, oncolytic therapies, and vaccine vector therapies (42, 145, 219). Studying these highly successful viruses has also provided a deeper understanding of the basic biology of viruses and immunology, the complexities of virus-host interactions, and the strategies utilized by viruses in general (55).

Poxviruses are notorious for their ability to interfere with the host immune response, made possible by their immense coding capacity (146, 191). Nearly half of the poxvirus genome is dedicated to encoding immunomodulatory proteins that are typically located within the termini (116, 146). The terminally-located B region of genes encoded by VACV includes, but is not limited to, a variety of immune evasion genes (200). While most genes found within the B region have been at least partially characterized, B6R has yet to gain any literary attention. An initial screen of the VACV genome identified B6 as a protein containing a putative C-terminal TMD (Dr. Michele Barry, unpublished). Based on the location and composition of the predicted TMD, we predicted that B6 is a characteristic TA protein that localizes to an intracellular membrane, such as the ER. We also proposed that, based on the position of the gene within the VACV genome, B6 may serve an immunomodulatory role during virus infection.

4.1 Summary of results. The present study demonstrated that while B6 and its homologues are actively expressed early during virus infection, its absence does

not attenuate virus growth *in vitro* (Figure 3.1, 3.2, 3.3). In addition to a C-terminal TMD, it is possible that B6 adopts a structure rich in alpha-helices (Figure 3.4, 3.5). We showed that B6 localizes to regions of the ER via the C-terminal 30 amino acids during both infection and transfection (Figure 3.6, 3.7, 3.8). We also demonstrated that B6 behaves like a TA protein, inserting post-translationally into the ER membrane with the N-terminus facing the cytosol (Figure 3.12, 3.13). Unexpectedly, we discovered the formation of ER- and B6-containing structures on the surface of infected cells when full-length B6 is over-expressed (Figure 3.8, 3.9, 3.10, 3.11). Functional analyses began by attempting to identify any B6 interacting partners, however our methods were unsuccessful (Figure 3.15). While exogenous expression of B6 did not prevent TNFα-induced activation of the classical NFκB pathway, it did appear to have an effect on mitochondrial membrane potential (Figure 3.16, 3.17, 3.18, 3.19). Together, this study provides evidence to suggest potential functions of B6 during VACV infection worth investigating in the future.

4.2 Initial characterization of B6. The poxvirus replication cycle is comprised of three temporal classes of gene expression: the early genes are involved in DNA replication, intermediate transcription, and virus-host interactions; intermediate genes are largely late gene transcription factors; late genes include those involved in structure and morphogenesis along with all of the machinery required for initiating the next infectious cycle (31, 146). The B6R homologue found in ECTV, ECTV161, exhibits the same expression pattern as that of ECTV004, a typical early protein of unknown function (244). It is therefore reasonable to believe that ECTV161, and presumably VACV-B6R, is involved in one of the functions ascribed to this temporal class of genes. While this does not significantly narrow down the potential roles of B6, these results, coupled with the fact that B6 has never been identified as a virion component, suggest that B6 is synthesized *de novo* early during virus infection, and is less likely to play a role in virion structure or morphogenesis. It is likely that B6R homologues found in

other orthopoxviruses are also expressed at early times of infection. However, it would be interesting to investigate whether the homologues that have undergone fragmentation in VARV strains and HSPV, are actually expressed at all. This information would provide useful insight as to the requirement of B6 for infection of different hosts.

Optimal conditions for growth and lack of an immune system in tissue culture can mask the effects of removing immunomodulatory genes from viruses. For example, removal of the VACV-N1L ORF has no effect on virus growth *in vitro*, however the knockout virus is attenuated *in vivo* (9). Thus, the indistinguishable growth patterns of VACV and VACVΔB6R-EGFP at both high and low MOI doesn't necessarily mean that the gene is dispensable. This result implies that B6 likely does not serve an essential role, such as expression, DNA replication, structure, or morphogenesis. Removing such a gene would attenuate or halt the growth of the virus even in tissue culture. In doing a single-step growth curve, we were able to observe the ability of VACV and VACVΔB6R-EGFP to replicate and generate progeny virions to the same extent (73). The multi-step growth curve also assessed replicative success, however it forces any defects masked by a high MOI to become obvious. A multi-step growth curve also indicates whether the progeny virions are capable of producing secondary infections. Thus, we can only conclude that B6 does not play a role that is required for growth in BGMK cells under optimal conditions *in vitro*. While these results lend further support to our hypothesis that B6 plays an immunomodulatory role, there still exists the potential that B6 is involved in host range (30, 137). To investigate this possibility, one could repeat these growth curves in a number of different cell lines to assess the ability of VACVΔB6R-EGFP to grow compared to VACV.

Tail-anchored proteins comprise a vast array of members that serve a multitude of functions (167). They are found in all domains of life, including

viruses (167). B6, like all TA proteins, contains a C-terminal TMD followed by a short tail (167). Thus, it came as no surprise that full-length B6 presented as an integral membrane protein that, like our positive control Bcl-2-Cyb5, was capable of inserting into microsomal membranes post-translationally (28). Though both proteins were also detected in microsomal pellets added during the transcription-translation reaction, these experimental conditions cannot discern true co-translational from post-translational insertion after ribosomal release. To better understand the mechanism of B6 insertion, one could test the insertion of B6 into membranes in systems containing different sets of chaperones and co-chaperones of the three known pathways, and even within systems devoid of ATP (50). Tail-anchored proteins are also united by their topology, such that the functional N-terminus faces the cytosol (167). We were able to confirm that B6 exhibits this topology both *in vitro* and during virus infection. Surprisingly, B6(1-142), which lacks the C-terminal TMD, was found in microsomal pellet fractions in both co- and post-translational conditions. We speculate that the slightly hydrophobic region spanning amino acids 82-100 could be responsible for this observation under saturated conditions. In future experiments, we could wash pellets containing B6(1-142) with the Na_2CO_3 solution to determine if this truncated protein is integral or just loosely associated with the microsomes. Either way, our results confirm that B6 is a bonafide tail-anchored protein, suggesting that its function relies on cytosolic localization of the N-terminus.

4.3 B6 binding partners have yet to be identified. Ankyrin domains are structural domains comprised of numerous alpha-helices that mediate protein-protein interactions (118). Considering that a number of B6 homologues are annotated as ankyrin-like proteins, it is not surprising that the secondary structure of B6 is predicted to be rich in alpha-helices (Figure 3.4). However, specifically looking for ankyrin motifs in the amino acid sequence of B6 reveals no obvious hits. Like other poxviral proteins, B6 may adopt an ankyrin-like fold in spite of its lack of sequence similarity, like how F1 adopts a Bcl-2-like fold with

very limited sequence similarity (114). Solving the crystal structure of B6 would be helpful to determine if it adopts an ankyrin-like structure.

Protein function often relies on interactions with other proteins, whether strong, weak, transient, or even within a larger complex of many proteins (232). We sought to identify proteins that interact with B6, however, our method of co-immunoprecipitating EGFP-B6(1-173) and any potential interacting partners from infected cell lysates proved unsuccessful. It is possible that interacting partners of B6 are only expressed at very low levels. Thus, an alternative, more sensitive approach would prove useful. Possible alternatives would be a yeast two-hybrid system, which would ultimately require at least a prediction as to what the interacting partner is, or a proteome chip (15, 128, 142). In a study done in 2000, a genome-wide screen of protein-protein interactions was performed on VACV, however B6 was not identified as having interactions with other viral proteins (136). Should B6 exhibit interactions with other proteins during virus infection, it may be more likely to involve host cell proteins. The case could also be that the protein-protein interactions exhibited by B6 are weak or even transient, making it very difficult to capture by IP. The same IP experiment could be done with the addition of cross-linkers to covalently join interacting proteins that normally interact weakly or transiently, thereby allowing us to pull them down with EGFP-B6(1-173) (15). Another important consideration would be the effect of over-expressing B6 on interactions or the formation of protein complexes. In this case, it would be beneficial to perform the experiments using antibodies raised to endogenous B6 itself, which could also circumvent our issues with expression of FLAG-tagged B6 from plasmids and viruses. This would allow us to IP endogenously expressed B6 within the context of infection, thus allowing the native post-translational modifications, interactions, and complex formations to be maintained.

While we were able to generate plasmids and viruses that express EGFP-tagged B6 constructs, expression of the FLAG-tagged counterparts was inconsistent. There could be an issue with protein stability that is remedied by the EGFP-tag but not the FLAG-tag. In this instance, we could use a B6-specific antibody to assess endogenous B6 expression. Though it is unlikely that the FLAG-tag itself is affecting protein expression levels, a different approach would be to append different N-terminal tags such as hemagglutinin (HA), hexahistidine (His), or Myc. It is widely known that the transient expression of poxvirus genes in uninfected mammalian cells can be very difficult to achieve due to inefficient codon usage (7). Expression deficiencies can be remedied by codon optimization of genes for expression, as it also removes other potentially problematic features such as cryptic splice sites or mRNA instability motifs (7). Considering that we were able to achieve expression of FLAG-B6(1-173) from the pCDNA3 plasmid, codon optimization may or may not solve the lack of expression of the two mutants. In addition, we observed the opposite within our recombinant viruses, in that FLAG-B6(1-142) expresses while expression of FLAG-B6(1-173) was lost after virus amplification. Again, an antibody raised to endogenous B6 would be an effective alternative.

4.4 B6 appears to localize to the ER. Using confocal microscopy, we were able to observe the sub-cellular localization of B6 during both transient expression and virus infection. The length of the predicted TMD of B6 is 23 amino acids long, and the only charged residue is a lysine on the 5' end, which suggests that B6 localizes to a fairly indiscriminate membrane such as the ER (193). Though our live cell images of full-length B6 showed only moderate overlap with ER tracker, it still exhibited an ER-like distribution reminiscent of the ER staining pattern in mock cells. We speculate that upon transfection, the RER of the cells expanded to accommodate the amount of protein synthesis occurring, while the SER contracted (42, 234). It is possible that ER tracker preferentially stains RER, which would explain its accumulation near the nucleus where the majority of the B6

protein was also localized. Removing the TMD rendered B6 cytoplasmic, demonstrating that this region is responsible for ER localization. Interestingly, infected cells were visibly rounded up but still exhibited a visible accumulation of ER tracker to one side of the nucleus, which may be due to an increase in RER or perhaps overlaps with the virus factory.

The ER is an extensive, heterogeneous organelle that can be described as a network of sub-organelles connected by a continuous lumen (126, 234). As such, it is not surprising that ER tracker is incapable of reliably staining the entirety of the ER under all conditions. Though our preliminary data supports that B6 is localizing to the ER, further analysis by confocal microscopy would require staining of additional ER markers to assess the precise localization. Sub-cellular fractionation would also be useful in determining the precise location of B6 (1). Fractions could be western blotted for subdomain-specific proteins to determine with which proteins B6 predominantly sediments. It is still possible, however, that B6 is simply found throughout the entire ER network. Localization to the ER may implicate B6 as being involved in an ER-related process like the UPR, calcium signalling, or in virus factory formation or virion morphogenesis (16, 36, 98, 188). However, there are ER-resident VACV proteins that have nothing to do with ER-specific processes, such as the NFκB inhibitor M2L (74, 91). In this case, it is possible that ER localization is optimal for M2L to prevent the ERK2 pathway (74).

4.5 Over-expression of B6 during virus infection induces ER morphological changes. The most unexpected, and perhaps most perplexing, result of this study was the formation of ER structures at the cell periphery at early times of infection with VACV-EGFP-B6R(1-173). Though we first observed the formation of the ER- and B6-containing structures in only half of the infected cells, this can be explained by the fact that we used a larger volume of inoculum, meaning that the infections were not closely synchronized within those samples. Based on our time-course images, it seems that some of the cells still exhibited the 6 hpi

phenotype, while others had already undergone dramatic ER morphological changes to the 8 hpi phenotype. In contrast, these ER structures were never observed throughout infection with VACV, which expresses endogenous B6, and VACV devoid of B6. From this we can deduce that it is the over-expression of B6 that is inducing the formation of these unique ER structures. This phenomenon has never been reported within the context of poxvirus infection, and it is difficult to speculate on the mechanisms behind such dramatic changes. Of note, these surface blebs were slightly reminiscent of apoptotic blebbing, though we cannot confirm this from our data (49).

The fact that these unique ER structures are the sole location of over-expressed EGFP-B6(1-173) for the first 6 hours of infection is also remarkable. Immediately upon cell infection, early gene transcription begins via the packaged viral transcription machinery, and expression of EGFP-B6(1-173) is driven by the synthetic poxviral early/late promoter (31, 37). While transcription of B6 could theoretically occur very close to the plasma membrane at very early time points, we never observe EGFP-B6(1-173) presumably in transit to these ER structures from 2-6 hpi. It would be informative to perform live cell imaging of cells infected with this same recombinant virus at additional time points during early stages of virus infection to determine where EGFP-B6(1-173) is being synthesized when under control of the synthetic poxviral promoter. After 6 hpi, both B6 and PDI exhibit characteristic ER distribution patterns, which at late times of infection accumulate in regions where the virus factory is. As several lines of study have suggested, the ER likely serves as the origin of membrane crescents at early stages of morphogenesis, which occur within the virus factories (98, 134). Thus, it is not surprising that the ER, along with ER resident proteins such as B6, were found in close proximity to virus factories at 12-24 hpi.

In addition to the formation of PDI-containing blebs on the cell surface, the over-expression of B6 also caused an exaggerated nuclear localization of PDI.

There was a slight increase in nuclear PDI when cells were infected with parental VACV, and even less so during VACVΔB6R-EGFP infection, which potentially implicates B6 in this phenomenon. Though localization of PDI isomers have been documented on both the cell surface and within the nucleus, the physiological relevance of these non-ER locations is still under investigation (224). Studies have shown that the redox action of PDI does play a role in these different locations (53, 224, 231). Cell surface localization has yet to be described in the context of infection, so we cannot discount that these results may be an artefact of the methods and recombinant virus we used. Three separate studies were done to identify all of the viral proteins within the VACV MV and EV, and B6 was not identified in any of them (45, 162, 173). It is therefore unlikely that EGFP-B6(1-173)-containing structures are from the MV or EV envelopes of infecting virions. Thus, there is some unknown mechanism underlying the mis-localization of over-expressed B6 along with ER proteins like PDI, to the cell surface. Such dramatic morphological changes could be the result of manipulations of ER structural proteins like RTN, atlastin, or DP1/Yop1p family proteins (59, 76). It would be interesting to test for potential interactions of B6 with any of these proteins.

4.6 Ectopic expression of B6 causes a loss of mitochondrial membrane potential. The immunomodulatory repertoire of poxviruses includes many redundancies, whereby numerous proteins target the same immune pathway (191, 200). Though VACV inhibitors of both apoptosis and the NFκB pathway have already been characterized, it is still possible that other proteins target these pathways as well (209, 244). Expression of B6 did not have an effect on TNFα-induced activation of the NFκB pathway under our experimental conditions; however, we did not assess the IL-1β-induced arm of this pathway (85). We also assessed the induction of the intrinsic apoptotic pathway in the presence of B6 upon TNFα treatment by looking at the loss of $\Delta\Psi_m$. While this is considered an acceptable indicator of the induction of apoptosis, it would still be

interesting to see if downstream events such as caspase-3 and poly(ADP-ribose) polymerase (PARP) cleavage are affected as well (217). Nonetheless, we are able to extract some interesting information from the $\Delta\Psi_m$ data. As expected, EGFP alone did not protect against TNFα-induced loss of $\Delta\Psi_m$, while cellular Bcl-2 and VACV-F1L conferred protection. Intriguingly, full-length B6 as well as the C-terminus and N-terminus alone only underwent an intermediate loss in $\Delta\Psi_{m.}$ This result implies that full-length B6, and surprisingly the N-terminus and C-terminus alone, are capable of reducing the loss of $\Delta\Psi_m$ experienced by cells upon TNFα stimulation, though the mechanism is not known.

Examining the effect of expression alone on TMRE uptake by cells provides some interesting information as well, which may or may not account for the intermediate loss of $\Delta\Psi_m$ caused by TNFα. Cells expressing EGFP-Bcl-2 exhibited two phenotypes depending on the level of protein expression: cells with very high expression exhibited low levels of TMRE, while those with lower Bcl-2 levels retained high levels of TMRE. This illustrates that over-expression of Bcl-2 ultimately causes a loss of $\Delta\Psi_m$, which is contrary to its ascribed anti-apoptotic function. The fact that full-length B6 caused the same expression level-dependent effect on $\Delta\Psi_m$ loss suggests that B6 may function like the cellular anti-apoptotic protein Bcl-2. This could also explain why B6 was able to provide intermediate protection against TNFα-induced loss in $\Delta\Psi_{m.}$

It has long been known that in addition to its role at the mitochondria, Bcl-2 is capable of preventing apoptosis at the ER (89, 179, 213). In this capacity, Bcl-2 exhibits a functional interaction with the ER membrane channel IP3R, which causes a slow leak of calcium from the ER lumen to the cytosol (179, 180). In essence, Bcl-2 decreases the pool of ER calcium that could potentially induce apoptosis at the mitochondria, thus desensitizing the cell to calcium-induced $\Delta\Psi_m$ and apoptosis (179). It is possible that B6 also functions to prevent pro-apoptotic calcium signalling from the ER, though its anti-apoptotic potency is less

than that of Bcl-2. The over-expression of both Bcl-2 and B6 appears to promote a slight loss of $\Delta\Psi_m$, which could be via the same mechanism, however we cannot speculate on this based on the results of this study. While expression of the N-terminus and C-terminus of B6 alone did not exhibit the same expression-dependent loss in $\Delta\Psi_m$, these two proteins still confer similar protective effects as their full-length counterpart. Once the function of full-length B6 is determined, it will be interesting to see how our observations of the two mutants add to the story.

4.7 Conclusions. The results of the present study provide information regarding the potential role of VACV-encoded B6 during virus infection. At early times of infection, artificially over-expressed B6 localizes to regions of the ER via the C-terminal TMD, and causes both the formation of cell surface structures, reminiscent of apoptotic blebbing, and induces a decrease in $\Delta\Psi_m$. At later times of infection, the ER surface structures are no longer present, and B6 accumulates around the nucleus near the virus factory. Expression of B6 is also able to moderately protect against TNFα-induced loss in $\Delta\Psi_m$. As to whether the primary role of B6 is in ER morphology or in modulating ER signalling events, we cannot say based on the present study. The observed phenomena were not seen under physiological conditions, but these exaggerated effects likely speak to the regular function performed by B6. Future work focused on dissecting the mechanisms underlying B6 effects on ER morphology and $\Delta\Psi_m$ will certainly shed light on the importance of this ER-resident virus protein.

In line with our original hypothesis that B6 serves an immunomodulatory role, future work with B6 in animal models is crucial. We attempted to generate a gene knockout in ECTV (ECTVΔ161-EGFP) to study the B6R homologue in a mouse model; however, we were not able to successfully remove the gene using our methods (66, 237). Nonetheless, generating a knockout virus in the future will allow us to assess any differences in virulence, pathogenicity, and virus spread in the absence of the B6 homologue (70). These results will confirm a role

for B6 in immune modulation, and demonstrate if the virus requires it at all. Identifying interacting proteins will also provide key information as to the function of B6, whether it is required or not. Given the fact that both VARV and HSPV homologues have undergone fragmentation and mutations that have likely rendered them pseudogenes, it is entirely possible that B6 was required by the ancestral virus of the *Orthopoxvirinae,* but has lost its necessity across divergence and evolution (79, 223). Continued work on VACV-B6R will allow us to better understand how these viruses are modulating the host cell and through what mechanism. This will also shed light on the evolutionary conservation of species-specific genes among poxvirus members (79).

Chapter 5

References

1. **Alberts, B., Johnson, A., Lewis, J.** 2002. Fractionation of Cells, Molecular biology of the cell. Garland Science, New York.
2. **Alcami, A.** 2003. Viral mimicry of cytokines, chemokines and their receptors. Nature reviews. Immunology **3:**36-50.
3. **Alcami, A., and G. L. Smith.** 1992. A soluble receptor for interleukin-1 beta encoded by vaccinia virus: a novel mechanism of virus modulation of the host response to infection. Cell **71:**153-167.
4. **Alcami, A., J. A. Symons, P. D. Collins, T. J. Williams, and G. L. Smith.** 1998. Blockade of chemokine activity by a soluble chemokine binding protein from vaccinia virus. Journal of immunology **160:**624-633.
5. **Altschul, S. F., W. Gish, W. Miller, E. W. Myers, and D. J. Lipman.** 1990. Basic local alignment search tool. Journal of molecular biology **215:**403-410.
6. **Banadyga, L., K. Veugelers, S. Campbell, and M. Barry.** 2009. The fowlpox virus BCL-2 homologue, FPV039, interacts with activated Bax and a discrete subset of BH3-only proteins to inhibit apoptosis. Journal of virology **83:**7085-7098.
7. **Barrett, J. W., Y. Sun, S. H. Nazarian, T. A. Belsito, C. R. Brunetti, and G. McFadden.** 2006. Optimization of codon usage of poxvirus genes allows for improved transient expression in mammalian cells. Virus genes **33:**15-26.
8. **Barry, M., and R. C. Bleackley.** 2002. Cytotoxic T lymphocytes: all roads lead to death. Nature reviews. Immunology **2:**401-409.
9. **Bartlett, N., J. A. Symons, D. C. Tscharke, and G. L. Smith.** 2002. The vaccinia virus N1L protein is an intracellular homodimer that promotes virulence. The Journal of general virology **83:**1965-1976.
10. **Bawden, A. L., K. J. Glassberg, J. Diggans, R. Shaw, W. Farmerie, and R. W. Moyer.** 2000. Complete genomic sequence of the Amsacta moorei entomopoxvirus: analysis and comparison with other poxviruses. Virology **274:**120-139.
11. **Baxby, D.** 1979. Edward Jenner, William Woodville, and the origins of vaccinia virus. Journal of the history of medicine and allied sciences **34:**134-162.
12. **Baxby, D.** 1977. The origins of vaccinia virus. The Journal of infectious diseases **136:**453-455.
13. **Beg, A. A., and A. S. Baldwin, Jr.** 1993. The I kappa B proteins: multifunctional regulators of Rel/NF-kappa B transcription factors. Genes & development **7:**2064-2070.
14. **Bengali, Z., A. C. Townsley, and B. Moss.** 2009. Vaccinia virus strain differences in cell attachment and entry. Virology **389:**132-140.
15. **Berggard, T., S. Linse, and P. James.** 2007. Methods for the detection and analysis of protein-protein interactions. Proteomics **7:**2833-2842.
16. **Berridge, M. J.** 2002. The endoplasmic reticulum: a multifunctional signaling organelle. Cell calcium **32:**235-249.
17. **Berridge, M. J.** 1995. Inositol trisphosphate and calcium signaling. Annals of the New York Academy of Sciences **766:**31-43.
18. **Berridge, M. J., P. Lipp, and M. D. Bootman.** 2000. The versatility and universality of calcium signalling. Nature reviews. Molecular cell biology **1:**11-21.
19. **Bertolotti, A., Y. Zhang, L. M. Hendershot, H. P. Harding, and D. Ron.** 2000. Dynamic interaction of BiP and ER stress transducers in the unfolded-protein response. Nature cell biology **2:**326-332.

20. **Bertrand, M. J., and P. Vandenabeele.** 2010. RIP1's function in NF-kappaB activation: from master actor to onlooker. Cell death and differentiation **17:**379-380.
21. **Bisht, H., A. S. Weisberg, P. Szajner, and B. Moss.** 2009. Assembly and disassembly of the capsid-like external scaffold of immature virions during vaccinia virus morphogenesis. Journal of virology **83:**9140-9150.
22. **Blasco, R., and B. Moss.** 1992. Role of cell-associated enveloped vaccinia virus in cell-to-cell spread. Journal of virology **66:**4170-4179.
23. **Blum H, B. H., Gross HJ.** 1987. Improved silver staining of plant proteins, RNA and DNA in polyacrylamide gels, p. 93-99, Electrophoresis, vol. 8.
24. **Boomker, J. M., L. F. de Leij, T. H. The, and M. C. Harmsen.** 2005. Viral chemokine-modulatory proteins: tools and targets. Cytokine & growth factor reviews **16:**91-103.
25. **Borgese, N., S. Brambillasca, and S. Colombo.** 2007. How tails guide tail-anchored proteins to their destinations. Current opinion in cell biology **19:**368-375.
26. **Borgese, N., and E. Fasana.** 2011. Targeting pathways of C-tail-anchored proteins. Biochimica et biophysica acta **1808:**937-946.
27. **Bork, P.** 1993. Hundreds of ankyrin-like repeats in functionally diverse proteins: mobile modules that cross phyla horizontally? Proteins **17:**363-374.
28. **Brambillasca, S., M. Yabal, M. Makarow, and N. Borgese.** 2006. Unassisted translocation of large polypeptide domains across phospholipid bilayers. The Journal of cell biology **175:**767-777.
29. **Brandstadter, J. D., and Y. Yang.** 2011. Natural killer cell responses to viral infection. Journal of innate immunity **3:**274-279.
30. **Bratke, K. A., A. McLysaght, and S. Rothenburg.** 2013. A survey of host range genes in poxvirus genomes. Infection, genetics and evolution : journal of molecular epidemiology and evolutionary genetics in infectious diseases **14:**406-425.
31. **Broyles, S. S.** 2003. Vaccinia virus transcription. The Journal of general virology **84:**2293-2303.
32. **Campbell, S., B. Hazes, M. Kvansakul, P. Colman, and M. Barry.** 2010. Vaccinia virus F1L interacts with Bak using highly divergent Bcl-2 homology domains and replaces the function of Mcl-1. The Journal of biological chemistry **285:**4695-4708.
33. **Carfi, A., C. A. Smith, P. J. Smolak, J. McGrew, and D. C. Wiley.** 1999. Structure of a soluble secreted chemokine inhibitor vCCI (p35) from cowpox virus. Proceedings of the National Academy of Sciences of the United States of America **96:**12379-12383.
34. **Carroll, K., O. Elroy-Stein, B. Moss, and R. Jagus.** 1993. Recombinant vaccinia virus K3L gene product prevents activation of double-stranded RNA-dependent, initiation factor 2 alpha-specific protein kinase. The Journal of biological chemistry **268:**12837-12842.
35. **Carter, G. C., M. Law, M. Hollinshead, and G. L. Smith.** 2005. Entry of the vaccinia virus intracellular mature virion and its interactions with glycosaminoglycans. The Journal of general virology **86:**1279-1290.
36. **Chakrabarti, A., A. W. Chen, and J. D. Varner.** 2011. A review of the mammalian unfolded protein response. Biotechnology and bioengineering **108:**2777-2793.

37. **Chakrabarti, S., J. R. Sisler, and B. Moss.** 1997. Compact, synthetic, vaccinia virus early/late promoter for protein expression. BioTechniques **23:**1094-1097.
38. **Chan, A., M. Baird, A. A. Mercer, and S. B. Fleming.** 2006. Maturation and function of human dendritic cells are inhibited by orf virus-encoded interleukin-10. The Journal of general virology **87:**3177-3181.
39. **Chang, H. W., J. C. Watson, and B. L. Jacobs.** 1992. The E3L gene of vaccinia virus encodes an inhibitor of the interferon-induced, double-stranded RNA-dependent protein kinase. Proceedings of the National Academy of Sciences of the United States of America **89:**4825-4829.
40. **Chen, R. A., G. Ryzhakov, S. Cooray, F. Randow, and G. L. Smith.** 2008. Inhibition of IkappaB kinase by vaccinia virus virulence factor B14. PLoS pathogens **4:**e22.
41. **Chen, S., P. Novick, and S. Ferro-Novick.** 2012. ER network formation requires a balance of the dynamin-like GTPase Sey1p and the Lunapark family member Lnp1p. Nature cell biology **14:**707-716.
42. **Chen, S., P. Novick, and S. Ferro-Novick.** 2013. ER structure and function. Current opinion in cell biology **25:**428-433.
43. **Chipuk, J. E., T. Moldoveanu, F. Llambi, M. J. Parsons, and D. R. Green.** 2010. The BCL-2 family reunion. Molecular cell **37:**299-310.
44. **Chiu, W. L., C. L. Lin, M. H. Yang, D. L. Tzou, and W. Chang.** 2007. Vaccinia virus 4c (A26L) protein on intracellular mature virus binds to the extracellular cellular matrix laminin. Journal of virology **81:**2149-2157.
45. **Chung, C. S., C. H. Chen, M. Y. Ho, C. Y. Huang, C. L. Liao, and W. Chang.** 2006. Vaccinia virus proteome: identification of proteins in vaccinia virus intracellular mature virion particles. Journal of virology **80:**2127-2140.
46. **Chung, C. S., J. C. Hsiao, Y. S. Chang, and W. Chang.** 1998. A27L protein mediates vaccinia virus interaction with cell surface heparan sulfate. Journal of virology **72:**1577-1585.
47. **Coe, H., and M. Michalak.** 2009. Calcium binding chaperones of the endoplasmic reticulum. General physiology and biophysics **28 Spec No Focus:**F96-F103.
48. **Colamonici, O. R., P. Domanski, S. M. Sweitzer, A. Larner, and R. M. Buller.** 1995. Vaccinia virus B18R gene encodes a type I interferon-binding protein that blocks interferon alpha transmembrane signaling. The Journal of biological chemistry **270:**15974-15978.
49. **Coleman, M. L., E. A. Sahai, M. Yeo, M. Bosch, A. Dewar, and M. F. Olson.** 2001. Membrane blebbing during apoptosis results from caspase-mediated activation of ROCK I. Nature cell biology **3:**339-345.
50. **Colombo, S. F., R. Longhi, and N. Borgese.** 2009. The role of cytosolic proteins in the insertion of tail-anchored proteins into phospholipid bilayers. Journal of cell science **122:**2383-2392.
51. **Condit, R. C., N. Moussatche, and P. Traktman.** 2006. In a nutshell: structure and assembly of the vaccinia virion. Advances in virus research **66:**31-124.
52. **Cooray, S., M. W. Bahar, N. G. Abrescia, C. E. McVey, N. W. Bartlett, R. A. Chen, D. I. Stuart, J. M. Grimes, and G. L. Smith.** 2007. Functional and structural studies of the vaccinia virus virulence factor N1 reveal a Bcl-2-like anti-apoptotic protein. The Journal of general virology **88:**1656-1666.

53. **Coppari, S., F. Altieri, A. Ferraro, S. Chichiarelli, M. Eufemi, and C. Turano.** 2002. Nuclear localization and DNA interaction of protein disulfide isomerase ERp57 in mammalian cells. Journal of cellular biochemistry **85:**325-333.
54. **Cullen, S. P., and S. J. Martin.** 2009. Caspase activation pathways: some recent progress. Cell death and differentiation **16:**935-938.
55. **Damon, I. K.** 2007. Poxviruses, p. 2947-2975. *In* H. P. M. Knipe D.M. (ed.), Fields Virology. Lippincott Williams & Wilkins, Philadelphia.
56. **Davies, M. V., H. W. Chang, B. L. Jacobs, and R. J. Kaufman.** 1993. The E3L and K3L vaccinia virus gene products stimulate translation through inhibition of the double-stranded RNA-dependent protein kinase by different mechanisms. Journal of virology **67:**1688-1692.
57. **Degenhardt, K., R. Sundararajan, T. Lindsten, C. Thompson, and E. White.** 2002. Bax and Bak independently promote cytochrome C release from mitochondria. The Journal of biological chemistry **277:**14127-14134.
58. **Dewson, G., T. Kratina, H. W. Sim, H. Puthalakath, J. M. Adams, P. M. Colman, and R. M. Kluck.** 2008. To trigger apoptosis, Bak exposes its BH3 domain and homodimerizes via BH3:groove interactions. Molecular cell **30:**369-380.
59. **Di Sano, F., P. Bernardoni, and M. Piacentini.** 2012. The reticulons: guardians of the structure and function of the endoplasmic reticulum. Experimental cell research **318:**1201-1207.
60. **Douglas, A. E., K. D. Corbett, J. M. Berger, G. McFadden, and T. M. Handel.** 2007. Structure of M11L: A myxoma virus structural homolog of the apoptosis inhibitor, Bcl-2. Protein science : a publication of the Protein Society **16:**695-703.
61. **Ea, C. K., L. Deng, Z. P. Xia, G. Pineda, and Z. J. Chen.** 2006. Activation of IKK by TNFalpha requires site-specific ubiquitination of RIP1 and polyubiquitin binding by NEMO. Molecular cell **22:**245-257.
62. **Earl, P., Moss, B, Wyatt, LS, Carroll MW** 1998. Generation of Recombinant Vaccinia viruses, p. 16.17.11-16.17.19. *In* B. R. Ausubel FM, Kingston RE, Moore DD, Seidman JG, et al. (ed.), Current protocols in molecular biology. Wiley Interscience, New York, NY.
63. **Earp, L. J., S. E. Delos, H. E. Park, and J. M. White.** 2005. The many mechanisms of viral membrane fusion proteins. Current topics in microbiology and immunology **285:**25-66.
64. **Elmore, S.** 2007. Apoptosis: a review of programmed cell death. Toxicologic pathology **35:**495-516.
65. **Emerson, G. L., Y. Li, M. A. Frace, M. A. Olsen-Rasmussen, M. L. Khristova, D. Govil, S. A. Sammons, R. L. Regnery, K. L. Karem, I. K. Damon, and D. S. Carroll.** 2009. The phylogenetics and ecology of the orthopoxviruses endemic to North America. PloS one **4:**e7666.
66. **Esteban, D. J., and R. M. Buller.** 2005. Ectromelia virus: the causative agent of mousepox. The Journal of general virology **86:**2645-2659.
67. **Esteban, D. J., A. A. Nuara, and R. M. Buller.** 2004. Interleukin-18 and glycosaminoglycan binding by a protein encoded by Variola virus. The Journal of general virology **85:**1291-1299.
68. **Everett, H., and G. McFadden.** 2002. Poxviruses and apoptosis: a time to die. Current opinion in microbiology **5:**395-402.

69. **Fagan-Garcia, K., and M. Barry.** 2011. A vaccinia virus deletion mutant reveals the presence of additional inhibitors of NF-kappaB. Journal of virology **85:**883-894.
70. **Fenner, F.** 2000. Adventures with poxviruses of vertebrates. FEMS microbiology reviews **24:**123-133.
71. **Fenner, F., D. A. Henderson, I. Arita, Z. Jezek, and I. D. Ladnyi.** 1988. Smallpox and Its Eradication, Geneva.
72. **Fenner, F., Wittek, R, Dumbell KR.** 1989. The Orthopoxviruses. Academic Press, San Diego.
73. **Furness, G., and J. S. Youngner.** 1959. One-step growth curves for vaccinia virus in cultures of monkey kidney cells. Virology **9:**386-395.
74. **Gedey, R., X. L. Jin, O. Hinthong, and J. L. Shisler.** 2006. Poxviral regulation of the host NF-kappaB response: the vaccinia virus M2L protein inhibits induction of NF-kappaB activation via an ERK2 pathway in virus-infected human embryonic kidney cells. Journal of virology **80:**8676-8685.
75. **Gottlieb, E., S. M. Armour, M. H. Harris, and C. B. Thompson.** 2003. Mitochondrial membrane potential regulates matrix configuration and cytochrome c release during apoptosis. Cell death and differentiation **10:**709-717.
76. **Goyal, U., and C. Blackstone.** 2013. Untangling the web: mechanisms underlying ER network formation. Biochimica et biophysica acta **1833:**2492-2498.
77. **Graham, S. C., M. W. Bahar, S. Cooray, R. A. Chen, D. M. Whalen, N. G. Abrescia, D. Alderton, R. J. Owens, D. I. Stuart, G. L. Smith, and J. M. Grimes.** 2008. Vaccinia virus proteins A52 and B14 Share a Bcl-2-like fold but have evolved to inhibit NF-kappaB rather than apoptosis. PLoS pathogens **4:**e1000128.
78. **Grimm, S.** 2012. The ER-mitochondria interface: the social network of cell death. Biochimica et biophysica acta **1823:**327-334.
79. **Gubser, C., S. Hue, P. Kellam, and G. L. Smith.** 2004. Poxvirus genomes: a phylogenetic analysis. The Journal of general virology **85:**105-117.
80. **Guerin, J. L., J. Gelfi, S. Boullier, M. Delverdier, F. A. Bellanger, S. Bertagnoli, I. Drexler, G. Sutter, and F. Messud-Petit.** 2002. Myxoma virus leukemia-associated protein is responsible for major histocompatibility complex class I and Fas-CD95 down-regulation and defines scrapins, a new group of surface cellular receptor abductor proteins. Journal of virology **76:**2912-2923.
81. **Guo, Z. S., Bartlett, DL.** 2004. Vaccinia as a vector for gene delivery. Expert Opinion on Biological Therapy **4:**901-917.
82. **Haga, I. R., and A. G. Bowie.** 2005. Evasion of innate immunity by vaccinia virus. Parasitology **130 Suppl:**S11-25.
83. **Halbach, A., C. Landgraf, S. Lorenzen, K. Rosenkranz, R. Volkmer-Engert, R. Erdmann, and H. Rottensteiner.** 2006. Targeting of the tail-anchored peroxisomal membrane proteins PEX26 and PEX15 occurs through C-terminal PEX19-binding sites. Journal of cell science **119:**2508-2517.
84. **Harding, H. P., Y. Zhang, A. Bertolotti, H. Zeng, and D. Ron.** 2000. Perk is essential for translational regulation and cell survival during the unfolded protein response. Molecular cell **5:**897-904.

85. **Hayden, M. S., and S. Ghosh.** 2012. NF-kappaB, the first quarter-century: remarkable progress and outstanding questions. Genes & development **26:**203-234.
86. **Hayden, M. S., and S. Ghosh.** 2008. Shared principles in NF-kappaB signaling. Cell **132:**344-362.
87. **Hayden, M. S., and S. Ghosh.** 2004. Signaling to NF-kappaB. Genes & development **18:**2195-2224.
88. **Hayden, M. S., A. P. West, and S. Ghosh.** 2006. NF-kappaB and the immune response. Oncogene **25:**6758-6780.
89. **He, H., M. Lam, T. S. McCormick, and C. W. Distelhorst.** 1997. Maintenance of calcium homeostasis in the endoplasmic reticulum by Bcl-2. The Journal of cell biology **138:**1219-1228.
90. **Hengartner, M. O.** 2000. The biochemistry of apoptosis. Nature **407:**770-776.
91. **Hinthong, O., X. L. Jin, and J. L. Shisler.** 2008. Characterization of wild-type and mutant vaccinia virus M2L proteins' abilities to localize to the endoplasmic reticulum and to inhibit NF-kappaB activation during infection. Virology **373:**248-262.
92. **Hofmann, K., Stoffel, W.** 1993. TMbase - A database of membrane spanning proteins segments, p. 374,166, Biol. Chem. . Hoppe-Seyler.
93. **Horie, C., H. Suzuki, M. Sakaguchi, and K. Mihara.** 2002. Characterization of signal that directs C-tail-anchored proteins to mammalian mitochondrial outer membrane. Molecular biology of the cell **13:**1615-1625.
94. **Hsiao, J. C., C. S. Chung, and W. Chang.** 1999. Vaccinia virus envelope D8L protein binds to cell surface chondroitin sulfate and mediates the adsorption of intracellular mature virions to cells. Journal of virology **73:**8750-8761.
95. **Hsiao, J. C., C. S. Chung, R. Drillien, and W. Chang.** 2004. The cowpox virus host range gene, CP77, affects phosphorylation of eIF2 alpha and vaccinia viral translation in apoptotic HeLa cells. Virology **329:**199-212.
96. **Hu, F. Q., C. A. Smith, and D. J. Pickup.** 1994. Cowpox virus contains two copies of an early gene encoding a soluble secreted form of the type II TNF receptor. Virology **204:**343-356.
97. **Hughes, A. L., S. Irausquin, and R. Friedman.** 2010. The evolutionary biology of poxviruses. Infection, genetics and evolution : journal of molecular epidemiology and evolutionary genetics in infectious diseases **10:**50-59.
98. **Husain, M., A. S. Weisberg, and B. Moss.** 2006. Existence of an operative pathway from the endoplasmic reticulum to the immature poxvirus membrane. Proceedings of the National Academy of Sciences of the United States of America **103:**19506-19511.
99. **Israel, A.** 2000. The IKK complex: an integrator of all signals that activate NF-kappaB? Trends in cell biology **10:**129-133.
100. **Johnston, J. B., and G. McFadden.** 2003. Poxvirus immunomodulatory strategies: current perspectives. Journal of virology **77:**6093-6100.
101. **Joseph, S. K.** 1996. The inositol triphosphate receptor family. Cellular signalling **8:**1-7.
102. **Kanayama, A., R. B. Seth, L. Sun, C. K. Ea, M. Hong, A. Shaito, Y. H. Chiu, L. Deng, and Z. J. Chen.** 2004. TAB2 and TAB3 activate the NF-kappaB pathway through binding to polyubiquitin chains. Molecular cell **15:**535-548.

103. **Katsafanas, G. C., and B. Moss.** 2007. Colocalization of transcription and translation within cytoplasmic poxvirus factories coordinates viral expression and subjugates host functions. Cell host & microbe **2:**221-228.
104. **Katz, E., B. M. Ward, A. S. Weisberg, and B. Moss.** 2003. Mutations in the vaccinia virus A33R and B5R envelope proteins that enhance release of extracellular virions and eliminate formation of actin-containing microvilli without preventing tyrosine phosphorylation of the A36R protein. Journal of virology **77:**12266-12275.
105. **Kennedy, R. B., I. G. Ovsyannikova, R. M. Jacobson, and G. A. Poland.** 2009. The immunology of smallpox vaccines. Current opinion in immunology **21:**314-320.
106. **Kerr, P. J., and S. M. Best.** 1998. Myxoma virus in rabbits. Revue scientifique et technique **17:**256-268.
107. **Kettle, S., A. Alcami, A. Khanna, R. Ehret, C. Jassoy, and G. L. Smith.** 1997. Vaccinia virus serpin B13R (SPI-2) inhibits interleukin-1beta-converting enzyme and protects virus-infected cells from TNF- and Fas-mediated apoptosis, but does not prevent IL-1beta-induced fever. The Journal of general virology **78 (Pt 3):**677-685.
108. **Kleizen, B., and I. Braakman.** 2004. Protein folding and quality control in the endoplasmic reticulum. Current opinion in cell biology **16:**343-349.
109. **Kotwal, G. J., S. N. Isaacs, R. McKenzie, M. M. Frank, and B. Moss.** 1990. Inhibition of the complement cascade by the major secretory protein of vaccinia virus. Science **250:**827-830.
110. **Kotwal, G. J., C. G. Miller, and D. E. Justus.** 1998. The inflammation modulatory protein (IMP) of cowpox virus drastically diminishes the tissue damage by down-regulating cellular infiltration resulting from complement activation. Molecular and cellular biochemistry **185:**39-46.
111. **Kozak, M.** 1987. An analysis of 5'-noncoding sequences from 699 vertebrate messenger RNAs. Nucleic acids research **15:**8125-8148.
112. **Kroemer, G.** 2003. Mitochondrial control of apoptosis: an introduction. Biochemical and biophysical research communications **304:**433-435.
113. **Kuznetsov, G., L. B. Chen, and S. K. Nigam.** 1997. Multiple molecular chaperones complex with misfolded large oligomeric glycoproteins in the endoplasmic reticulum. The Journal of biological chemistry **272:**3057-3063.
114. **Kvansakul, M., H. Yang, W. D. Fairlie, P. E. Czabotar, S. F. Fischer, M. A. Perugini, D. C. Huang, and P. M. Colman.** 2008. Vaccinia virus anti-apoptotic F1L is a novel Bcl-2-like domain-swapped dimer that binds a highly selective subset of BH3-containing death ligands. Cell death and differentiation **15:**1564-1571.
115. **Lalani, A. S., K. Graham, K. Mossman, K. Rajarathnam, I. Clark-Lewis, D. Kelvin, and G. McFadden.** 1997. The purified myxoma virus gamma interferon receptor homolog M-T7 interacts with the heparin-binding domains of chemokines. Journal of virology **71:**4356-4363.
116. **Lefkowitz, E. J., C. Wang, and C. Upton.** 2006. Poxviruses: past, present and future. Virus research **117:**105-118.
117. **Li, H., H. Zhu, C. J. Xu, and J. Yuan.** 1998. Cleavage of BID by caspase 8 mediates the mitochondrial damage in the Fas pathway of apoptosis. Cell **94:**491-501.
118. **Li, J., A. Mahajan, and M. D. Tsai.** 2006. Ankyrin repeat: a unique motif mediating protein-protein interactions. Biochemistry **45:**15168-15178.

119. **Li, Z. W., W. Chu, Y. Hu, M. Delhase, T. Deerinck, M. Ellisman, R. Johnson, and M. Karin.** 1999. The IKKbeta subunit of IkappaB kinase (IKK) is essential for nuclear factor kappaB activation and prevention of apoptosis. The Journal of experimental medicine **189:**1839-1845.
120. **Liptakova, H., E. Kontsekova, A. Alcami, G. L. Smith, and P. Kontsek.** 1997. Analysis of an interaction between the soluble vaccinia virus-coded type I interferon (IFN)-receptor and human IFN-alpha1 and IFN-alpha2. Virology **232:**86-90.
121. **Liszewski, M. K., M. K. Leung, R. Hauhart, C. J. Fang, P. Bertram, and J. P. Atkinson.** 2009. Smallpox inhibitor of complement enzymes (SPICE): dissecting functional sites and abrogating activity. Journal of immunology **183:**3150-3159.
122. **Loparev, V. N., J. M. Parsons, J. C. Knight, J. F. Panus, C. A. Ray, R. M. Buller, D. J. Pickup, and J. J. Esposito.** 1998. A third distinct tumor necrosis factor receptor of orthopoxviruses. Proceedings of the National Academy of Sciences of the United States of America **95:**3786-3791.
123. **Luik, R. M., M. M. Wu, J. Buchanan, and R. S. Lewis.** 2006. The elementary unit of store-operated Ca2+ entry: local activation of CRAC channels by STIM1 at ER-plasma membrane junctions. The Journal of cell biology **174:**815-825.
124. **Luttichau, H. R., J. Gerstoft, and T. W. Schwartz.** 2001. MC148 encoded by human molluscum contagiosum poxvirus is an antagonist for human but not murine CCR8. Journal of leukocyte biology **70:**277-282.
125. **Luttichau, H. R., J. Stine, T. P. Boesen, A. H. Johnsen, D. Chantry, J. Gerstoft, and T. W. Schwartz.** 2000. A highly selective CC chemokine receptor (CCR)8 antagonist encoded by the poxvirus molluscum contagiosum. The Journal of experimental medicine **191:**171-180.
126. **Lynes, E. M., and T. Simmen.** 2011. Urban planning of the endoplasmic reticulum (ER): how diverse mechanisms segregate the many functions of the ER. Biochimica et biophysica acta **1813:**1893-1905.
127. **Ma, Y., J. W. Brewer, J. A. Diehl, and L. M. Hendershot.** 2002. Two distinct stress signaling pathways converge upon the CHOP promoter during the mammalian unfolded protein response. Journal of molecular biology **318:**1351-1365.
128. **MacBeath, G.** 2002. Protein microarrays and proteomics. Nature genetics **32 Suppl:**526-532.
129. **Macen, J. L., C. Upton, N. Nation, and G. McFadden.** 1993. SERP1, a serine proteinase inhibitor encoded by myxoma virus, is a secreted glycoprotein that interferes with inflammation. Virology **195:**348-363.
130. **Malhotra, J. D., and R. J. Kaufman.** 2007. The endoplasmic reticulum and the unfolded protein response. Seminars in cell & developmental biology **18:**716-731.
131. **Maluquer de Motes, C., S. Cooray, H. Ren, G. M. Almeida, K. McGourty, M. W. Bahar, D. I. Stuart, J. M. Grimes, S. C. Graham, and G. L. Smith.** 2011. Inhibition of apoptosis and NF-kappaB activation by vaccinia protein N1 occur via distinct binding surfaces and make different contributions to virulence. PLoS pathogens **7:**e1002430.
132. **Maruri-Avidal, L., A. Domi, A. S. Weisberg, and B. Moss.** 2011. Participation of vaccinia virus l2 protein in the formation of crescent membranes and immature virions. Journal of virology **85:**2504-2511.

133. **Maruri-Avidal, L., A. S. Weisberg, and B. Moss.** 2013. Direct formation of vaccinia virus membranes from the endoplasmic reticulum in the absence of the newly characterized L2-interacting protein A30.5. Journal of virology **87:**12313-12326.
134. **Maruri-Avidal, L., A. S. Weisberg, and B. Moss.** 2011. Vaccinia virus L2 protein associates with the endoplasmic reticulum near the growing edge of crescent precursors of immature virions and stabilizes a subset of viral membrane proteins. Journal of virology **85:**12431-12441.
135. **Mazzon, M., N. E. Peters, C. Loenarz, E. M. Krysztofinska, S. W. Ember, B. J. Ferguson, and G. L. Smith.** 2013. A mechanism for induction of a hypoxic response by vaccinia virus. Proceedings of the National Academy of Sciences of the United States of America **110:**12444-12449.
136. **McCraith, S., T. Holtzman, B. Moss, and S. Fields.** 2000. Genome-wide analysis of vaccinia virus protein-protein interactions. Proceedings of the National Academy of Sciences of the United States of America **97:**4879-4884.
137. **McFadden, G.** 2005. Poxvirus tropism. Nature reviews. Microbiology **3:**201-213.
138. **McGuffin, L. J., K. Bryson, and D. T. Jones.** 2000. The PSIPRED protein structure prediction server. Bioinformatics **16:**404-405.
139. **Messud-Petit, F., J. Gelfi, M. Delverdier, M. F. Amardeilh, R. Py, G. Sutter, and S. Bertagnoli.** 1998. Serp2, an inhibitor of the interleukin-1beta-converting enzyme, is critical in the pathobiology of myxoma virus. Journal of virology **72:**7830-7839.
140. **Michalak, M., J. Groenendyk, E. Szabo, L. I. Gold, and M. Opas.** 2009. Calreticulin, a multi-process calcium-buffering chaperone of the endoplasmic reticulum. The Biochemical journal **417:**651-666.
141. **Miller, C. G., S. N. Shchelkunov, and G. J. Kotwal.** 1997. The cowpox virus-encoded homolog of the vaccinia virus complement control protein is an inflammation modulatory protein. Virology **229:**126-133.
142. **Miller, J., and I. Stagljar.** 2004. Using the yeast two-hybrid system to identify interacting proteins. Methods in molecular biology **261:**247-262.
143. **Mohamed, M. R., and G. McFadden.** 2009. NFkB inhibitors: strategies from poxviruses. Cell cycle **8:**3125-3132.
144. **Mohamed, M. R., M. M. Rahman, J. S. Lanchbury, D. Shattuck, C. Neff, M. Dufford, N. van Buuren, K. Fagan, M. Barry, S. Smith, I. Damon, and G. McFadden.** 2009. Proteomic screening of variola virus reveals a unique NF-kappaB inhibitor that is highly conserved among pathogenic orthopoxviruses. Proceedings of the National Academy of Sciences of the United States of America **106:**9045-9050.
145. **Moss, B.** 1996. Genetically engineered poxviruses for recombinant gene expression, vaccination, and safety. Proceedings of the National Academy of Sciences of the United States of America **93:**11341-11348.
146. **Moss, B.** 2007. Poxviridae: The Viruses and Their Replication, p. 2905-2946. *In* H. P. M. Knipe D.M. (ed.), Fields Virology. Lippincott Williams & Wilkinson, Philadelphia.
147. **Moss, B.** 2012. Poxvirus cell entry: how many proteins does it take? Viruses **4:**688-707.
148. **Moss, B.** 2006. Poxvirus entry and membrane fusion. Virology **344:**48-54.

149. **Moss, B.** 2011. Smallpox vaccines: targets of protective immunity. Immunological reviews **239:**8-26.
150. **Moss, B.** 1991. Vaccinia virus: a tool for research and vaccine development. Science **252:**1662-1667.
151. **Mossman, K., C. Upton, and G. McFadden.** 1995. The myxoma virus-soluble interferon-gamma receptor homolog, M-T7, inhibits interferon-gamma in a species-specific manner. The Journal of biological chemistry **270:**3031-3038.
152. **Najarro, P., P. Traktman, and J. A. Lewis.** 2001. Vaccinia virus blocks gamma interferon signal transduction: viral VH1 phosphatase reverses Stat1 activation. Journal of virology **75:**3185-3196.
153. **Nash, P., M. Barry, B. T. Seet, K. Veugelers, S. Hota, J. Heger, C. Hodgkinson, K. Graham, R. J. Jackson, and G. McFadden.** 2000. Post-translational modification of the myxoma-virus anti-inflammatory serpin SERP-1 by a virally encoded sialyltransferase. The Biochemical journal **347:**375-382.
154. **Nechushtan, A., C. L. Smith, Y. T. Hsu, and R. J. Youle.** 1999. Conformation of the Bax C-terminus regulates subcellular location and cell death. The EMBO journal **18:**2330-2341.
155. **Nicholls, C., H. Li, and J. P. Liu.** 2012. GAPDH: a common enzyme with uncommon functions. Clinical and experimental pharmacology & physiology **39:**674-679.
156. **Nicholson, D. W.** 1999. Caspase structure, proteolytic substrates, and function during apoptotic cell death. Cell death and differentiation **6:**1028-1042.
157. **Oda, Y., N. Hosokawa, I. Wada, and K. Nagata.** 2003. EDEM as an acceptor of terminally misfolded glycoproteins released from calnexin. Science **299:**1394-1397.
158. **Odom, M. R., R. C. Hendrickson, and E. J. Lefkowitz.** 2009. Poxvirus protein evolution: family wide assessment of possible horizontal gene transfer events. Virus research **144:**233-249.
159. **Pahl, H. L.** 1999. Activators and target genes of Rel/NF-kappaB transcription factors. Oncogene **18:**6853-6866.
160. **Parker, S., A. Nuara, R. M. Buller, and D. A. Schultz.** 2007. Human monkeypox: an emerging zoonotic disease. Future microbiology **2:**17-34.
161. **Paulose, M., B. L. Bennett, A. M. Manning, and K. Essani.** 1998. Selective inhibition of TNF-alpha induced cell adhesion molecule gene expression by tanapox virus. Microbial pathogenesis **25:**33-41.
162. **Payne, L.** 1978. Polypeptide composition of extracellular enveloped vaccinia virus. Journal of virology **27:**28-37.
163. **Perdiguero, B., and M. Esteban.** 2009. The interferon system and vaccinia virus evasion mechanisms. Journal of interferon & cytokine research : the official journal of the International Society for Interferon and Cytokine Research **29:**581-598.
164. **Petit, F., S. Bertagnoli, J. Gelfi, F. Fassy, C. Boucraut-Baralon, and A. Milon.** 1996. Characterization of a myxoma virus-encoded serpin-like protein with activity against interleukin-1 beta-converting enzyme. Journal of virology **70:**5860-5866.
165. **Pichler, H., B. Gaigg, C. Hrastnik, G. Achleitner, S. D. Kohlwein, G. Zellnig, A. Perktold, and G. Daum.** 2001. A subfraction of the yeast endoplasmic reticulum

associates with the plasma membrane and has a high capacity to synthesize lipids. European journal of biochemistry / FEBS **268:**2351-2361.

166. **Price, N., D. C. Tscharke, M. Hollinshead, and G. L. Smith.** 2000. Vaccinia virus gene B7R encodes an 18-kDa protein that is resident in the endoplasmic reticulum and affects virus virulence. Virology **267:**65-79.
167. **Rabu, C., V. Schmid, B. Schwappach, and S. High.** 2009. Biogenesis of tail-anchored proteins: the beginning for the end? Journal of cell science **122:**3605-3612.
168. **Rabu, C., P. Wipf, J. L. Brodsky, and S. High.** 2008. A precursor-specific role for Hsp40/Hsc70 during tail-anchored protein integration at the endoplasmic reticulum. The Journal of biological chemistry **283:**27504-27513.
169. **Rahighi, S., F. Ikeda, M. Kawasaki, M. Akutsu, N. Suzuki, R. Kato, T. Kensche, T. Uejima, S. Bloor, D. Komander, F. Randow, S. Wakatsuki, and I. Dikic.** 2009. Specific recognition of linear ubiquitin chains by NEMO is important for NF-kappaB activation. Cell **136:**1098-1109.
170. **Rahman, M. M., M. R. Mohamed, M. Kim, S. Smallwood, and G. McFadden.** 2009. Co-regulation of NF-kappaB and inflammasome-mediated inflammatory responses by myxoma virus pyrin domain-containing protein M013. PLoS pathogens **5:**e1000635.
171. **Raturi, A., and T. Simmen.** 2013. Where the endoplasmic reticulum and the mitochondrion tie the knot: the mitochondria-associated membrane (MAM). Biochimica et biophysica acta **1833:**213-224.
172. **Ray, C. A., R. A. Black, S. R. Kronheim, T. A. Greenstreet, P. R. Sleath, G. S. Salvesen, and D. J. Pickup.** 1992. Viral inhibition of inflammation: cowpox virus encodes an inhibitor of the interleukin-1 beta converting enzyme. Cell **69:**597-604.
173. **Resch, W., K. K. Hixson, R. J. Moore, M. S. Lipton, and B. Moss.** 2007. Protein composition of the vaccinia virus mature virion. Virology **358:**233-247.
174. **Resch, W., A. S. Weisberg, and B. Moss.** 2005. Vaccinia virus nonstructural protein encoded by the A11R gene is required for formation of the virion membrane. Journal of virology **79:**6598-6609.
175. **Riedl, S. J., and G. S. Salvesen.** 2007. The apoptosome: signalling platform of cell death. Nature reviews. Molecular cell biology **8:**405-413.
176. **Riedl, S. J., and Y. Shi.** 2004. Molecular mechanisms of caspase regulation during apoptosis. Nature reviews. Molecular cell biology **5:**897-907.
177. **Roberts, K. L., and G. L. Smith.** 2008. Vaccinia virus morphogenesis and dissemination. Trends in microbiology **16:**472-479.
178. **Ron, D., and P. Walter.** 2007. Signal integration in the endoplasmic reticulum unfolded protein response. Nature reviews. Molecular cell biology **8:**519-529.
179. **Rong, Y., and C. W. Distelhorst.** 2008. Bcl-2 protein family members: versatile regulators of calcium signaling in cell survival and apoptosis. Annual review of physiology **70:**73-91.
180. **Rong, Y. P., G. Bultynck, A. S. Aromolaran, F. Zhong, J. B. Parys, H. De Smedt, G. A. Mignery, H. L. Roderick, M. D. Bootman, and C. W. Distelhorst.** 2009. The BH4 domain of Bcl-2 inhibits ER calcium release and apoptosis by binding the regulatory and coupling domain of the IP3 receptor. Proceedings of the National Academy of Sciences of the United States of America **106:**14397-14402.

181. **Sahu, A., S. N. Isaacs, A. M. Soulika, and J. D. Lambris.** 1998. Interaction of vaccinia virus complement control protein with human complement proteins: factor I-mediated degradation of C3b to iC3b1 inactivates the alternative complement pathway. Journal of immunology **160:**5596-5604.
182. **Sambrook, R.** 2001. Molecular Cloning: A Laboratory Manual. Cold Spring Harbor Laboratory Press, Cold Spring Harbor, NY.
183. **Saraiva, M., and A. Alcami.** 2001. CrmE, a novel soluble tumor necrosis factor receptor encoded by poxviruses. Journal of virology **75:**226-233.
184. **Savill, J., and V. Fadok.** 2000. Corpse clearance defines the meaning of cell death. Nature **407:**784-788.
185. **Scaduto, R. C., Jr., and L. W. Grotyohann.** 1999. Measurement of mitochondrial membrane potential using fluorescent rhodamine derivatives. Biophysical journal **76:**469-477.
186. **Scherer, D. C., J. A. Brockman, Z. Chen, T. Maniatis, and D. W. Ballard.** 1995. Signal-induced degradation of I kappa B alpha requires site-specific ubiquitination. Proceedings of the National Academy of Sciences of the United States of America **92:**11259-11263.
187. **Schmelz, M., B. Sodeik, M. Ericsson, E. J. Wolffe, H. Shida, G. Hiller, and G. Griffiths.** 1994. Assembly of vaccinia virus: the second wrapping cisterna is derived from the trans Golgi network. Journal of virology **68:**130-147.
188. **Schramm, B., and J. K. Locker.** 2005. Cytoplasmic organization of POXvirus DNA replication. Traffic **6:**839-846.
189. **Sedger, L., and G. McFadden.** 1996. M-T2: a poxvirus TNF receptor homologue with dual activities. Immunology and cell biology **74:**538-545.
190. **Seet, B. T., J. Barrett, J. Robichaud, B. Shilton, R. Singh, and G. McFadden.** 2001. Glycosaminoglycan binding properties of the myxoma virus CC-chemokine inhibitor, M-T1. The Journal of biological chemistry **276:**30504-30513.
191. **Seet, B. T., J. B. Johnston, C. R. Brunetti, J. W. Barrett, H. Everett, C. Cameron, J. Sypula, S. H. Nazarian, A. Lucas, and G. McFadden.** 2003. Poxviruses and immune evasion. Annual review of immunology **21:**377-423.
192. **Shamas-Din, A., H. Brahmbhatt, B. Leber, and D. W. Andrews.** 2011. BH3-only proteins: Orchestrators of apoptosis. Biochimica et biophysica acta **1813:**508-520.
193. **Shao, S., and R. S. Hegde.** 2011. Membrane protein insertion at the endoplasmic reticulum. Annual review of cell and developmental biology **27:**25-56.
194. **Shen, J., X. Chen, L. Hendershot, and R. Prywes.** 2002. ER stress regulation of ATF6 localization by dissociation of BiP/GRP78 binding and unmasking of Golgi localization signals. Developmental cell **3:**99-111.
195. **Shevchenko, A., M. Wilm, O. Vorm, and M. Mann.** 1996. Mass spectrometric sequencing of proteins silver-stained polyacrylamide gels. Analytical chemistry **68:**850-858.
196. **Shisler, J. L., and B. Moss.** 2001. Molluscum contagiosum virus inhibitors of apoptosis: The MC159 v-FLIP protein blocks Fas-induced activation of procaspases and degradation of the related MC160 protein. Virology **282:**14-25.
197. **Siegel, R. M.** 2006. Caspases at the crossroads of immune-cell life and death. Nature reviews. Immunology **6:**308-317.

198. **Smith, C. A., T. Farrah, and R. G. Goodwin.** 1994. The TNF receptor superfamily of cellular and viral proteins: activation, costimulation, and death. Cell **76:**959-962.
199. **Smith, C. A., F. Q. Hu, T. D. Smith, C. L. Richards, P. Smolak, R. G. Goodwin, and D. J. Pickup.** 1996. Cowpox virus genome encodes a second soluble homologue of cellular TNF receptors, distinct from CrmB, that binds TNF but not LT alpha. Virology **223:**132-147.
200. **Smith, G. L., C. T. Benfield, C. Maluquer de Motes, M. Mazzon, S. W. Ember, B. J. Ferguson, and R. P. Sumner.** 2013. Vaccinia virus immune evasion: mechanisms, virulence and immunogenicity. The Journal of general virology **94:**2367-2392.
201. **Smith, G. L., and G. McFadden.** 2002. Smallpox: anything to declare? Nature reviews. Immunology **2:**521-527.
202. **Smith, G. L., A. Vanderplasschen, and M. Law.** 2002. The formation and function of extracellular enveloped vaccinia virus. The Journal of general virology **83:**2915-2931.
203. **Smith, M. H., H. L. Ploegh, and J. S. Weissman.** 2011. Road to ruin: targeting proteins for degradation in the endoplasmic reticulum. Science **334:**1086-1090.
204. **Sonnberg, S., S. B. Fleming, and A. A. Mercer.** 2011. Phylogenetic analysis of the large family of poxvirus ankyrin-repeat proteins reveals orthologue groups within and across chordopoxvirus genera. The Journal of general virology **92:**2596-2607.
205. **Sood, C. L., J. M. Ward, and B. Moss.** 2008. Vaccinia virus encodes I5, a small hydrophobic virion membrane protein that enhances replication and virulence in mice. Journal of virology **82:**10071-10078.
206. **Spriggs, M. K., D. E. Hruby, C. R. Maliszewski, D. J. Pickup, J. E. Sims, R. M. Buller, and J. VanSlyke.** 1992. Vaccinia and cowpox viruses encode a novel secreted interleukin-1-binding protein. Cell **71:**145-152.
207. **Stefanovic, S., and R. S. Hegde.** 2007. Identification of a targeting factor for posttranslational membrane protein insertion into the ER. Cell **128:**1147-1159.
208. **Stephens, D. J., N. Lin-Marq, A. Pagano, R. Pepperkok, and J. P. Paccaud.** 2000. COPI-coated ER-to-Golgi transport complexes segregate from COPII in close proximity to ER exit sites. Journal of cell science **113 (Pt 12):**2177-2185.
209. **Stewart, T. L., S. T. Wasilenko, and M. Barry.** 2005. Vaccinia virus F1L protein is a tail-anchored protein that functions at the mitochondria to inhibit apoptosis. Journal of virology **79:**1084-1098.
210. **Stornaiuolo, M., L. V. Lotti, N. Borgese, M. R. Torrisi, G. Mottola, G. Martire, and S. Bonatti.** 2003. KDEL and KKXX retrieval signals appended to the same reporter protein determine different trafficking between endoplasmic reticulum, intermediate compartment, and Golgi complex. Molecular biology of the cell **14:**889-902.
211. **Su, J., G. Wang, J. W. Barrett, T. S. Irvine, X. Gao, and G. McFadden.** 2006. Myxoma virus M11L blocks apoptosis through inhibition of conformational activation of Bax at the mitochondria. Journal of virology **80:**1140-1151.
212. **Symons, J. A., D. C. Tscharke, N. Price, and G. L. Smith.** 2002. A study of the vaccinia virus interferon-gamma receptor and its contribution to virus virulence. The Journal of general virology **83:**1953-1964.

213. **Szegezdi, E., D. C. Macdonald, T. Ni Chonghaile, S. Gupta, and A. Samali.** 2009. Bcl-2 family on guard at the ER. American journal of physiology. Cell physiology **296:**C941-953.
214. **Tait, S. W., and D. R. Green.** 2010. Mitochondria and cell death: outer membrane permeabilization and beyond. Nature reviews. Molecular cell biology **11:**621-632.
215. **Taylor, J. M., and M. Barry.** 2006. Near death experiences: poxvirus regulation of apoptotic death. Virology **344:**139-150.
216. **Taylor, J. M., D. Quilty, L. Banadyga, and M. Barry.** 2006. The vaccinia virus protein F1L interacts with Bim and inhibits activation of the pro-apoptotic protein Bax. The Journal of biological chemistry **281:**39728-39739.
217. **Taylor, R. C., S. P. Cullen, and S. J. Martin.** 2008. Apoptosis: controlled demolition at the cellular level. Nature reviews. Molecular cell biology **9:**231-241.
218. **Tewari, M., W. G. Telford, R. A. Miller, and V. M. Dixit.** 1995. CrmA, a poxvirus-encoded serpin, inhibits cytotoxic T-lymphocyte-mediated apoptosis. The Journal of biological chemistry **270:**22705-22708.
219. **Thorne, S. H.** 2008. Oncolytic vaccinia virus: from bedside to benchtop and back. Current opinion in molecular therapeutics **10:**387-392.
220. **Timmer, J. C., and G. S. Salvesen.** 2007. Caspase substrates. Cell death and differentiation **14:**66-72.
221. **Townsley, A. C., A. S. Weisberg, T. R. Wagenaar, and B. Moss.** 2006. Vaccinia virus entry into cells via a low-pH-dependent endosomalpathway. J. Virology **80:**8899-8908.
222. **Tulman, E. R., C. L. Afonso, Z. Lu, L. Zsak, G. F. Kutish, and D. L. Rock.** 2004. The genome of canarypox virus. Journal of virology **78:**353-366.
223. **Tulman, E. R., G. Delhon, C. L. Afonso, Z. Lu, L. Zsak, N. T. Sandybaev, U. Z. Kerembekova, V. L. Zaitsev, G. F. Kutish, and D. L. Rock.** 2006. Genome of horsepox virus. Journal of virology **80:**9244-9258.
224. **Turano, C., S. Coppari, F. Altieri, and A. Ferraro.** 2002. Proteins of the PDI family: unpredicted non-ER locations and functions. Journal of cellular physiology **193:**154-163.
225. **Turner, P. C., M. T. Baquero, S. Yuan, S. R. Thoennes, and R. W. Moyer.** 2000. The cowpox virus serpin SPI-3 complexes with and inhibits urokinase-type and tissue-type plasminogen activators and plasmin. Virology **272:**267-280.
226. **Turner, P. C., and R. W. Moyer.** 1995. Orthopoxvirus fusion inhibitor glycoprotein SPI-3 (open reading frame K2L) contains motifs characteristic of serine proteinase inhibitors that are not required for control of cell fusion. Journal of virology **69:**5978-5987.
227. **Upton, C., S. Slack, A. L. Hunter, A. Ehlers, and R. L. Roper.** 2003. Poxvirus orthologous clusters: toward defining the minimum essential poxvirus genome. Journal of virology **77:**7590-7600.
228. **Vallabhapurapu, S., and M. Karin.** 2009. Regulation and function of NF-kappaB transcription factors in the immune system. Annual review of immunology **27:**693-733.
229. **van Meer, G.** 2005. Cellular lipidomics. The EMBO journal **24:**3159-3165.

230. **Vancova, I., C. La Bonnardiere, and P. Kontsek.** 1998. Vaccinia virus protein B18R inhibits the activity and cellular binding of the novel type interferon-delta. The Journal of general virology **79 (Pt 7):**1647-1649.
231. **VanderWaal, R. P., D. R. Spitz, C. L. Griffith, R. Higashikubo, and J. L. Roti Roti.** 2002. Evidence that protein disulfide isomerase (PDI) is involved in DNA-nuclear matrix anchoring. Journal of cellular biochemistry **85:**689-702.
232. **Vazquez, A., A. Flammini, A. Maritan, and A. Vespignani.** 2003. Global protein function prediction from protein-protein interaction networks. Nature biotechnology **21:**697-700.
233. **Vembar, S. S., and J. L. Brodsky.** 2008. One step at a time: endoplasmic reticulum-associated degradation. Nature reviews. Molecular cell biology **9:**944-957.
234. **Voeltz, G. K., M. M. Rolls, and T. A. Rapoport.** 2002. Structural organization of the endoplasmic reticulum. EMBO reports **3:**944-950.
235. **Wajant, H., and P. Scheurich.** 2011. TNFR1-induced activation of the classical NF-kappaB pathway. The FEBS journal **278:**862-876.
236. **Ward, B. M.** 2005. The longest micron; transporting poxviruses out of the cell. Cellular microbiology **7:**1531-1538.
237. **Wasilenko, S. T., L. Banadyga, D. Bond, and M. Barry.** 2005. The vaccinia virus F1L protein interacts with the proapoptotic protein Bak and inhibits Bak activation. Journal of virology **79:**14031-14043.
238. **Wasilenko, S. T., A. F. Meyers, K. Vander Helm, and M. Barry.** 2001. Vaccinia virus infection disarms the mitochondrion-mediated pathway of the apoptotic cascade by modulating the permeability transition pore. Journal of virology **75:**11437-11448.
239. **Wasilenko, S. T., T. L. Stewart, A. F. Meyers, and M. Barry.** 2003. Vaccinia virus encodes a previously uncharacterized mitochondrial-associated inhibitor of apoptosis. Proceedings of the National Academy of Sciences of the United States of America **100:**14345-14350.
240. **Wei, M. C., T. Lindsten, V. K. Mootha, S. Weiler, A. Gross, M. Ashiya, C. B. Thompson, and S. J. Korsmeyer.** 2000. tBID, a membrane-targeted death ligand, oligomerizes BAK to release cytochrome c. Genes & development **14:**2060-2071.
241. **Welsch, S., L. Doglio, S. Schleich, and J. Krijnse Locker.** 2003. The vaccinia virus I3L gene product is localized to a complex endoplasmic reticulum-associated structure that contains the viral parental DNA. Journal of virology **77:**6014-6028.
242. **Wilkinson, B., and H. F. Gilbert.** 2004. Protein disulfide isomerase. Biochimica et biophysica acta **1699:**35-44.
243. **Willis, K. L., J. O. Langland, and J. L. Shisler.** 2011. Viral double-stranded RNAs from vaccinia virus early or intermediate gene transcripts possess PKR activating function, resulting in NF-kappaB activation, when the K1 protein is absent or mutated. The Journal of biological chemistry **286:**7765-7778.
244. **Wilton, B. A., S. Campbell, N. Van Buuren, R. Garneau, M. Furukawa, Y. Xiong, and M. Barry.** 2008. Ectromelia virus BTB/kelch proteins, EVM150 and EVM167, interact with cullin-3-based ubiquitin ligases. Virology **374:**82-99.
245. **Xiang, Y., and B. Moss.** 2003. Molluscum contagiosum virus interleukin-18 (IL-18) binding protein is secreted as a full-length form that binds cell surface glycosaminoglycans through the C-terminal tail and a furin-cleaved form with only the IL-18 binding domain. Journal of virology **77:**2623-2630.

246. **Yoshida, H., T. Matsui, A. Yamamoto, T. Okada, and K. Mori.** 2001. XBP1 mRNA is induced by ATF6 and spliced by IRE1 in response to ER stress to produce a highly active transcription factor. Cell **107:**881-891.
247. **Youle, R. J., and A. Strasser.** 2008. The BCL-2 protein family: opposing activities that mediate cell death. Nature reviews. Molecular cell biology **9:**47-59.
248. **Zhang, Y.** 2008. I-TASSER server for protein 3D structure prediction. BMC bioinformatics **9:**40.
249. **Zhao, G., L. Droit, R. B. Tesh, V. L. Popov, N. S. Little, C. Upton, H. W. Virgin, and D. Wang.** 2011. The genome of Yoka poxvirus. Journal of virology **85:**10230-10238.